**WORKING DRAFT**

# EFFECTIVENESS OF FUEL ROD CLADDING AS AN ENGINEERED BARRIER IN THE YUCCA MOUNTAIN REPOSITORY

Prepared by:
S. Cohen & Associates, Inc.
1355 Beverly Road, Suite 250
McLean, VA 22101

Under

Contract No. 68D70073
Work Assignment 2-05

Prepared for:

U.S. Environmental Protection Agency
Office of Radiation and Indoor Air
401 M Street, SW
Washington, D.C. 20460

Dr. Kenneth Czyscinski
Work Assignment Manager

November 5, 1998

main/Legacy - RD

TABLE OF CONTENTS

Table of Contents (Continued)

# LIST OF TABLES

LIST OF TABLES (Continued)

# LIST OF FIGURES

LIST OF FIGURES (Continued)

# EFFECTIVENESS OF FUEL ROD CLADDING AS AN ENGINEERED BARRIER IN THE YUCCA MOUNTAIN REPOSITORY

## 1.0 INTRODUCTION

As part of its effort to develop proposed 40 CFR 197 regulations for Yucca Mountain, the EPA is characterizing technical factors important to provisions of the proposed rule. This effort is aimed at identifying repository system performance factors and characterizing their uncertainties. Results can then be used to show that the regulatory provisions are compatible with characteristics of the site and the proposed repository and to provide perspective on where design selections and performance parameter assumptions lie within the spectrum of options and uncertainties.

One of the repository features potentially important to repository system performance is the cladding on commercial spent nuclear fuel (CSNF) disposed in the repository. This report addresses this performance factor by providing an information base for characterizing the effectiveness of spent fuel cladding as a barrier to release of radionuclides from a repository at Yucca Mountain. To develop the contents of the report, available information concerning the incidence of, and the mechanisms for, penetrations of cladding that could establish or compromise barrier effectiveness was reviewed and evaluated.

The information and findings presented here can be used to characterize uncertainty in the effectiveness of cladding as a repository system barrier. The information can also be used to characterize cladding performance assumptions (e.g., their position in the uncertaintly range) that are made and used, for example, in performance assessments included in the Department of Energy's (DOE) Viability Assessment for development of a repository at Yucca Mountain. The Viability Assessment was not available for characterization of its cladding performance assumptions at the time of preparation of this report.

In evaluating the barrier performance potential for CSNF cladding, it is important to estimate the time at which the fuel cladding is breached by some degradation mechanism(s). This time is an uncertain variable depending on such factors as the cladding temperature history, exposure to water, exposure to mechanical stress, initial condition of the fuel, *etc.*

As important as the time at which the fuel cladding is breached is the amount of fuel exposed as a function of time after breach and therefore potentially accessible for radionuclide transport mechanisms to become operative. A small pinhole in the cladding occurring at some time, t, after disposal is much less detrimental than a fuel rod in which the cladding has split along a significant length over the same time interval. This report provides discussion of uncertainty both as to the time of cladding failure and the fraction of fuel exposed as a function of time.

Uncertainty in the fraction of fuel exposed at various times cannot be treated independently of other factors such as the time of waste package breach or the time at which a failed waste package becomes filled with water. For example, if waste package failure occurs at a time sufficiently long after disposal that the fuel temperature is below the temperature at which the $UO_2$ fuel can oxidize to $U_3O_8$, then longitudinal cracking (and unzipping) of the cladding caused by the volume increase associated with $U_3O_8$ formation cannot occur in flawed rods. In such a situation uncertainty associated with the time dependence for cracking and unzipping is eliminated. Similarly, if some threshold temperature exists for Zircaloy corrosion and the time at which the breached waste package is filled with water is such that the threshold temperature is not exceeded, then uncertainty associated with the time to penetrate the cladding by corrosion can be eliminated from the analysis process. Additionally, if the waste package is breached at a time beyond some regulatory limit (*e.g.*, 10,000 years) or, if the fuel rod degradation processes are extant only beyond the regulatory limit, then the uncertainty associated with such failures is irrelevant from a regulatory perspective.

Prior total system performance assessments conducted by EPRI (EPRI 1996) and DOE (DOE 1995) did not consider the effects of fuel element cladding as a barrier to radionuclide release from spent fuel stored in a geologic repository at Yucca Mountain. However, in the 1996 Performance Allocation (DOE 1996), the efficacy of the fuel element cladding was considered by DOE and beneficial effects were identified. This report provides a further examination of the role that the fuel element cladding can play as part of an engineered barrier system to prevent or delay the release of radionuclides from a geologic repository.

The Performance Assessment Peer Review Panel formed by DOE "to provide formal, independent evaluation and critique of Total System Performance Assessment - Viability Assessment" had not addressed performance of spent fuel cladding as of their June 1997 report (DOE 1997).

To estimate the value of fuel rod cladding as a barrier to radionuclide releases in a high-level waste repository, it is important to know, *inter alia*, the condition of fuel element cladding at the time of disposal (i.e., the number of failed fuel pins and the distribution within the fuel assemblies) and the causes of the fuel pin failures. The initial condition of the fuel pin cladding will set the lower limit on the number of fuel pins which can leak radioactivity out of the waste container after the integrity of the waste container is lost. In addition, analysis of the causes of fuel pin failure can provide insight into some of the mechanisms which may remain in play after disposal.

Having established the initial condition of the fuel pins and the initial causes of failure, it is even more important to understand the mechanisms by which the cladding can fail after fuel assemblies are isolated in the geologic repository. Using this information combined with initial failure levels, one can model the temporal behavior of the cladding and predict radionuclide releases over time.

Conceptually, fuel pin failures prior to emplacement of the spent fuel in the waste package for final geologic disposal can result from:

- Initial manufacturing defects
- In-service failures
- In-storage failures (wet)
- In-storage failures (dry)
- Handling failures during removal from reactor, during pool storage, during removal to dry storage, during shipment to an interim storage or disposal facility, or during packaging for final disposal

After the spent fuel is placed in the repository, additional degradation of the cladding may occur. Time-dependent cladding degradation processes are affected by the cladding temperature, the presence or absence of air within the waste package, and access of the cladding surface to water that has entered the package interior as a result of corrosion and penetration of the package wall.

During the period prior to any breach of the waste package, the degradation mechanisms will be limited to those which occur in an inert environment since the waste packages are hermetically-sealed with an internal helium (or similar gas) atmosphere. Once the waste package is breached at some future time, additional fuel pin degradation mechanisms involving air (oxygen) and water (liquid or gas and its radiolytic decomposition products) are possible. A key factor in assessing the fuel pin degradation mechanisms is the spatial and temporal temperature distribution of the fuel pins in the repository.

The subsequent sections of this report discuss fuel pin failure mechanisms during various stages of operation and disposal. Section 2 discusses fuel pin failures prior to disposal, Section 3 discusses post-disposal failure mechanisms, Section 4 provides modeling recommendations to estimate the number of fuel pin failures within the Yucca Mountain environment based on the mechanisms described in Section 3, Section 5 presents a perspective on the DOE approach to modeling of fuel rod cladding as a barrier to radionuclide release, and Section 6 provides a discussion of some the elements of uncertainness in the treatment of cladding as an engineered barrier.

Specific post-disposal failure mechanisms addressed in Section 3, which can only occur after the waste package is breached by corrosion or some indeterminate failure mechanism, include cladding oxidation, fuel oxidation, cladding corrosion, and mechanical ruptures due to rock falls. Post-disposal mechanisms considered in Section 3, which are independent of whether or not the waste package has been breached, include creep, delayed hydride cracking, and fuel side stress corrosion cracking. As noted above, most of these processes are highly sensitive to the temperature profiles assigned to the fuel cladding. In this review, as discussed in Section 4, the temperature profiles developed by DOE in its 1996 Advanced Conceptual Design Report (ACD 1996) were used for the quantitative analyses. The temperature profiles were based on the peak cladding temperatures for design basis fuel[1]. Consequently, the analyses are expected to be bounding with most of the fuel cladding being at lower temperatures. While these temperature estimates are believed to be realistic, further studies in the Yucca Mountain

[1] Assumptions include a thermal loading in the repository of 83 MTU/acre, a 19.5 m waste package spacing, 10-year old fuel exposed to a burnup of 48,000 Mwd/MTU, and use of smeared thermal conductivity for the waste package internals.

program may generate new profiles which will require some of the conclusions presented here to be modified.

Information presented in this report shows that the incidence of cladding penetrations has been low, and the size of penetrations has been small, for service and storage experience to date. There are several reasons for this record of high integrity of the cladding and the limited number and size of cladding penetrations. In terms of historical sequence, the first principal reason was the nuclear navy's need for cladding integrity. In the initial stages of nuclear submarine use, cladding penetrations associated with manufacturing defects were present. These defects produced fission-recoil radionuclide releases to the reactor coolant, which led to delays in completion of maintenance operations and adverse effects on operational readiness at the height of the Cold War. As a result, Naval Reactors embarked on a fuel manufacturing quality assurance program to eliminate cladding defects. Today, there are no cladding defects in navy fuel, and a naval reactor is never refueled from start of operations to decommissioning.

The second incentive for cladding integrity was provided by the Fast Flux Test Facility (FFTF). The FFTF was designed to test fuel to failure, by achieving burnups on the order of 200 GWd/MTU. The evidence of failure would be releases of radioactivity to the reactor coolant as a result of cladding failure. If there was a baseline coolant concentration as a result of cladding defects at the start of operations, the failure could be masked. The FFTF project therefore embarked on a QA/QC program for fuel manufacture that was designed to produce fuel elements with no cladding defects. The technology and quality controls were subsequently adopted for manufacture of fuel rods for commercial power reactors.

The commercial power reactors also have need for high integrity cladding. Fission product contamination in the reactor coolant as a result of releases from cladding defects could impede the rate of execution of maintenance work during outages, with a lost-revenue cost impact of about one million dollars per day for every day the outage is extended. The electric utilities have therefore had keen interest in zero-defect fuel manufacturing.

Because of the widespread interest in, and need for, fuel cladding integrity, a large data base derived from post-service examinations has been developed. Extensive research and testing has also been done to establish the boundaries and mechanisms for potential cladding failures. These efforts are summarized in the next section.

## 2.0 FAILURES PRIOR TO DISPOSAL

It is known that some fraction of the fuel rods will have cladding failures at the time the rods are emplaced in the repository. These initial failures will have no impact on repository performance unless or until the waste packages in which they are contained are breached. The initial failures may have occurred during reactor service, handling, wet or dry storage, or transportation prior to disposal.

The U.S. Nuclear Regulatory Commission (NRC) has published annually reports on fuel element performance from which some service failure information can be distilled (NUREG/CR-3950, vol. 1-9). The most recent report in the series (vol. 9) is for 1991. Under NRC regulations in effect since 1984, license event reports (LERs) are required for a nuclear power plant when the plant, including its principal safety barriers, is seriously degraded or in an unanalyzed condition. This would require that "fuel cladding failures in the reactor or the storage pool that exceed expected values, that are unique or widespread, or that resulted from unexpected factors" be addressed (NRC 1994). If cladding failure levels are within expected value ranges, reporting is not required.

At the end of 1991 there were 111 licensed, operable nuclear power plants in the United States. Fuel for these plants was supplied by five fuel element manufacturers who produced over 112,000 fuel assemblies containing approximately 12 million fuel pins. According to TSPA-1993, a total of 40.3 million reactor fuel rods will ultimately be available for disposal (Wilson, *et al.* 1994). This equates to 86,000 MTU of fuel. Based on a Yucca Mountain repository limit of 63,000 MTU for commercial fuel (Andrews in DOE 1998a), the total number of fuel rods scheduled for disposal is 29.5 million. These fuel rods are contained in 96,684 BWR and 131,208 PWR fuel assemblies. Most of these fuel rods use Zircaloy-2 or Zircaloy-4 as the fuel rod cladding. As will be discussed subsequently, five reactors (four PWR and one BWR ) used stainless steel cladding for some of the core loadings. A total of 2,179 irradiated stainless steel fuel assemblies are available for disposal from commercial light water reactors.

Additional details on numbers of waste packages, fuel assemblies and fuel rods based on 63,000 tonnes of commercial SNF are summarized below:

PWR

Number of waste packages - 4,604
Number of fuel assemblies per package - 21
Number of fuel rods per package - 4,851 (per TSPA 1993)
Number of PWR assemblies in repository - 96,684
Number of PWR fuel rods in repository - 22,334,004

BWR

Number of waste packages - 2,982
Number of fuel assemblies per package - 44
Number of fuel rods per package - 2,400 (per TSPA 93)
Number of BWR assemblies in repository - 131,208
Number of BWR fuel rods in repository - 7,156,800

TOTALS

Number of CSNF waste packages in repository - 7,586
Number of fuel assemblies in repository - 227,892
Number of fuel rods in repository - 29,490,804

A typical Zircaloy-4 clad fuel rod for a PWR fuel assembly is about 4 m long, has an outside diameter of 9 to 11 mm and a cladding thickness of 0.58 to 0.78 mm. A typical Zircaloy-2 clad BWR fuel rod is also about 4 m long, has an outside diameter of 11 to 13 mm and a cladding thickness of 0.76 to 0.86 mm. During reactor exposure to a burnup of 40,000 to 50,000 MWd/MT, PWR fuel rods are exposed for about three years to a dynamic high-temperature (320°C), high-pressure (15.5 MPa) environment.

## 2.1 MANUFACTURING DEFECTS

No detailed information has been uncovered on manufacturing defects in the course of this study. Presumably, such defects will be detected and included with in-reactor service failures. Section 4.2, Fuel System Design of the NRC's Standard Review Plan includes preirradiation verification of cladding integrity.

## 2.2 IN-SERVICE FAILURES

Fuel rod reliability as of 1991 for the U.S. nuclear industry was quoted to be greater that 99.98% excluding debris-induced fretting corrosion (NRC 1994). Fuel rod reliability continuously improved during the 1980s but appeared to have leveled off by 1991.

In-reactor failure mechanisms which have been identified include (NRC 1994, SNL 1992):

- Debris- or flow-induced fretting
- Hydriding
- Pellet cladding interaction (PCI)
- Crud-induced localized corrosion (CILC)
- Baffle jetting

These failures are typically no longer reported to the NRC either by the utilities or the fuel vendors, so detailed statistics on failure levels are not available. However, some data have been assembled which will be described subsequent paragraphs.

Debris-induced fretting is caused by mechanical erosion of the exterior surface of the fuel rod by foreign material. This foreign material may be metallic debris introduced during the coring of plugged steam generators or materials introduced during refueling or other repair outages (NRC 1994, SNL 1992). Although debris traps have been added to fuel element assemblies to help alleviate this problem, debris-induced fretting remains the most significant failure mechanism (NRC 1994). The report from Sandia National Laboratory (SNL), SNL 1992, estimated the number of in-service breaches from this mechanism as 0.03% in 1983 and 0.0007% in 1986.

Flow-induced fretting results from the vibration of fuel rods against fuel assembly spacer grids and typically occurs at the bottom grid where turbulence is greatest. Five instances of fretting were reported in PWRs from 1971 to 1977 and two breaches were reported in BWRs from 1969 to 1971. In the period 1985-1986 two fuel rods in Yankee Rowe and one in Salem-2 failed by flow-induced fretting. The estimated failure level was 0.00001% (SNL 1992).

Baffle jetting failures are caused by excessive fuel rod vibration driven by coolant in PWRs jetting through baffle joints. SNL estimated that 197 rods had been breached by this mechanism during the period 1973 through 1986 resulting in a failure level of 0.0025%.

PCI failures are caused by the mechanical interaction of the fuel and the cladding. The problem is more prevalent in BWRs. According to SNL 1992, the failure level for BWRs was 0.01 to 0.06% and for PWRs was 0.007 to 0.04% through 1977. Only one instance of PCI failures was reported between 1977 and 1986. During a sipping test at the Oyster Creek BWR Plant, cladding breaches were detected in 47 assemblies. General Electric (GE) has introduced a pure Zr liner bonded to the inner wall of its fuel pins to absorb pellet stresses and reduce the incidence of PCI failures.

SNL divides corrosion related failures into those caused by crud deposition and CILC. Normal crud deposition primarily involves $Fe_2O_3$ while CILC crud is approximately 50% CuO and 20% $Fe_2O_3$. The BWR failure level from crud deposition was 0.002% from 1973 through 1976. The estimated crud failure level in 1979 was 0.05% for BWRs and 0.007% for PWRs. CILC failures occur primarily in BWRs due to copper contamination from condensers. The estimated failure rate for CILC from GE 8 x 8 assemblies was 0.02 to 0.07% from 1981 to 1983 (SNL 1992). This problem is gradually being reduced as brass condensers are being replaced in the power plants and water chemistry is more rigorously controlled.

Hydriding failures were the dominant breach mechanism for BWR fuel rods in the early 1970s (SNL 1992). The principal cause of this hydriding was residual moisture in the fuel rods at the time of manufacture. This moisture caused localized blisters on the inner surface of the cladding and created weak areas which could subsequently fail. The maximum BWR failure level for hydriding, ca. 0.5%, occurred in 1969 and had declined to less than 0.01% by 1977 as manufacturing procedures were improved. During the same period, hydriding failures in PWR rods dropped from 0.35 to 0.01%. No hydriding failures were reported in 1986, indicating that improved manufacturing procedures had solved this problem..

Failure levels from SNL 1992 are summarized in Table 2.1. It should be noted that, although this report was published in 1992, only data through 1986 were included. Taking the 1986 quoted experience for each failure mechanism, the failure level in BWR rods is 0.07% and the failure level in PWR rods is 0.014%. SNL 1992 states that "Since 1978 the breach fraction for PWR rods has leveled off at ~0.02%. ..... BWR rates are similar, with some sporadically higher years."

Table 2.1. Operational Fuel Rod Failure Levels (SNL 1992)

| Failure Mechanism | BWR Failures (%) | PWR Failures (%) | Time Period |
|---|---|---|---|
| Hydriding | 0.5 to 0.01 | 0.35 to 0.01 | 1969 - 1977 |
| PCI | 0.06 to 0.01-0.06 | 0.04 to 0.007 | 1964 to 1985-1986 |
| Debris-induced fretting | N/A[a] | 0.03 to 0.0007 | 1983 to 1986 |
| Flow-induced fretting | 0.05 to 0.01 | 0.01 to 0.004 | 1969 to 1986 |
| Baffle jetting | N/A | 0.0024 | 1973 to 1986 |
| Cladding corrosion-CILC | 0.002<br>0.02 to 0.07 | 0.002<br>N/A | 1973 to 1976<br>1981 to 1983 |
| Crud | 0.002<br>0.05 | 0.002<br>0.007 | 1973 to 1976<br>1979 |

[a] not applicable

To obtain an overall failure level, fuel rod failures must be weighted by the mix of BWRs and PWRs. Of the 109 reactors on-line in 1995, 37 were BWRs and 72 were PWRs (NRC 1996). Assuming 264 fuel rods per assembly and 193 assemblies per core for PWRs (Westinghouse - 17x17) and 63 fueled rods per assembly and 560 assemblies per core for BWRs (GE - 8x8) (Appendix A), the weighted average failure level using the data in Table 2.1 and the current mix of operating reactors is 0.03% (for comparable PWR and BWR burnup rates). McCoy and Doering 1994 quote a range of 0.02 to 0.05% leaking rods based on recent reactor experience.

Fuel element reliability as reported by each of the five fuel manufacturers is reproduced from NRC 1994 in Tables 2.2 through 2.6. Fuel element reliability is based on standardized procedures developed by the Institute for Nuclear Power Operations (INPO). For PWRs the procedure involves measuring the I-131 level in the reactor coolant while for BWRs the procedure involves measuring fission gas release at the steam jet air ejector. As a cautionary note, the reliability data reported in these tables may or may not include all causes of failure.

Careful reading of the footnotes is advised. For example, in Table 2.5 (Siemens), the reported reliability prior to 1988 does not include failures from plant-related causes such as debris-induced fretting. The reliability quoted for 1987 is ≥99.995%. The reliability in that year (through September), based on all failures of Siemens/ANF fuel, was 99.98% (NRC 1990).

Table 2.2. Reliability of Babcock and Wilcox Nuclear Fuel

| Year | Zircaloy-Clad Fuel Rod Reliability[a] (%) | Stainless Steel Clad Fuel Reliability[a] (%) | Average Plant Coolant I-131 Activity (μCi/g) |
|---|---|---|---|
| 1991[b] | | | |
| 1990[b] | | | |
| 1989 | 99.997 | 98.6 | 0.023 |
| 1988 | 99.99 | 99.98 | 0.035 |
| 1987 | 99.98 | 99.98 | 0.028 |
| 1986 | 99.999 | 99.998 | 0.014 |
| 1985 | 99.995 | 99.997 | 0.031 |
| 1984 | 99.990 | 100 | 0.051 |
| 1983 | 99.991 | 100 | 0.041 |
| 1982 | 99.994 | | 0.031 |
| 1981 | 99.992 | | 0.046 |
| 1980 | 99.997 | | 0.086 |
| 1979 | 99.97 | | |
| 1978 | 99.9 to 99.99 | | |

[a] B&W has defined fuel reliability as follows:
[(total # of rods irradiated during calendar year) - (estimated # of rods with defects)] x 100%
(total # of rods irradiated during calendar year)

[b] B&W has not provided information for these years.

Table 2.3. Reliability of ABB Combustion Engineering Nuclear Fuel

| Year | Zircaloy-Clad Fuel Rod Reliability (%) | Average Plant Corrected Coolant I-131 Activity[e] ($\mu$Ci/g) |
|---|---|---|
| 1991 | 99.998[a,b] | 0.0074 |
| 1990 | 99.998[a,b] | 0.0055 |
| 1989 | 99.997[a,b] | 0.0096 |
| 1988 | (c) | 0.014 |
| 1987 | (c) | 0.0304 |
| 1986 | (c) | -- |
| 1985 | (c) | -- |
| 1984 | 99.98 | -- |
| 1983 | 99.98 | -- |
| 1982 | 99.98 | -- |
| 1981 | (d) | -- |
| 1980 | (d) | -- |
| 1979 | >99.99 | -- |
| 1978 | 99.99 | -- |
| 1977 | 99.98 | -- |
| 1976 | 99.98 | -- |
| 1975 | 99.97 | -- |
| 1974 | >99.75 | -- |
| 1973 | 99.96 | -- |
| 1972 | 99.99 | -- |
| 1971 | 99.99 | -- |

[a] ABB CENF has defined fuel reliability for these years in terms of the overall reliability of ABB CE fuel fabricated since 1983.
[b] Excluding failures caused by debris-induced fretting wear.
[c] ABB CENF did not report fuel rod reliability for these years, instead they provided data on coolant activity. In their 1988 annual report, ABB CENF indicated that their overall fuel rod reliability for fuel fabricated after 1984 was estimated to be 99.997%--excluding failures caused by debris-induced fretting wear and by baffle jetting in the Yankee Rowe plant.
[d] Reliability of 8 x 8 fuel if fuel failures involving CILC are excluded.
[e] INPO Standard Method.

Table 2.4. Reliability of General Electric Nuclear Fuel

| Year | Zircaloy-Clad Fuel Rod Reliability (%) | Comments Regarding GE Fuel Reliability |
|---|---|---|
| 1991 | >99.98 | GE 8x8 Fuel Types, 1974-1991 |
| 1990 | >99.98 | All Fuel Types, 1974-1990 |
| 1989 | 99.98 | All Fuel Types, 1974-1989 |
| 1988 | >99.97 | All Fuel Types, 1974-1988 |
| 1987 | >99.99 | All Fuel Types, 1974-1987 |
| | >99.999 | Barrier Types, 1987 |
| 1986 | >99.99 | All Fuel Types, 1974-1986 |
| | 99.994 | All Fuel Types, 1986 |
| | >99.999 | Barrier Types, 1986 |
| 1985 | >99.99 | All Fuel Types, 1974-1985 |
| 1984 | >99.99 | All Fuel Types, 1974-1984 |
| | 100.00 | Barrier Types, 1984 |
| 1983 | 99.993 | All Fuel Types, 1974-1983 |
| | 99.998 | All Fuel Types, 1974-1983[a] |
| 1982 | >99.98 | All Fuel Types, 1974-1982 |
| 1981 | >99.98 | All Fuel Types, 1974-1981 |
| 1980 | >99.98 | All Fuel Types, 1974-1980 |
| 1979 | 99.984 | All Fuel Types, 1974-1979 |
| | 99.998 | For 8x8R plus 8x8R(PP) Types[b] |

[a] Reliability of 8 x 8 fuel if fuel failure involving CILC are excluded.
[b] R = retrofit design, PP = prepressurized.

Table 2.5. Reliability of Siemens Power Corporation Nuclear Fuel

| Year | Fuel Rod Reliability[a] (%) | Median Plant (PWR) Corrected Coolant I-131 Activity[e] (μCi/ml) | Median Plant (BWR) FGR Measured at Steam Jet Air Ejector[e] (μCi/sec) |
|---|---|---|---|
| 1991 | 99.998 | 0.0023 | 46 |
| 1990 | 99.997 | 0.00166 | 159 |
| 1989 | 99.997 | 0.00126 | 370 |
| 1988 | >99.994 | 0.000102 | (g) |
| 1987 | ≥99.995[b,c] | (f) | -- |
| 1986 | 99.995[b,c] | -- | -- |
| 1985 | 99.994[b,c] | -- | -- |
| 1984 | 99.995[b,c] | -- | -- |
| 1983 | 99.998,[b,c] 99.87[b,d] | -- | -- |
| 1982 | 99.998[b,c] | -- | -- |
| 1981 | 99.998,[b,c] 99.987[b,d] | -- | -- |
| 1980 | 100 | -- | -- |

[a] Includes the reliability for both PWR and BWR fuel rods. Please refer to previous annual fuel performance reports for specific PWR and BWR reliability values.
[b] On a cumulative basis.
[c] The fuel reliability value is based on fuel failures that were judged to be from fuel-related or unknown causes and were not directly attributable to external causes (e.g., plant-related causes such as baffle jetting, fretting from the presence of foreign objects or other off-normal core conditions).
[d] The fuel reliability value is based on fuel failures from all causes.
[e] INPO Standard Methods.
[f] SPC began reporting INPO fuel reliability indicator (FRI) values for PWR plants in 1988.
[g] SPC began reporting INPO FRI values for BWR plants in 1989.

Table 2.6. Reliability of Westinghouse Corporation Nuclear Fuel

| Year | Zircaloy-Clad Fuel Rod Reliability (%) | Average Plant Corrected Coolant I-131 Activity[a] ($\mu$Ci/g) |
|---|---|---|
| 1991 | | 0.00019 |
| 1990 | 99.998[b] | 0.0021 |
| 1989 | 99.994[b] | 0.0047 |
| 1988 | 99.994[b] | 0.0049 |
| 1987 | 99.994[b] | 0.0045 |
| 1986 | (c) | 0.0044 |
| 1985 | (c) | 0.0086,[d] 0.0092[e] |
| 1984 | (c) | 0.008[d] |
| 1983 | (c) | 0.030[d] |
| 1982 | (c) | 0.0296,[d] 0.041[e] |
| 1981 | (c) | -- |
| 1980 | (c) | -- |
| 1979 | ~99.983 | -- |
| 1978 | (c) | -- |
| 1977 | 99.938-99.9999 | -- |
| 1976 | (c) | -- |
| 1975 | 99.75-100.00[f] | -- |
| 1974 | 99.790-99.999[f] | -- |
| 1973 | 99.91-99.999[f] | -- |
| 1972 | 99.74-100[f] | -- |
| 1971 | 99.23-100[f] | -- |
| 1970 | 99.24-99.999[f] | -- |
| 1969 | 99.64-100[f] | -- |

[a] Westinghouse began reporting fuel performance in terms of coolant activity level starting June 30, 1976. In 1982, Westinghouse provided data on average coolant activity levels in terms of $\mu$Ci/g for Westinghouse fueled plants. Beginning 1991, Westinghouse began to also report the distribution of coolant activities for Westinghouse-fueled plants.

[b] The fuel reliability value is based on fuel failures from all causes.

[c] Westinghouse did not state a fuel rod reliability (integrity) value. Westinghouse continues to evaluate fuel performance in terms of coolant activity level.

[d] Uncorrected activity, excludes fuel failures due to baffle jetting.

[e] Uncorrected activity, includes fuel failures due to baffle jetting.

[f] The range of values for individual plants in all four quarters of the given year are provided.

In addition to the fuel rod reliability data reported in Table 2.6, Westinghouse conducted ultrasonic fuel rod testing at 12 reactor sites in 1991 (NRC 1994). Sixty-one leaking fuel rods were identified in 21 assemblies. If one assumes that there are 193 fuel assemblies per core and each assembly has 264 fuel rods (see Appendix A), an overall reliability rate of 99.99% can be estimated. TV camera examination of the rods from 10 of the 21 assemblies which were reconstituted indicated nine failures from debris-induced fretting, 40 failures from grid-rod fretting, and three rods where no primary failure mechanism was identified.

In an effort to provide greater precision in the definition of failed fuel under 10 CFR Part 961, *Standard Contract for Disposal of Spent Nuclear Fuel and/or High-Level Radioactive Waste,* EPRI has prepared an analysis of methods for classifying failures (EPRI 1997). Historical failure levels, through 1996, for fuel assemblies from the EPRI study are summarized in Table 2.7. Numbers of failed assemblies were recalculated here using the basic data in the EPRI report and slightly different values were obtained than those quoted by EPRI as shown in the last line of the table. It is not clear from the EPRI report what constitutes a fuel assembly failure. Is it mechanical failure (e.g. rod bowing or twisting) or is it fuel rod breach? If these data are extrapolated to the current Yucca Mountain design basis of 63,000 MTU for commercial fuel (total 96,684 PWR assemblies and 131,208 BWR assemblies) using the 1985 to 1996 EPRI failure level, an additional 592 to 3,556 failed assemblies (118,528[2] x 0.005 or 0.03) would be expected in the future. Based on the minimum expected total of 5,111 (4,519 + 592) failed assemblies, not every one of the more than 7,000 Yucca Mountain waste packages would contain a failed assembly.

DOE reported that the total numbers of defective fuel assemblies discharged through 1985 ranged from 3,119 to 4,691[3] (DOE 1987). Defective assemblies include assemblies with bowing, mechanical parts failure, and handling damage. Not all defective assemblies contain

---

[2] Based on the information in EPRI 1997, it can be estimated that 47,830 PWR and 61,540 BWR fuel assemblies were discharged through 1996. Subtracting these from a total of 227,892 assemblies, leaves a total of 118,522 assemblies yet to be discharged..

[3] According to Table 2.3.4 in DOE 1987, as of December 31, 1985, 45,814 assemblies had been permanently discharged and of these 3,119 were defective. In Section 2.5.6.6 of the report DOE states that 45,569 assemblies had been discharged with 4,691 being defective. In Table 2.5.6 DOE lists 45,569 discharged assemblies of which 4,691 are defective. In Table 2.5.7 DOE lists 4,650 and 4,691 assemblies as defective. The information in Section 2.5.6.6 was used for the estimates cited here.

breached fuel rods. The DOE reported minimum (3,119) is about 75% of the EPRI reported minimum (4,181) for defective assemblies through 1985. The DOE reported maximum (4,691) is substantially lower than the comparable figure reported by EPRI (8,364). Reasons for these differences are not apparent.

Table 2.7. Historical Failure Levels for Fuel Assemblies

| Time Period | Failure Level (%) | No. of Failed Assemblies |
|---|---|---|
| 1970-81 | 10 to 20 | 2573 to 5147 |
| 1981-85 | 10 to 20 | 1608 to 3217 |
| 1985-96 | 0.5 to 3.0 | 338 to 2026 |
| Revised Total | | 4519 to 10390 |
| EPRI Total | | 4864 to 9728 |

Data on fuel rods failures are estimated in Table 2.8 using the failure rates quoted in EPRI 1997 and SC&A estimates of the total number of fuel rods assuming 55 fuel rods per BWR[4] assembly and 231 rods per PWR assembly (based on data from TSPA-93, p.5- 4 and 21 assemblies per PWR waste package and 44 assemblies per BWR waste package). Extrapolations to 63,000 MTU assume that the 1985-96 failure rate in EPRI 1997 is extended to all subsequent years.

The minimum calculated number of rod failures (3,221) in Table 2.8 is inconsistent with the minimum number of failed assemblies (5,111) if there must be at least one failed rod per failed assembly. This may be due to the fact that some of the failed assemblies are the result of mechanical failures where the cladding is not breached. If this explanation is correct, about 40% of the failed fuel assemblies would be mechanical without cladding breach. This inconsistency may also be due to uncertainties in the failure level estimates for rods and assemblies. For example, if the minimum number of failed assemblies (5,111) is coupled with the maximum number of failed fuel rods (11,394), then there would be about two failed rods per failed assembly.

[4] Based on these data the number of fuel rods per waste package would be 2420 rather than 2400 as quoted in TSPA-93. The difference is not substantive.

Table 2.8. Estimated Total Fuel Rod Failures Based on EPRI Failure Level Estimates

| Time Period | Fuel Rod Failures (%) | No. of Failed Rods |
|---|---|---|
| 1970-81 | 0.04 to 0.08 | 1358/2717 |
| 1981-85 | 0.02 to 0.07 | 424/1486 |
| 1985-96 | 0.006 to 0.03 | 535/2674 |
| After 1996 | 0.006 to 0.03 | 904/4518 |
| Total | 0.011 to 0.039 | 3221/11394 |

DOE has developed fuel rod failure level estimates based on numbers of defective assemblies for the same time periods which are somewhat higher than the EPRI estimates (DOE 1987). The DOE fuel rod failure estimates are as follows:

| | BWRs | PWRs |
|---|---|---|
| Prior to 1981 | 0.06 to 1.13% | 0.02 to 0.28% |
| 1981-1985 | 0.03 to 0.55% | 0.02 to 0.17% |

This presentation by DOE is misleading and confusing. From information contained on pages 2.5-13 and 2.5-15 of DOE 1987, there are 3,374 defective BWR fuel assemblies with 1.6 defective rods per assembly, 90% of the defects are leakers, and there are 49 rods per assembly. This yields an overall failure level through 1985 for 27,446 discharged assemblies of 0.36% ([3,374x1.6x0.9]/[27,446x49]x100). Similarly for PWR fuel assemblies, there are 1,317 defective assemblies in 18,123 discharged assemblies, 2.1 defective rods per defective assembly, 54% of the defective rods are leakers, and each assembly contains 205 fuel rods. This yields an overall failure level for PWR fuel rods through 1985 of 0.04%. The combined failure level through 1985, based on DOE 1987, is 0.12%.

It was estimated in EPRI 1997 that less than 1% of the failed fuel assemblies have "severe" failures, 10 to 20% are "of intermediate condition," and the balance have "pinhole" or "hairline crack" failures. The report does not further define these conditional terms, other than to state that severe failures are those with loss of rod or assembly integrity, nor does the report indicate the basis upon which the failure distribution was estimated. DOE is apparently

using this information to develop cladding failure boundary conditions for TSPA-VA (Siegmann in DOE 1998).

Another EPRI study developed slightly different values based on experience for the year 1989 (Yang *et al.* 1991). For PWRs, the assembly failure level was 6.7% and the fuel rod failure level was 0.004%. For BWRs, the assembly failure level was 1.8% and the fuel rod failure level was 0.003%. Using these assembly failure levels, on average, a PWR waste package would contain 1.4 failed assemblies and a BWR waste package would contain 0.8 failed assemblies. Information on the number of failed assemblies is useful in estimating the probability that a failed waste package will contain failed fuel rods.

GE experience with Zircaloy-2 clad BWR fuel pins completing at least one operational cycle through August 1990 is summarized in Table 2.9 (Baily *et al.* 1991). Fretting failures are much less prevalent in BWRs than in PWRs. When fretting does occur, it is "generally characterized by a single smoothly abraded area and perforation, often accompanied by secondary hydride damage away from the primary defect" *(ibid.)*. Crud-induced localized corrosion (CILC) is the major cause of fuel rod failures in GE BWR fuel accounting for about 80% of all failures. CILC failures are specific to certain plants where copper is available from coolant system components such as condenser tubes. "CILC failures are generally characterized by regions of the cladding outer surface oxide spalling with pinhole cladding perforations, often accompanied by secondary hydride bulges and longitudinal splits" *(ibid.)*. Pellet-cladding interaction (PCI) is the source of about 14% of all GE fuel rod failures. "PCI failures are generally characterized by tight, longitudinal cracks in the cladding often accompanied by secondary hydride damage in a region away from the primary defect. The secondary hydride damage may appear as hydride bulges and accompanying cracks in the cladding, or as hydrided and fractured areas in or near the upper and lower end plug welds." If a defective fuel rod is operated for an extended period, the fuel can oxidize and swell causing the crack to widen and propagate axially.

Peehs and Fleisch 1986 quote an operational defect rate for fuel rods in FRG as 2 to 5 in $10^5$ which is equivalent to a 99.995% reliability.

Table 2.9. GE 8X8 Fuel Performance as of August 1990

| | All 8X8 | Zr Liner 8X8 |
|---|---|---|
| Date introduced to mfg. | 1973 | 1983 |
| Cumulative rods loaded | 3,900,000 | 1,250,000 |
| Reliability inc. CILC failures[a] | 99.981% | 99.988% |
| Reliability exc. CILC failures | 99.996 | 99.998 |
| Fretting failures | <15 | 2 |

a - CILC: Crud-Induced Localized Corrosion

The International Atomic Energy Agency (IAEA) stated in 1982, based on PWR experience, that a failure level of 0.01 to 0.02% was typical, while for BWRs a failure level of 0.02 to 0.07% "can be maintained" (IAEA 1982). The IAEA observed that the nature of in-reactor defects was dependent on the type of cladding. "SS-clad fuel develops long axial cracks exposing the fuel to water; experience has shown that the fuel remains inert and that no measurable radioactivity is released except during handling of the assemblies. Zircaloy-clad fuel usually has pinhole defects, sometimes small cracks or perforations and unfrequently a rupture of the rod; no further extensions of the defects were noticeable during subsequent storage of the spent fuel."

Data on the historical performance of fuel rods is summarized in Table 2.10 based on information presented in the preceding paragraphs. From this information, the expected value of the initial failure level is <0.1%. As noted previously, these initial failures are of no consequence until the integrity of the waste packages in which they reside is breached so that air and water can contact the fuel cladding.

Table 2.10 Summary of Fuel Rod Failure Levels

| Fuel | Period | Failure Level (%) | Reference |
|---|---|---|---|
| GE 8x8 | 1973-1990 | 0.019 | Baily et al. 1991 |
| GE Zr liner 8x8 | 1983-1990 | 0.012 | Baily et al. 1991 |
| All PWR | Through 1985 | 0.04 | DOE 1987 |
| All BWR | Through 1985 | 0.36 | DOE 1987 |
| BWR + PWR | Through 1985 | 0.12 | DOE 1987 |
| All PWR | 1989 | 0.004 | Yang et al. 1991 |
| All BWR | 1989 | 0.003 | Yang et al. 1991 |
| All | 1970-1981 | 0.04 to 0.08 | EPRI 1997 |
| | 1981-1985 | 0.02 to 0.07 | EPRI 1997 |
| | After 1985 | 0.006 to 0.03 | EPRI 1997 |
| All BWR | 1986 | 0.07 | SNL 1992 |
| All PWR | 1986 | 0.014 | SNL 1992 |

### 2.2.1 In-Service Failures of Stainless Steel Fuel Rods

As shown in Table 2.11, McCoy 1998 identified 2,179 stainless steel fuel assemblies for disposal. The number of rods in each assembly was obtained from the Energy Information Agency (EIA) data assembly code descriptors (*e.g.*, XHN15B is a 15 x15 array manufactured by B&W for Haddam Neck) and the total number of stainless steel fuel rods was then calculated with the results presented in Table 2.11. Total fuel rod positions per assembly were adjusted for control rods guide tubes in PWR assemblies and water rods and tie rods for BWR assemblies based on information contained in SAND90-2046 (Sanders et al. 1992) and in EIA 1996. The cladding thickness in the XHN15B, XSO14W, and XHN15W assemblies is 0.0165 in (0.42 mm)(EIA 1996).

If one assumes that 397,048 stainless steel clad fuel rods were irradiated in commercial reactors as indicated in Table 2.11, then the fraction of the total fuel rods which are stainless steel clad is 1.35% based on the commercial fuel limit of 63,000 MTU and assuming that all stainless steel rods are included in the repository inventory. The difference between this value and the DOE estimate of 1.15%, discussed in Section 5, may be due to slightly different assumptions about the total fuel rod inventory.

Table 2.11. Summary of Stainless Steel Fuel Rods Available for Disposal

| EIA Assembly Code | Cladding Material | Reactor | Fuel Manufacturer | Assemblies Discharged | Rods per Assembly | Active Rods per Assembly | Total Rods |
|---|---|---|---|---|---|---|---|
| XHN15B | 304 S.S. | Haddam Neck | B&W | 633[a] | 225 | 204 | 129,132 |
| XHN15HS (XHN15IS) | 304 S.S. | Haddam Neck | Gulf | 1 | 225 | 204 | 204 |
| XHN15MS | 304 S.S. | Haddam Neck | Numec | 2 | 225 | 204 | 408 |
| XHN15W | 304 S.S. | Haddam Neck | West. | 309 | 225 | 204 | 63,036 |
| XIP14W | 304 S.S. | Indian Point 1 | West. | 160 | 196 | 180 | 28,800 |
| XLC10L | 348H S.S. | LaCrosse | Allis Chalmers | 155 | 100 | 100 | 15,500 |
| XLC10A | 348H S.S. | LaCrosse | ANF | 178 | 100 | 96 | 17,088 |
| XSO14W | 304 S.S. | San Onofre 1 | West. | 665 | 196 | 180 | 119,700 |
| XYR18W | 348H S.S. | Yankee Rowe | West. | 76[b] | 324 | 305 | 23,180 |
| TOTAL | | | | 2179 | | | 397,048 |

a - Bailey et al., 1992 indicates that 678 stainless steel-clad assemblies had been discharged as of December 31, 1989 and that no S.S. assemblies remained in the reactor core.
b - According to EIA 1996 most of these assemblies were reprocessed at West Valley; this is the balance.

There is some confusion in the literature about the number of B&W stainless steel clad fuel assemblies used at Haddam Neck. EIA 1996 quotes 576 as the number. However, McCoy 1998 determined, based on more recent information obtained from the staff at the reactor site, that 633 is the correct number. Bailey et al. 1992 stated that 678 stainless-clad B&W assemblies had been discharged as of December 31, 1989 (682 minus 4 Zircaloy-clad lead assemblies) and that no assemblies remained in the core. At that time, Haddam Neck was temporarily shut down for debris cleaning. In addition, Pasupathi and Klingensmith 1981 state that batch 7 fuel for Haddam Neck was manufactured by Gulf United Nuclear Fuels, but no evidence of this is provided in EIA 1996. For purposes of this report, we have used the data obtained by McCoy as being the most recent and provided directly by the reactor staff.

Some ambiguity also exists in EIA 1996 about Yankee Rowe stainless steel-clad assemblies. Table B4 of that report states that most of the XYR18W fuel assemblies had been reprocessed at West Valley while Table B8 states that 76 of these assemblies were discharged from the reactor between 1972 and 1975. It is not clear from the report whether the 76 assemblies were those remaining after reprocessing or whether some portion of the 76 had been reprocessed. The EIA confirmed on June 23, 1998 that there were 76 stainless-steel clad assemblies currently in the storage pool at Yankee Rowe.

The discharge schedule for all these stainless steel assemblies is included in Table 2.12. About 40% of these assemblies were discharged at least 20 years ago.

No spent fuel at Yankee Rowe, San Onofre 1, Indian Point 1, or LaCrosse is stored in canisters (EIA 1996). This indicates that the stainless-steel clad fuel has not deteriorated to the extent that additional containment is required. At Haddam Neck, four canisters containing fuel and one canister containing fuel and non-fuel components are stored in the pool (EIA 1996).

Table 2.12. Discharge Dates Of Spent Stainless Steel Fuel Assemblies (EIA 1996)

| Year | XHN15W | XHN15B | XIP14W | XSO14W | XYR18W | XLC10L | XLC10A |
|---|---|---|---|---|---|---|---|
| 1970/71 | 103 | | | 97 | | | |
| 1972/73 | 102 | 2[a] | 40 | 57 | 36 | 56 | |
| 1974/75 | 48 | 1[b] | 120 | 53 | 40 | 25 | |
| 1976/77 | 56 | 50 | | 53 | | 32 | |
| 1978/79 | | 49 | | 52 | | 28 | |
| 1980/81 | | 106 | | 52 | | 12 | |
| 1982/83 | | 49 | | | | 2 | 50 |
| 1984/85 | | 53 | | 52 | | | 28 |
| 1986/87 | | 109 | | | | | 100 |
| 1988/89 | | 54 | | 52 | | | |
| 1990/91 | | 53 | | 40 | | | |
| 1992/93 | | 53 | | 157 | | | |
| 1994/95 | | 57[c] | | | | | |
| Total | 309 | 636 | 160 | 665 | 76 | 155 | 178 |

a - XHN15MS
b - XHN15HS
c - Assumed in order to reconcile McCoy 1998 and EIA 1996.

To gather additional insight into the condition of stainless steel fuel assemblies in storage, telephone inquiries were made to various reactors where the spent stainless steel clad assemblies are stored. R. Willams, plant manager at Yankee Rowe, said, based on superficial visual inspection and monitoring of pool chemistry, there is no evidence of any significant deterioration of the 76 assemblies which have been in storage since 1975 (Williams 1998). The fuel in the pool has been reshuffled from time to time to meet operational needs and receives limited inspection during such operations. Although this fuel had been discharged prior to Williams' arrival at the site in the late 1970's, he was not aware, based on heresay, that there were any defects in the assemblies when they were discharged.

At the La Crosse boiling water reactor, which is now in SAFSTOR, Dr. Seymour Rafferty provided information on the status of spent stainless fuel there (Rafferty 1998). No operational failures occurred in the XLC10A assemblies built by ANF (see Table 2.11). However, a number of stress corrosion failures occurred in the XLC10L assemblies manufactured by Allis Chalmers. According to Rafferty, flaws were detected in 54 assemblies by sipping tests, and visual evidence of circumferential cracking was observed in an additional 31 assemblies with one to two rods containing 4 to 5 cracks per assembly. Eighteen assemblies had gross failures including severe cracking in three to four rods per assembly. In five of these assemblies, sections of the fuel rods were missing. The issue of fuel assemblies with lost fuel is also described in La Crosse 1979. This reference notes that 22 defective fuel rods or 0.3% of the total fuel rods in the core were identified at the end of cycle 5. In particular, La Crosse 1979 describes failures in fuel assemblies 2-33 and 2-13. In assembly 2-33, fuel was observed to fall from one rod ($P_{39}$) as the assembly was being moved to the storage well. Approximately 8.5 in of the fuel column was lost. Another rod ($P_{29}$) in the same assembly appeared to have a circumferential crack. In fuel assembly 2-13, significant cladding degradation was noted in rods $P_{07}$ and $P_{09}$ over a length of about seven inches. About 3.5 inches of fuel was lost from rod $P_{07}$.

In commenting on why the ANF fuel was superior, Rafferty noted that a tighter chemistry specification with low Si and low P was used, the cladding was about 2 mils thicker, fuel pellets were shorter and the pellet-clad gap was larger. Rafferty said that there was no obvious evidence of fuel deterioration during storage although this was not an issue that is specifically addressed. He noted that eight fuel assemblies had been shipped to Morris IL and back during a pool reshuffling. No problems were encountered. .

At Indian Point, Donald Maffei, the Unit 1 Project Manager, said that they were currently doing work in the fuel storage pool and had looked at some of the assemblies with an underwater camera. No degradation was apparent although the fuel was not moved to provide a more complete examination (Maffei 1998). It should be noted that the Indian Point 1 fuel assemblies use a perforated can so that only a limited amount of cladding surface is visible through the perforations, which are about 0.5 in. dia. Maffei said that the fuel is currently stored in baskets, each containing four fuel bundles. The reactor staff is considering moving the fuel from the current concrete lined pool to a stainless steel lined pool. If that is done, an

opportunity will exist to inspect the fuel more closely. Maffei suggested that Charles Limoges be contacted for information on the condition of the fuel at the time it was discharged from the reactor. Limoges advised that there were no known leakers although there was some evidence of elevated coolant activity levels when the fuel was discharged (Limoges 1998). No sipping tests were done to confirm the presence or absence of leaks.

According to Paul Myers of Southern California Edison Company, some failures were experienced towards the end of reactor life at San Onofre #1 (Myers 1998). When the reactor was shut down in 1992, some of the fuel assemblies had been in the core for about 10 years. This unusual situation apparently resulted from the fact the reactor was off-line for a considerable period due to steam generator problems. The maximum number of failed fuel rods based on coolant activity levels was estimated to be 6 to 10. Myers believed the number could be smaller if the individual defects were large. There has been no evidence of additional deterioration since discharge although no special efforts have been devoted to examining the discharged stainless steel fuel assemblies.

A significant source of failed stainless steel rods is the Haddam Neck (Connecticut Yankee) reactor, where the first problem occurred when using batch 8 fuel. This fuel batch was irradiated in reactor cycles 6, 7, and 8. Prior to the end of cycle 7 *(i.e.*, for the period 1969-78) the fuel was "essentially" free of failures (Pasupathi and Klingensmith 1981) although cracks were observed on the outer surface of some batch 7 fuel. Based on information in Table 1 of that report (*ibid.*), it can be deduced that there were essentially no failures in assemblies designated XHN15W, XHN15MS, XHN15HS (312 assemblies). In fact, the report documents the total absence of failures associated with Type 304 S.S. cladding in U.S. commercial power reactors prior to the problem with the batch 8 fuel at Haddam Neck. This conclusion is supported by Graves 1979 who stated that no failures had occurred prior to the end of cycle 7.

At the end of reactor cycle 8 on January 28, 1979, 36 of 48 batch 8 assemblies showed leaks when tested in a wet sipping system, but six assemblies with batch 7 fuel and five assemblies

batch 9 fuel were sound (Graves 1979)[5]. Based on iodine isotope concentrations it was estimated that 60 fuel rods were leaking at the end of Cycle 8 (Graves 1979). This value was subsequently reported to be about 150 rods (Goncarovs 1991). Visual examination of 24 of the batch 8 assemblies with underwater television equipment detected four assemblies with visible axial cracks of varying lengths and widths[6]. Three of these assemblies contained two failed rods each while the fourth contained eight failed rods (assembly HO7). All four assemblies were known to leak based on the sipping tests.

To understand the cause of these failures, a fuel assembly from batch 8 (HO7) as well as one from batch 7 (assembly G11, as a problem-free control) were taken to a hot cell for detailed examination. The following factors were identified as contributing to the batch 8 failures:

- High localized cladding stresses resulting from fuel pellet chips wedged in the fuel-clad gap
- Low propensity for in-reactor fuel densification of batch 8 fuel
- Power change maneuver near the end of cycle 7 (2nd cycle for batch 8 rods)

The diameter increase in one of the failed rods at a crack location was about 0.015 in. and the axial crack was about 4 in long. A photomicrograph suggests that the crack was actually about 0.032 in wide.

Another major failure mechanism at Haddam Neck was debris induced fretting which occurred during cycle 15 (Bailey *et al.* 1992., p. 4.9). Of 32,028 rods manufactured by B&W that were discharged from this reactor in 1989 at the end of cycle 15, a total of 450 (1.4%) was leaking[7]. In contrast, during 1988, only seven leaking stainless steel fuel rods were reported by B&W (Bailey and Wu 1990). Reliability was at least as good in prior years as it was in

[5] Some (unquantified) failures were subsequently detected in batch 9 fuel at the end of cycle 9 (Pasupathi and Kligensmith 1981).

[6] Visual examination is limited to the outer fuel rods which constitute about 25% of the total rods in an assembly (Graves 1979).

[7] Goncarovs 1991 quotes a value of 456 instead of 450.

1988 (Painter *et al.* 1994, Table A-10 reproduced as Table 2.2 here). Elsewhere, Goncarovs reported that two rods with known cladding defects were reloaded at the start of cycle 15 (March 1988) and, based on I-131 coolant activity, the Haddam Neck staff estimated that four additional failures occurred during Cycle 15 startup (Goncarovs 1991). The four failures were initially attributed to pellet/clad interaction but subsequently reclassified as being the result of debris-induced fretting *(ibid.)* .

The debris-induced failures were caused by small metal chips, generated when the core shield was replaced, being trapped under the bottom spacer grid. The chips cut through the cladding near the bottom fuel plug much like a metal cutting tool would do. B&W replaced all the defective rods as well as about an equal number of rods that were damaged but not leaking (Mitchell 1998). While the intention was to remove all known damaged rods including those which had not developed leaks during cycle 15, a unknown number of damaged but not failed rods were introduced into the reconstituted assemblies used in cycle 16 (Goncarovs 1991). Based on coolant activity levels, an additional 15-20 debris induced fretting failures occurred in cycle 16 *(ibid.)*. The fuel manufacturer is unaware of any subsequent deterioration of the Haddam Neck assemblies during storage (Mitchell 1998).

Table 2.13 summarizes the available information of failures in stainless steel clad assemblies.

Additional details on failures at Haddam Neck are included in Table 2.14.

Based on Table 2.14, the maximum number of failed stainless steel fuel rods at Haddam Neck is about 650 (650/129,132=0.005%) and the maximum number of failed fuel assemblies is about 230 (230/633=36%). A bounding estimate of total stainless steel cladding failures based on the worst year reported for fuel rods manufactured by B&W would be 5559 fuel rods (397,048 x 1.4%). A more realistic estimate is 840 failed fuel rods based on the information included in Tables 2.13 and 2.14.

Table 2.13. Failures in Stainless Steel Clad Fuel Assemblies

| EIA Assembly Code | Assemblies Discharged | Active Rods per Assembly | Total Rods | Failed Assemblies | Failed Rods per Assembly | Defect Size |
|---|---|---|---|---|---|---|
| XHN15B | 633[a] | 204 | 129,132 | 36 of 48 (batch 8 fuel), 0 of 11 (batch 7 plus 9 fuel); 230 (max.) with debris induced fretting (see Table 2.14) | 2 to 8[a] | max. crack about 4 in x 0.032 in |
| XHN15HS (=XHN15IS) | 1 | 204 | 204 | 0 | 0 | 0 |
| XHN15MS | 2 | 204 | 408 | 0 | 0 | 0 |
| XHN15W | 309 | 204 | 63,036 | 0 | 0 | 0 |
| XIP14W | 160 | 180 | 28,800 | 0 | 0 | 0 |
| XLC10L | 155 | 100 | 15,500 | 103 | max. of 1to 2 in assemblies w/ visible cracks; 3-4 in assemblies w/ gross failures | 54 assemblies with sipping leaks, 31 with visual failures, 18 with gross cracks inc. 5 with lost fuel |
| XLC10A | 178 | 96 | 17,088 | 0 | 0 | 0 |
| XSO14W | 665 | 180 | 119,700 | 6-10 max.[b] | 6-10 max. | |
| XYR18W | 76[b] | 305 | 23,180 | 0 | 0 | 0 |
| TOTAL | 2179 | | 397,048 | | | |

a - based on four Batch 8 assemblies only
b - assuming one failed rod per assembly

## Table 2.14. Failures in Stainless Steel Clad Fuel Elements at Haddam Neck

| Cycle/end date | Fuel Batch | Fuel Mfg. | Failed Assemblies | Failed Rods | Comments/References |
|---|---|---|---|---|---|
| 1 | | West. | 0 | 0 | |
| 2 | | West. | 0 | 0 | |
| 3 | | West. | 0 | 0 | |
| 4 | | West. | 0 | 0 | |
| 5 (mid-1975) | | West. | 0 | 0 | |
| 6 (mid-1976 | 8 + ? | | 0 | 0 | |
| 7 (ca. 1/78) | 8 + ? | | ? | ? | Increased coolant activity at end of cycle |
| 8 (1/29/79) | 8 | BNFL/B&W | 36 of 48 | 2 to 8 per assembly, [a] 60/150 rods total based on I | PCI causing stress corrosion cracking NP-2119 |
| | 7 | GUNF | 0 of 6 | | |
| | 9 | B&W | 0 of 5 | | |
| 9 | 9 | B&W | some | some | NP-2119 |
| ???? | | | | | |
| 12/31/83 | | B&W | 0 | 0 | NUREG/CR-3950, v. 1 |
| 12/31/.84 | | B&W | 0 | 0 | NUREG/CR-3950, v. 2 |
| 12/31/85 | | B&W | 1 | 1 | NUREG/CR-3950, v. 3 |
| 12/31/86 | | B&W | 1 | 1 | NUREG/CR-3950, v. 4 |
| 12/31/87 | | B&W | ? (7 max.) | 7 | NUREG/CR-3950, v. 5 |
| 12/31/88 | | B&W | ? (7 max.) | 7 | NUREG/CR-3950, v. 6 |
| Cycle 15 9/2/89 | | B&W | b (157 max.) | 456 | debris induced fretting, NUREG/CR-3950, v. 7 Goncarovs 1991 |
| Cycle 16 | | B&W | ? (15-20 max.) | 15-20 | debris induced fretting, Goncarovs 1991 |
| ????[c] | | | | | |

a - Based on visual examination of 24 assemblies with batch 8 pellets using underwater television camera. Four assemblies showed visible cracks including three assemblies with two cracked rods each and one assembly with eight cracked rods.
b - 157 assemblies were inspected and 456 failed rods were detected, but number of failed assemblies not cited.
c - B&W stopped providing information for NUREG/CR-3950 after 1989.
???? - History not available during this period.

## 2.3 IN-STORAGE FAILURES

### 2.3.1 Pool Storage

In 1982, the IAEA conducted an extensive worldwide survey of operator experience with storage of spent fuel in pools (IAEA 1982). The survey included 115 pools, some of which were used to store fuel assemblies other than discharged assemblies from commercial LWRs. The pool water is typically at approximately 40°C. The fuel center temperature in spent fuel elements is 100°C, while the inside diameter cladding temperature is 30-60°C during pool storage after removal from the reactor. The external pressure in the pool is approximately 0.2 MPa.

To quote the study, "There is a substantial basis to conclude from pool operator observations and from specific fuel examinations that Zircaloy-clad water reactor spent fuel has not degraded appreciably in up to 20 years; SS-clad water reactor fuel has been examined after 5 years of storage and has resided in pools for up to about12 years without evidence of pool-induced degradation. Most pools store defective fuel assemblies on the same basis as intact assemblies. IAEA reported no further degradation of defective rods. Obviously, fission gases and other volatile or readily-leachable fission products would be removed from the defective rods either during operation or pool storage. At temperatures of 95°C, air exposure of irradiated $UO_2$ should not produce $U_3O_8$ with attendant volume increases and clad degradation for times of less than 2,000 years (Einziger et al., 1992)."

Pool storage is required in the U.S. for a minimum of five years (see Appendix E to 10 CFR 961). Under these conditions little degradation of intact fuel rods is expected.

It was reported in SNL 1992 that no breaches had occurred during wet storage as of December 31, 1986.

Discussions with operators of reactors which had employed stainless steel fuel assemblies did not reveal any evidence of in-pool deterioration (see Section 2.2.1 above).

### 2.3.2 Dry Storage

Authors of SNL 1992 reported that the dry storage failure level for PWR rods was 0.03% but that no data were available for BWR rods. BWR failure levels in dry storage are expected to be less than or equal to those for PWR rods because of lower fill gas pressures and thicker cladding.

McKinnon and Doherty 1997 summarized results of dry storage tests with spent fuel casks of various designs. Two leaking rods (one BWR and one PWR) were detected during cask performance testing with unconsolidated fuel. The leaking BWR rod was in a cask (REA-2023) containing 52 BWR assemblies of a General Electric 7x7 design. The fuel in the cask had been discharged from Nebraska Power's Cooper reactor in 1981-82 after a burnup of 24-28 GWd/MTU. Peak cladding temperatures were estimated to range from 110 to 227°C depending on the test configuration. Gas sampling was conducted over a 5½ month period. The leaking PWR rod was detected in cask TN-24P loaded with 24 Westinghouse 15x15 assemblies. The fuel was discharged from VEPCO's Surry reactors in 1981 after a burnup of 29-32 GWd/MTU. During storage tests, the peak cladding temperatures were estimated to range from 215 to 290°C. Gas sampling of the cask was conducted over a period of about 17 months. Testing of fuel rods after consolidation indicated that about ten rods had developed leaks probably associated with the additional handling. Details are presented in Table 2.15. It is noteworthy that the test of the CASTOR-V/21 cask has continued for about 11 years without apparent fuel rod failures.

Table 2.15 Summary of Fuel Rod Failures During Cask Dry Storage Tests

| Cask | Assemblies | Assembly Design | Consolidated? | Test Duration (months) | | Cladding Temperature (°C)[a] | Burnup (GWd/MTU) | Fuel Rod Failures |
|---|---|---|---|---|---|---|---|---|
| | | | | Active | Post | | | |
| REA-2023 | 52 | GE BWR 7x7 | No | 5½ | 0 | 110-227 | 24-28 | 1 |
| TN-24P | 24 | W PWR 15x15 | No | ½ | 16 | 215-290 | 29-32 | 1 |
| TN-24P | 24 Canisters[b] | -- | Yes | 2 | 5½ | 205-293 | 24-35 | 12 |
| CASTOR V/21 | 21 | W PWR 15x15 | No | ½ | 130 | 352-424 | 24-25 | 0 |
| MC-10 | 24 | W PWR 15x15 | No | 1 | 20 | 139-217 | 24-35 | 0 |
| VSC-17 | 17 Canisters[b] | -- | Yes | 2 | 69 | 321-397 | 26-35 | 0 |

a -during active portion of test only
b - 410 rods per canister

## 2.4 HANDLING FAILURES

### 2.4.1 Consolidation Failures

SNL indicated that the level of consolidation failures for PWR fuel rods was <0.005% and no breaches of BWR rods had been reported as of December 31, 1986 (SNL 1992). The indicated failure level was based on one fuel rod breach during rod pulling while performing wet consolidation at the West Valley Demonstration project. These failure levels are not representative of what might occur during production line rod consolidation.

Other information on consolidation failures is presented in Table 2.15. Based on information from the canistered fuel in TN-24P it appears that the SNL estimate may be too low. This table suggests that the failure rate could be about 0.1%. However, the point is moot since fuel rod consolidation is not commercially practiced in the US at the present time.

### 2.4.2 Other Handling Failures

A fuel handling failure level of 0.0003% was quoted by SNL for BWR rods but no handling breaches of PWR rods had been noted (SNL 1992). The BWR handling failure level was based on a 1982 incident in which some fuel rods broke in two places when two assemblies were mishandled. To develop the estimated failure level, SNL assumed that 27,446 fuel assemblies had been discharged from BWRs at the end of 1986 and that each damaged assembly contained two broken rods. Fuel assemblies built prior to 1979 were assumed to be 7 x 7 arrays of fuel rods while those built after 1979 were assumed to be 8 x 8 arrays.

Based on its 1982 survey, the IAEA reported that spent fuel pool handling mechanisms had malfunctioned but the resulting events had minimal impact on the spent fuel. About 65% of the operators reported no drops during handling, 12% reported one drop and 23% reported more than one drop (IAEA 1982). "A total of about 30 water reactor fuel assemblies were dropped without serious consequences such as contamination or fission product release."

A summary of reported handling incidents in the U.S. from 1978 through 1989 is presented in Table 2.16 (NRC 1990). Unfortunately, Table 2.16 does not indicate whether the incidents resulted in fuel rod damage; however, some information in presented for 1987-89 in the text of NRC 1990. In the 1989 incident at Limerick-1, a fuel rod was dropped during reconstitution activities. There was no release of radioactivity from the rod and inspection showed that it was undamaged. The rod was returned to its proper location in the fuel assembly. In the 1987 Oyster Creek incident, several rods separated from a previously damaged BWR bundle during handling. While some spacer grid and end plug damage occurred, the fuel cladding appeared to be intact. In the 1988 Vogtle-1 incident, a power failure during refueling caused a bundle to be improperly inserted into the core. The bundle was removed to the fuel handling building where visual examination revealed no apparent damage. In the 1988 Palisades incident, a fuel bundle was stuck to the upper guide structure and inadvertently lifted with the guide structure. No physical damage was noted.

The Table 2.16 handling experience is based on approximately 123,100 fuel assemblies that were in or had completed operation in the U.S., including 78,700 BWR assemblies and 44,400 PWR assemblies. Assuming that the number of assemblies in operation was 36,000, then the

Table 2.16 Fuel Handling Events Involving Irradiated Fuel

| Year | Plant | Fuel Assembly Fell, Dropped, or Bumped | Fuel Rod Broken | Fuel Rod Damaged | Fuel Rod Dropped | Fuel Assembly Improperly Grappled | Fuel Assembly Inadvertently Lifted | Spacer Grids Damaged |
|---|---|---|---|---|---|---|---|---|
| 1989 | Limerick-1 | | | | X | | | |
| 1988 | Palisades<br>Vogtle-1 | <br>X | | | | | X | |
| 1987 | Oyster Creek<br>North Anna | <br>[b] | | <br>X[a] | | | | <br>X[a] |
| 1986 | Diablo Canyon-1<br>Haddam Neck | X<br>X[c] | | | | | <br>X[c] | |
| 1985 | Cooper<br>Fitzpatrick<br>Summer-1 | | | | | X | <br>X | <br><br>X |
| 1984 | | | | | | | | |
| 1983 | Beaver Valley-1<br>Turkey Point-4 | X[d]<br>X,X[e] | | | | | | |
| 1982 | Browns Ferry-2<br>Hatch-1 | | X<br>X | | | | | |
| 1981 | Cook-1<br>Millstone-1<br>Prairie Island-1 | X<br>X<br>X | | | | | | |
| 1980 | | | | | | | | |
| 1979 | | | | | | | | |
| 1978 | Dresden-1 | X | | | | | | |

[a] Upper tie plate and the eight tie rods separated from the remainder of the previously damaged spent fuel bundle during movement in the spent fuel pool.

[b] Fuel assembly undamaged, but there was potential for damage (assembly hooked to crane but still in storage rack when crane moved laterally.)

[c] One fuel assembly was lifted and dropped.

[d] A rod cluster control assembly was also damaged.

[e] Two events occurred at this plant.

number discharged was 87,100 and the total reported incidents involved 21 assemblies, an incidence level of 0.02% is indicated. As discussed above, several of these incidents did not result in fuel rod damage. Based on this more recent information, it appears that the 0.0003%

failure level for handling cited above is conservative since more than twice as many assemblies had been discharged through the end of 1988 with no additional rod breaches recorded.

### 2.4.3 Transportation Failures

A truck carrying 14 unirradiated fuel assemblies for Callaway overturned in 1987. No details were provided (NRC 1990).

A survey conducted by PNL (Bailey and Langstaff 1980) revealed two cases where damage to spent stainless steel fuel assemblies had occurred (one domestic and one non-U.S.). The results are obfuscated by the facts that, in one instance, the fuel bundles initially contained failed rods and, in the other case, the fuel was from a lot which had encountered service problems. The survey concluded that "Little is known about damage to fuel during shipments; however, such damage, if any, is minor."

# 3.0 DISPOSAL FAILURES

Possible failure mechanisms in fuel rods after the spent fuel has been placed in the inerted waste package include (Pescatore et al. 1990, Blackburn et al. 1978, Rothman 1984):

- Creep (stress) rupture
- Mechanical overload
- Fuel side stress corrosion cracking (FSSCC)
- Rapid fracture of flawed cladding
- Delayed hydride cracking (DHC) and fatigue crack propagation
- Internal hydriding
- Pellet-cladding interaction (PCI)
- Oxidation

Of the items listed, the NRC identified only creep rupture, DHC, and FSSCC as important failure modes in the dry storage of spent fuel elements (Pescatore, et.al., 1990).

Some of these mechanisms are operative only if the waste package is eventually breached by a corrosion mechanism. For example, oxidation of the fuel cladding can occur as humid air enters the waste package interior. If the fuel pin had developed a defect at some time prior to breach of the waste package, the $UO_2$ can begin to oxidize, as well. This oxidation can ultimately cause the cladding to split. These and other post-disposal failure mechanisms are discussed in the following sections.

If an initial pinhole defect develops during storage, fission gases in the fuel rod plenum would be released into the waste package. Once the cladding is breached by a pinhole or small crack, the driving force for those mechanisms which rely on internal stress would be eliminated and the opportunity to release solid particulates would be negligible.

DOE has recently added, to the above list, mechanical failure of the fuel rods due to rock falls after the structural integrity of the waste packages has been destroyed and a generic corrosion mechanism (DOE 1998, McNeish in DOE 1998a).

Potential cladding failure mechanisms examined in this section include creep, fuel side stress corrosion cracking, delayed hydride cracking, mechanical rupture due to rock falls, cladding oxidation, fuel oxidation, and cladding corrosion. The first three mechanisms listed can occur

regardless of whether or not the integrity of the waste package has been breached while the remaining four mechanisms can occur only after the waste package has been breached. Mechanical shearing of the fuel pins due to rock falls can only occur after the waste package has been breached and its load-bearing capabilities have been destroyed.

## 3.1 OXIDATION OF CLADDING AND FUEL

Oxidation of the cladding can occur only after the wall of the waste package is breached; oxidation of the fuel can occur only after the package wall and the cladding have been breached.

The following equation for the oxidation of Zircaloy fuel rod cladding is proposed in Einziger 1994:

$$t_{ox} = 5.76 \times 10^{-10} \times (\%) \times \exp(27000/RT) \quad (1)$$

where $t_{ox}$ is the time in years to oxidize a specified % of the cladding thickness at an absolute temperature T (K) and R is the universal gas constant (1.9865 cal/mole•K). This equation is based on measurements in air and steam down to about 250°C with agreement between tests in the two gaseous media characterized as "good." Extension of this expression below 250°C is judged to be "probably a valid one" (Einziger 1994). Times to produce 25 and 100% cladding oxidation at various temperatures are summarized in Table 3.1. The plot of oxidation time (25%) versus absolute temperature in Figure 3.1 emphasizes the very strong temperature dependence of this process.

Above approximately 300°C, the cladding will have limited viability as a barrier in an oxidizing environment (i.e., a few hundred years). Assuming that a 25% percent thickness loss represents the end of useful cladding life, the cladding can be expected to effectively resist oxidation for 10,000 years at temperatures below 225°C.

Table 3.1. Times in Years to Produce Specified Percentages of Zircaloy Cladding Oxidation

| Temperature (°C) | Temperature (K) | 25% Oxidation | 100% Oxidation |
|---|---|---|---|
| 125 | 398 | 9,760,000 | 39,000,000 |
| 150 | 423 | 1,300,000 | 5,200,000 |
| 175 | 448 | 216,000 | 864,000 |
| 200 | 473 | 43,400 | 174,000 |
| 225 | 498 | 10,300 | 44,700 |
| 250 | 523 | 2,800 | 11,200 |
| 275 | 548 | 850 | 3,400 |
| 300 | 573 | 290 | 1,200 |

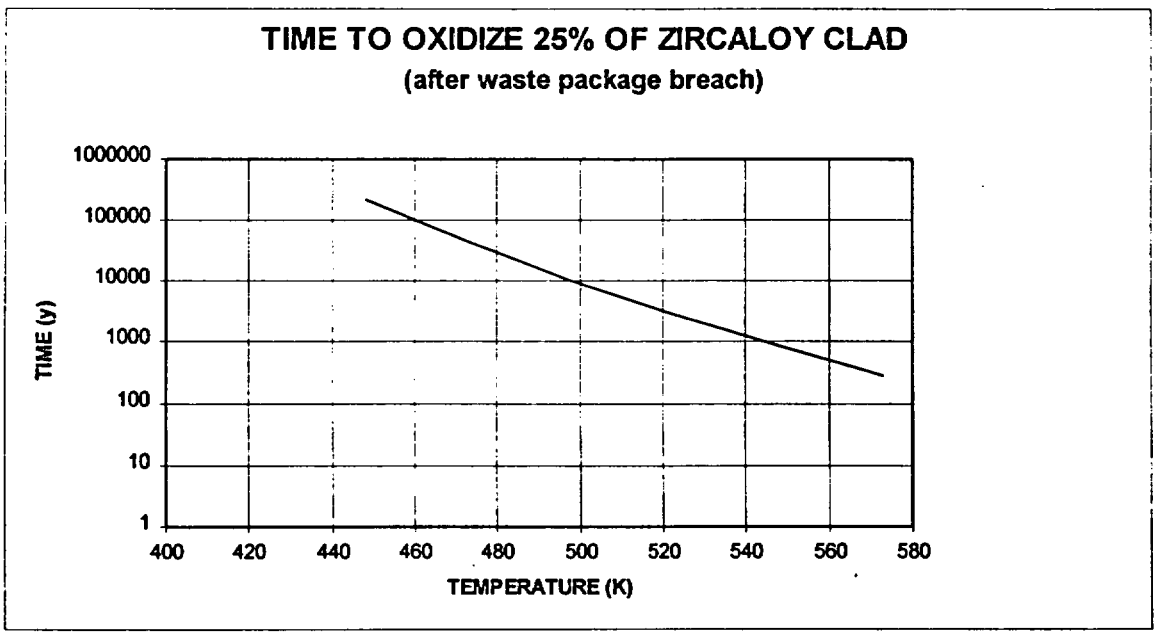


Figure 3.1 Temperature Dependence for Time (y) to Oxidize 25% of Zircaloy Cladding (After Waste Package Breach)

The work of several investigators on the oxidation of Zircaloy in air, steam and water was reviewed in Rothman 1984. The behavior of Zircaloy was similar in all three media. The depth of Zircaloy oxidation at 180°C for 10,000 years was estimated to range from 4 to 53 $\mu$m which would be equivalent to a maximum cladding thickness reduction of approximately 8%. Based on equation 1, the time to oxidize 8% of the cladding at 180°C would be approximately 49,000 years, indicating reasonable agreement between Einziger and the earlier work discussed by Rothman.

Peehs et al. 1986b proposed the following equation for the increase in oxide thickness ($\Delta$d) during steam oxidation of Zircaloy:

$$\Delta d = k_o \exp(-\frac{Q_c}{RT})\Delta t \qquad (2)$$

where $k_o$ is 1.7 mm/s, $Q_c$ is 118kJ/mol, and $\Delta t$ is the exposure time. The same equation is applicable to Zircaloy in air. This equation gives results that are in good agreement with equation 1 when a typical fuel rod cladding thickness (0.6 to 0.7 mm) is considered.

The oxidation degradation mechanism will not be initiated until after the waste package is breached by pitting corrosion. Once the waste package is breached, $UO_2$ can begin to oxidize if a cladding pinhole defect exists. Einziger 1994 proposed that, as the $UO_2$ oxidizes locally in the vicinity of the pinhole, the cladding may become stressed due to the formation of $U_3O_8$. This oxidation reaction results in about a 30% volume increase in the fuel. The time for this mechanism to initiate a crack in the fuel pin can be represented by the following equation:

$$t_i = 9.8 \times 10^{-21} \times \exp(47{,}400/RT) \qquad (3)$$

where $t_i$ is the time in years for crack initiation in a defective rod. This time is measured from the time of waste package breach or from the time which a pinhole defect forms in a fuel pin, whichever is longer.

After the crack has been initiated at a time defined by Equation (3), the time to split or unzip the cladding for a specified length can be represented by the equation:

$$t_s = 1.14 \times 10^{-9} \times d \times \exp(18{,}400/RT) \quad (4)$$

where $t_s$ is the time (years) to split the cladding a distance d (inches) in one direction. Values of $t_i$ and $t_s$ at various temperatures are presented in Table 3.2. As will be discussed in Section 4.2, the axial temperature profile shows about a factor of two difference between the maximum point and the ends of the fuel rods. This gradient can affect the time for the cladding to split. For example, from Table 3.2 the difference in $t_s$ at 250°C and 125°C is over 1400 years. If this temperature profile was integrated into equation 4, the time to split the cladding a distance of 39.4 cm (100 inches) would lie between the two extremes (i.e., between 6 years and 1,460 years, per Table 3.2).

Time-temperature plots for crack initiation and clad splitting are presented in Figures 3.2 and 3.3.

In earlier work described by Kohli et al.1985, a BWR fuel rod with several cladding splits developed during operation was subjected to oxidation at 598K for 2100 hours. The maximum defect length after the test was 10 cm. Equation 4 predicts that only 218 hours would be required to unzip the cladding for this distance.

Table 3.2. Times for Crack Initiation ($t_i$) and Crack Propagation ($t_s$) in Zircaloy Fuel Rods in Oxidizing Atmospheres

| Temperature (°C) | Temperature (K) | $t_i$ (years) | $t_s$ (years)[a] |
|---|---|---|---|
| 125 | 398 | 1,070,000 | 1,460 |
| 150 | 423 | 30,900 | 370 |
| 175 | 448 | 1,300 | 110 |
| 200 | 473 | 80 | 36 |
| 225 | 498 | 6 | 14 |
| 250 | 523 | <1 | 6 |
| 275 | 548 | <1 | 2 |
| 300 | 573 | <1 | 1 |

a - for d = 39.4 cm (100 inch), one direction splitting

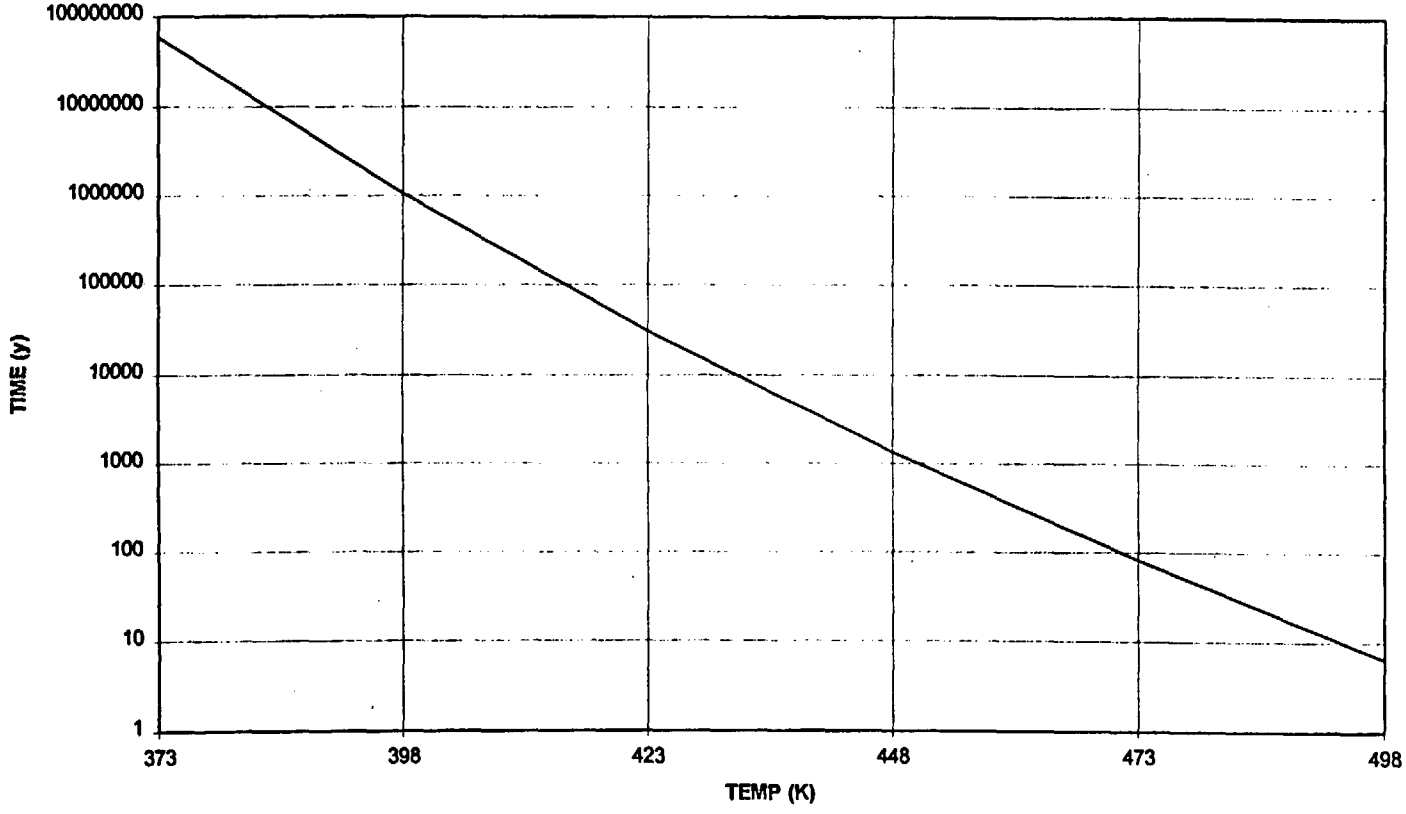


Figure 3.2. Time to Initiate Crack in Defective Zircaloy Fuel Rod (After Waste Package Breach.)

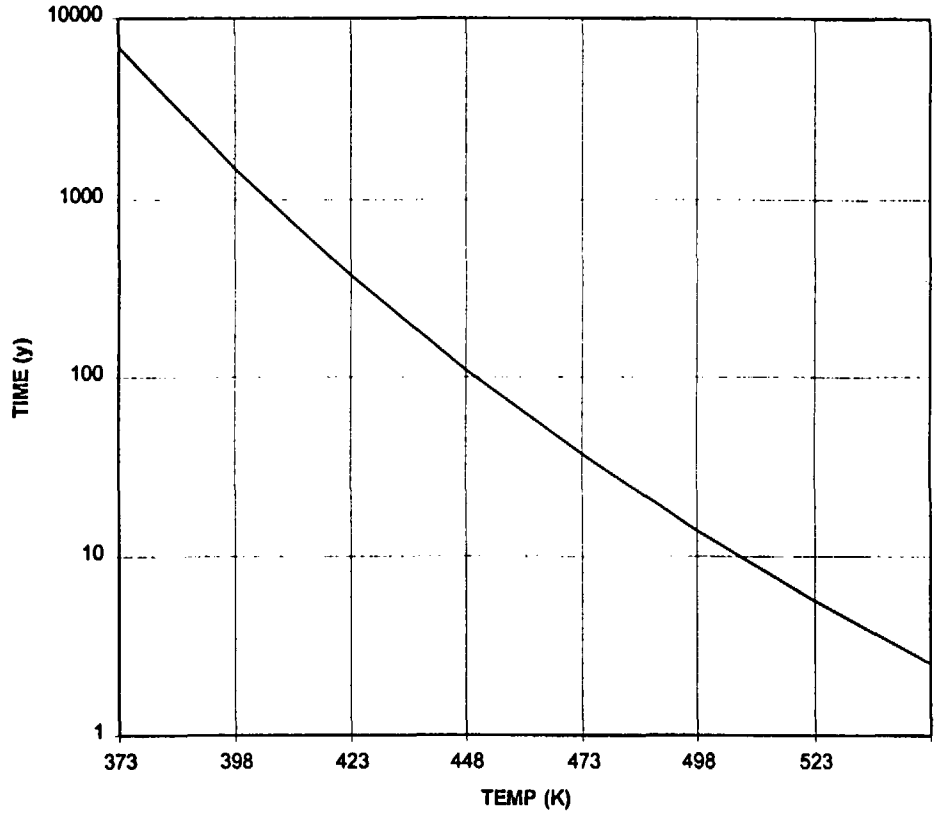


Figure 3.3. Time for Zircaloy Clad to Unzip after Crack Initiation.

During the low temperature oxidation of $UO_2$, $U_4O_9$ is initially produced which results in a slight volume decrease (Einziger 1997). The $U_4O_9$ is then converted to $U_3O_8$ with a 30% volume increase and attendant stressing of the cladding. Below 100°C, bulk oxidation of the fuel does not proceed past $U_4O_9$ (Eingziger 1994), so the mechanisms described in Equations (3) and (4) will not occur. Einziger states that, for irradiated $UO_2$, the oxidation rate for conversion to $U_4O_9$ is not altered for dew points up to 80°C.

## 3.2 FUEL SIDE STRESS CORROSION CRACKING (FSSCC)

The possibility that the fuel rod cladding can fail from stress corrosion cracking initiated on the inner cladding surface and catalyzed by fission product iodine has been examined by numerous investigators (Peehs et al.1986a, Peehs et al.1986b, Pescatore and Cowgill 1994). According to Pescatore and Cowgill 1994, FSSCC has occurred during reactor service but is not expected during spent fuel storage because the stress levels and free iodine contents are lower than during reactor operation. A stress intensity factor $K_{IC} > 3$ MPa•m$^{½}$ and an iodine surface concentration $> 1.5 \times 10^{-6}$ g/cm$^2$ are necessary for the process to occur.

Peehs et al. 1986a conducted tests with Zircaloy at temperatures of 100°C and 300°C and hoop stress levels of 62 and 95 MPa, respectively, for 2300 days with a maximum iodine inventory of $10 \times 10^{-5}$ g/cm$^2$. No cladding defects were noted; however, no comments were made as to the initial inner surface quality of the cladding. One-year tests were conducted at 440°C and hoop stresses of 75, 112, and 150 MPa with an iodine inventory of $1 \times 10^{5}$ g/cm$^2$. Again, no cladding defects resulted. On the basis of this experimental work, the authors concluded that iodine stress corrosion cracking "can be ruled out as a defect mechanism under dry inert storage conditions."

Additional studies of FSSCC have been reported in EPRI 1989. Figure 3.4 shows the envelope of conditions for FSSCC failures as a function of time, temperature, and pre-disposal crack depth. For a given crack depth failure is predicted to occur if the temperature is above the lines shown. For example, failure is predicted to occur in 10,000 years at temperatures above 300°C, if pre-disposal cracks exist which are greater than about 9% of the wall thickness, if the fission gas release is 50%, and if the $I_2$ concentrations are greater than $10^{-4}$ g/cm$^2$. As noted in the figure, 50% fission gas release is equated to a temperature-dependent stress $\sigma$(MPa)=0.155T(K).

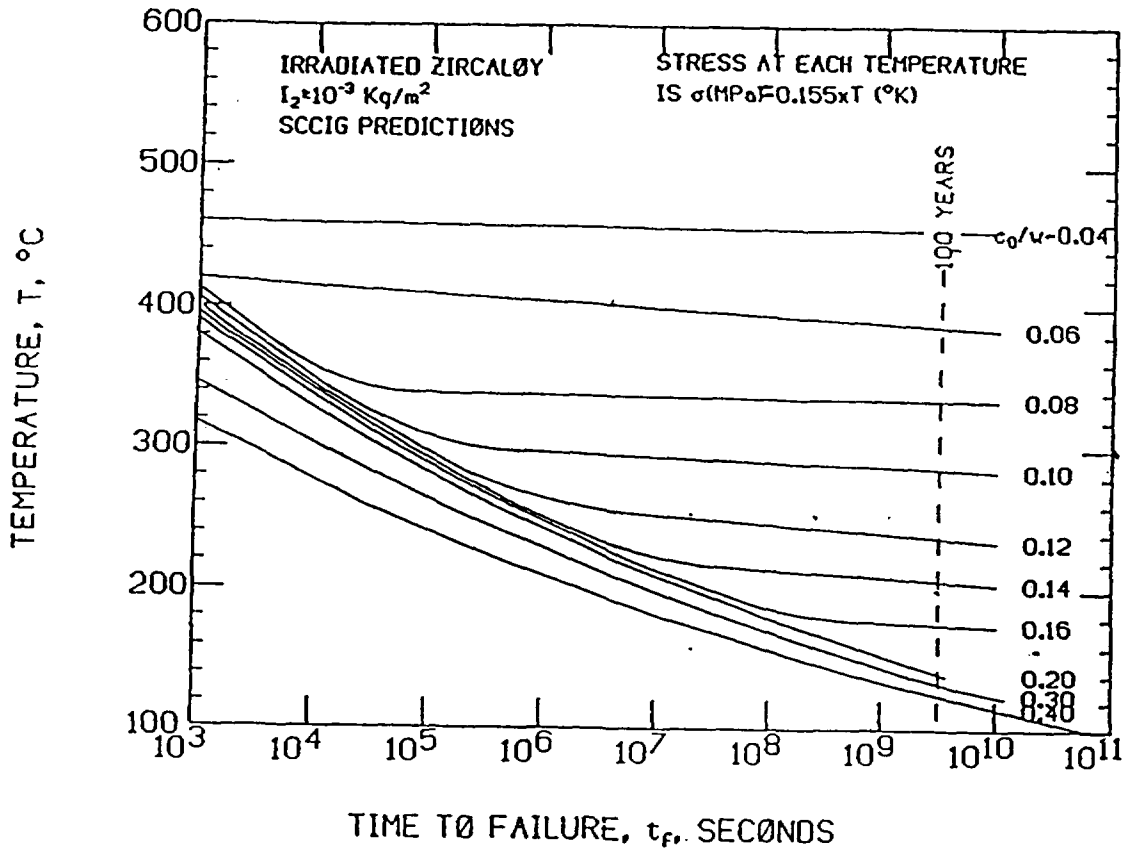


Figure 3.4. Predictions of allowable temperature versus time to failure for various initial crack depths in Zircaloy fuel cladding. Stresses and iodine concentrations correspond to "worst case" conditions (i.e. 50% fission gas release and iodine saturation level). $c_o$/w is the ratio of the crack depth to the tube wall thickness.

## 3.3 CREEP RUPTURE

Deformation of cladding can occur by thermal creep if the hoop stress caused by internal pressure in the fuel rod exceeds the creep strength at a given temperature. If sufficient deformation (strain) occurs, the cladding can rupture. Crack propagation ceases after the internal pressure is relieved. Potential for creep rupture is independent of the condition of the waste package.

### 3.3.1 Mechanistic Models

Mechanistic modeling of the creep rupture behavior of Zircaloy has been extensively described by Chin and his co-workers (Chin and Gilbert 1989, Kahn, Madsen and Gilbert 1985, Santanum, Ragahaven and Chin 1992). Chin et al. have mathematically described nine creep

deformation processes and five fracture mechanisms. The relevant equations are presented in Tables 3.3 and 3.4. Deformation and fracture maps developed by Chin are included as Figures 3.5 and 3.6. For perspective, the expected range of values of $T_m/T$ during disposal is 3.3 to 5.8 and for $\ln(\sigma/E)$ is -6.9 to -7.7 which is at the top of the cavity diffusion controlled region in Figure 3.6.

The so-called reduced forms of these equations were included in 1995 total system performance assessment (TSPA 1995, pages 5-20 through 5-22). These reduced-form equations contain several numerical errors which appeared in the source paper by Santanam et al. 1992. In addition, the equations are stated to calculate the rupture time in years but the units are actually seconds. These equations were presented but not used in the TSPA modeling.

The life fraction rule which relates the fraction of the creep rupture life expended at each cladding temperature increment can be used with the time-to-failure expressions in Table 3.4 to predict the percentage of the total cladding life consumed for any time-temperature profile. The life fraction rule is stated as follows:

$$\sum_{n=1}^{N} \frac{t_i}{\tau_i} \leq 1 \qquad (5)$$

where $t_i$ is the time under stress at any temperature [$T=f(t)$] and $\tau_i$ is the rupture life for the limiting fracture mechanism at that temperature. When the life fraction is unity, failure has occurred.

Table 3.3a Deformation Equations (Chin and Gilbert 1989)

| | |
|---|---|
| Theoretical strength | $\dot{\epsilon}_{TH} = \infty \;\; for \;\; \sigma > \sigma_{TH}$ , $where \;\; \sigma_{TH} \left( \frac{E\gamma_s}{\alpha_0} \right)^{1/2} \simeq \frac{E}{10}$ <br> $\dot{\epsilon}_{TH} = 0 \;\; for \;\; \sigma < \sigma_{TH}$ |
| Dislocation glide | $\dot{\epsilon}_{DG} = exp\left[ -(S-\sigma)\frac{ba}{kT} \right] \;\; for \;\; \sigma > \sigma_0$ <br> $\dot{\epsilon}_{DG} = 0 \;\; for \;\; \sigma < \sigma_0$ |
| High-temperature climb | $\dot{\epsilon}_{HT} = A_l D_{0l} exp\left( \frac{-Q_l}{RT} \right) \left( \frac{Eb}{kT} \right) \left( \frac{\sigma}{E} \right)^n$ |
| Low-temperature climb | $\dot{\epsilon}_{LT} = 50 A_l D_{0c} exp\left( \frac{-Q_c}{RT} \right) \left( \frac{Eb}{kT} \right) \left( \frac{\sigma}{E} \right)^{n+2}$ |
| Harper-Dorn climb | $\dot{\epsilon}_{HD} = A_{HD} D_{0l} exp\left( \frac{-Q_l}{RT} \right) \left( \frac{Eb}{kT} \right) \left( \frac{\sigma}{E} \right)$ |
| Grain boundary sliding (grain boundary diffusion) | $\dot{\epsilon}_{GBS} = A_{GBS} D_{0gb} exp\left( \frac{-Q_{gb}}{RT} \right) \left( \frac{Eb}{kT} \right) \left( \frac{b}{d} \right)^3 \left( \frac{\sigma}{E} \right)^2$ |
| Grain boundary sliding (lattice diffusion) | $\dot{\epsilon}_{GBL} = A_{GBL} D_{0l} exp\left( \frac{-Q_l}{RT} \right) \left( \frac{Eb}{kT} \right) \left( \frac{b}{d} \right)^2 \left( \frac{\sigma}{E} \right)^2$ |
| Nabarro-Herring creep | $\dot{\epsilon}_{NH} = A_{NH} D_{0l} exp\left( \frac{-Q_l}{RT} \right) \left( \frac{Eb}{kT} \right) \left( \frac{b}{d} \right)^2 \left( \frac{\sigma}{E} \right)$ |
| Coble creep | $\dot{\epsilon}_{CO} = A_{CO} D_{0gb} exp\left( \frac{-Q_{gb}}{RT} \right) \left( \frac{Eb}{kT} \right) \left( \frac{b}{d} \right)^3 \left( \frac{\sigma}{E} \right)$ |

Table 3.3b Symbols and Coefficient Values for Deformation Equations (Chin and Gilbert 1989)

| | | |
|---|---|---|
| $\dot{\epsilon}$ | = | strain rate ($s^{-1}$) |
| $\sigma$ | = | stress (MPa) |
| $T$ | = | temperature (K) |
| $R$ | = | gas content = 8.3144 J/mol·K |
| $k$ | = | Boltzmann's constant = $1.38 \times 10^{-29}$ MJ/K |
| $b$ | = | Burger's vector = $3.23 \times 10^{-10}$ m |
| $d$ | = | grain size = $5.0 \times 10^{-6}$ m |
| $T_m$ | = | melting temperature of Zircaloy = 2125 K |
| $E$ | = | Young's modulus $(11.81 - 14.59T/T_m) \times 10^4$ Mpa, $T_m/T > 4.06$ for $T < 865°C$ $(11.09 - 11.61T/T_m) \times 10^4$ Mpa, $T_m/T < 4.06$ |
| $n$ | = | stress exponent = 5 |
| $Q$ | = | activation energy (kJ/mol) |
| $Q_l$ | = | 250 kJ/mol |
| $Q_{gb}$ | = | 175 kJ/mol |
| $Q_c$ | = | 180 kJ/mol |
| $D_0$ | = | diffusivity coefficient ($m^2/s$) |
| $D_{0l}$ | = | $2.00 \times 10^{-4}$ $m^2/s$ |
| $D_{0gb}$ | = | $3.89 \times 10^{-6}$ $m^2/s$ |
| $D_{0c}$ | = | $2.26 \times 10^{-6}$ $m^2/s$ |
| $A$ | = | strain rate coefficient |
| $A_l$ | = | $7.4 \times 10^7$ |
| $A_{CO}$ | = | $5.362 \times 10^2$ |
| $A_{GBS}$ | = | $8.85 \times 10^6$ |
| $A_{NH}$ | = | 0.92 |
| $A_{GBL}$ | = | $5 \times 10^2$ |
| $S$ | = | $\frac{Eb}{3l}$ |
| $l$ | = | obstacle spacing (m) |
| $\alpha$ | = | activation area ($m^2$) |
| $\sigma_0$ | = | cutoff stress = $2.4 \times 10^{-2}E$ |

Table 3.4a Fracture Equations (Pescatore et al. 1990)

| | |
|---|---|
| Theoretical shear strength | $\sigma_{th} = \left( \frac{E\gamma_f}{\alpha_0} \right)^{1/2} \simeq \frac{E}{10}$ |
| Transgranular fracture | $t_f^{TG} = \left[ \epsilon_n + \left( \frac{1}{4.937} \right) \left( \frac{n}{n-1} \right) \ln \left( \frac{0.38}{f_v^{1/2}} - 1 \right) \right] \dot{\epsilon}^{-1}$ |
| Triple-point cracking | $t_f^{TP} = \frac{\gamma_f}{Ed\xi} \left( \frac{\sigma}{E} \right)^{-1} \dot{\epsilon}^{-1}$ |
| Cavitation-diffusional growth | $t_f^{CD} = \frac{2.525 \times 10^{-3} l^3}{\delta D_{0gb} b^2 exp \left( \frac{-Q_{gb}}{RT} \right)} \left( \frac{kT}{Eb} \right) \left( \frac{\sigma}{E} \right)^{-1}$ |
| Cavitation-power law growth | $t_f^{CP} = \left[ \frac{(1 - 0.78 P_0 l_0)}{4.87} \right] \dot{\epsilon}^{-1}$ |

Table 3.4b Symbols and Coefficient Values for Fracture Equations (Pescatore et al. 1990)

| | | |
|---|---|---|
| $t_f$ | = | time to fracture (s) |
| $\epsilon_n$ | = | hole nucleation strain = 0.08 |
| $f_v$ | = | volume fraction of intragranular inclusions = 0.025 |
| $P_0$ | = | average particle diameter = 10 nm (100Å) |
| $l_0$ | = | particle spacing along boundary = $2.0 \times 10^{-6}$ m |
| $\xi$ | = $\dot{\epsilon}_{GBS}$ | = contribution of grain boundary strain rate to total strain rate - 0.2 |
| $l$ | = | average cavity spacing = $2.6 \times 10^{-6}$ m (6/grain segment) |
| $\delta$ | = | width of grain boundary = $1.6 \times 10^{-8}$ m (50 Burger's vectors) |
| $\gamma_f$ | = | free surface energy created by fracture = 35 J/m$^2$ |
| $\alpha_0$ | = | lattice spacing (m) |
| $\sigma_{th}$ | = | maximum theoretical stress |

$D_{ogb}$ = Grain boundary self-diffusion coefficient ≡ $3.89 \times 10^{-6}$ m$^2$ /sec.
$Q_{gb}$ = Activation energy for grain boundary diffusion ≡ 175 k/J/mol
b = Burger's vector ≡ $3.23 \times 10^{-10}$m
E = Young's modulus

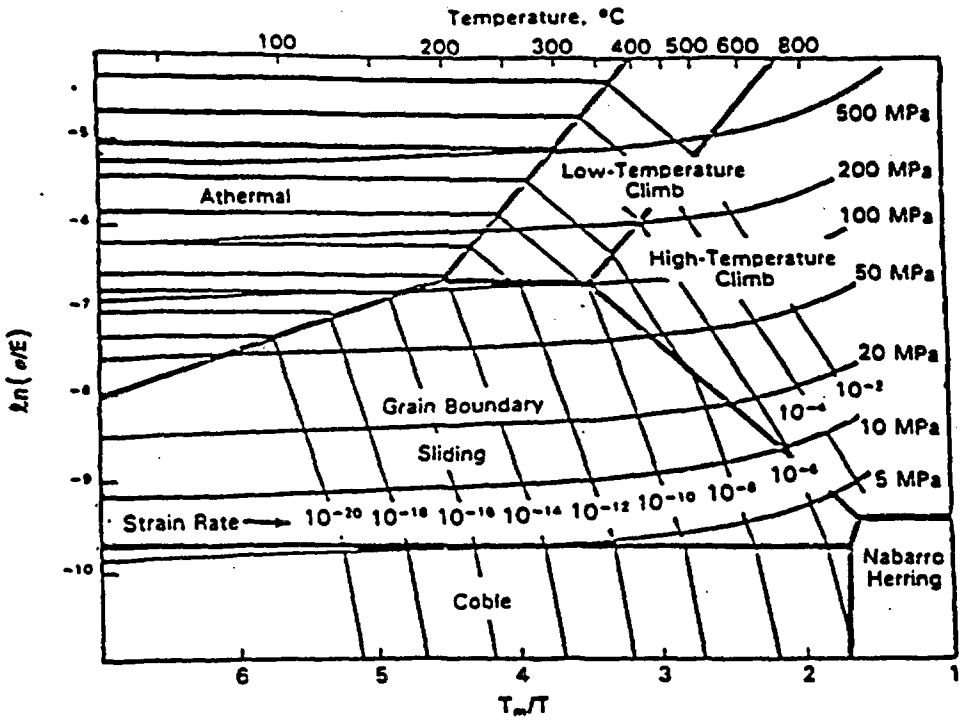


Figure 3.5. Deformation map for Zircaloy with constant stress and strain rate ($s^{-1}$) contours.

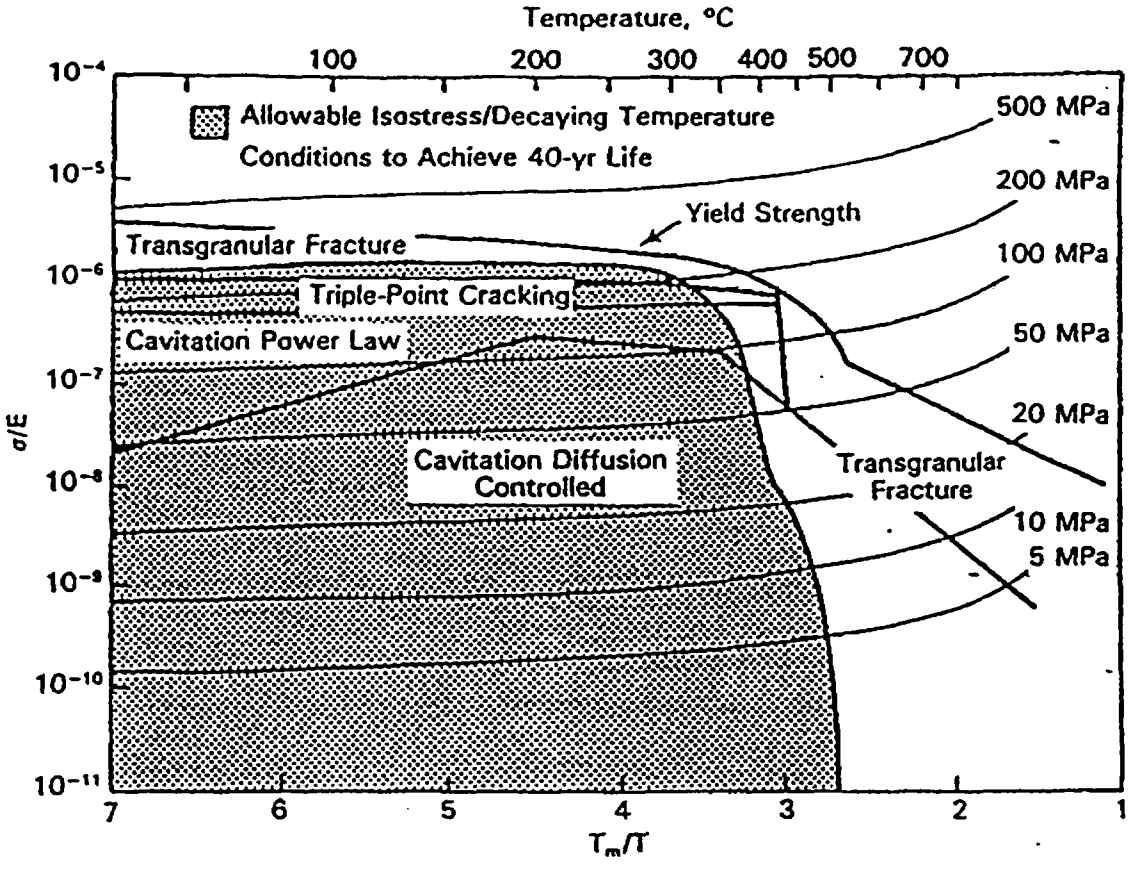


Figure 3.6. Fracture Map of Zircaloy Showing Dominant Fracture Mechanisms.

According to Chin and Gilbert 1989, diffusion controlled cavity growth (DCCG) is conceptually the dominant failure mechanism under expected disposal conditions. DCCG is an element of the Chin mechanistic fracture model. Pescatore and Cowgill 1994 question the validity of DCCG to describe creep in Zircaloy. They note that cavities are seldom observed in irradiated Zircaloys. In a limited number of instances cavities have been seen in irradiated Zircaloy-2 but the numbers of cavities have been "very few." Voids or cavities have not been detected in irradiated Zircaloy-4 (the primary cladding alloy for PWRs). The DCCG model was designed to describe intergranular fracture at high temperature. As modeled by Chin, failure occurs when there is 100% decohesion of the grain boundaries. However, the model, as implemented by NRC, assumes that 15% grain boundary decohesion is the failure criterion. With the DCCG mechanisms, it is assumed that a fixed number of voids must initially be present and grow under applied stress. The model requires inclusion-free grain boundaries, only two grain boundaries, and a stress normal to the boundaries. Voids are assumed to grow by diffusion of matter along the grain boundaries away from the voids.

Concerns expressed by Pescatore and Cowgill with the DCCG model include the facts that it describes tertiary creep (which does not occur at low stresses), that voids are seldom seen in irradiated Zircaloys, that the model has not been tested against actual Zircaloy creep data, and that the model has not been tested against other models. In addition, no strain rate dependency is assumed.

### 3.3.2 Empirical Models

An empirical model for the creep behavior of Zircaloy has been developed by Peehs and his co-workers (Peehs et al. 1986b) based on testing unirradiated, internally pressurized Zircaloy-4 samples at hoop stresses of 150 and 200 MPa over the temperature range from 250 to 400°C.

The creep strain was measured as a function of time for periods up to about 4,000 h and the results were fitted to the following equation[8]:

$$\epsilon = M\left(\frac{a}{T} - \frac{\ln\sigma - \ln k}{\ln t} - 1\right)^{-n} \qquad (6)$$

[1] This equation is sometimes presented in the literature with the time dependency shown as ln(t+1) rather than ln t, but for large times there is no difference.

where $\epsilon$ is the strain (%), $\sigma$ is the hoop stress (MPa), t is time (h), T is the temperature (K) and M, n, a, and ln k are experimentally determined empirical constants with the following values:

$a = 610$
$M = 1.89 \times 10^{-3}$
$\ln k = 6.11$
$n = 2.584$

Presumably, this equation embraces both transient and steady state creep.

The predictions from this empirical model were compared with two sets of irradiated samples in Peehs et. al. 1986a. The first set of 14 internally pressurized Zircaloy PWR cladding samples were irradiated at 400 °C in a fast neutron flux of $3 \times 10^{13}$ n/cm$^2$•s for 540 and 1,170 hours resulting in a relatively low neutron fluence of approximately $10^{20}$ n/cm$^2$. The samples were kept under tensile and compressive hoop stresses varying from 70 to 120 MPa during irradiation (Pescatore et al. 1990). Post-irradiation creep testing was done at a tensile hoop stress of 70 MPa and temperatures of 380°C for the first 1,000 hours and 395°C for the remainder of the test. After 8,000 hours, the creep strain for the irradiated samples was approximately half that predicted with Equation 6 suggesting that irradiation had increased the creep strength. The second set of 10 cladding samples were irradiated at 300°C and a compressive hoop stress of 65 MPa (i.e., with external overpressure) accumulating a fast neutron fluence of 0.5 to $1 \times 10^{22}$ n/cm$^2$. Post irradiation testing was conducted at a tensile hoop stress of 50 MPa and a temperature of 350°C for up to 8,000 hours. Unlike the first set of samples, the actual test data bracketed the creep strain predicted by equation 6 suggesting no creep strength alteration from irradiation. The difference is attributed to residual stresses associated with the in-pile pressurization mode - tensile hoop stresses with internal pressurization and compressive hoop stresses with external pressurization. Based on the two data sets, use of equation 6 should produce results which are either representative or conservative for irradiated fuel rods.

Significant spread was reported in the creep data on the irradiated specimens. For example, for the 14 samples tested at 380/395°C, the creep at 8,000 hours ranged from about 0.19 to 0.29% hoop strain while for the 10 samples tested at 350°C, the spread was from 0.06 to 0.11%.

Mayazumi and Onchi 1990b developed an empirical equation for creep strain based on experiments with unirradiated Zircaloy-4 samples pressurized to achieve stresses of 51 to 121 MPa at temperatures of 577 to 693 K (304 to 420°C)[2]. Tests were for durations of up to 7,400 hours.

Based on this work, the following empirical equation for creep strain ($\epsilon$) including transient and steady-state creep strain was proposed:

$$\epsilon = \epsilon_t^s\{1 - \exp(-D(\dot{\epsilon}_s t)^{0.63})\} + \dot{\epsilon}_s t \quad (7)$$

where D is a non-dimensional variable, $\epsilon_t^s$, is the saturated transient creep strain, and $\dot{\epsilon}_s$ is the steady-state creep rate ($s^{-1}$). Equations for these parameters are listed below:

$$D = 9.28x10^{7}\exp(-0.0212T) \quad (8)$$

$$\epsilon_t^s = \exp(-0.0866T + 64.1)(\dot{\epsilon}_s)^{-0.00336T + 2.81} \quad (9)$$

$$\dot{\epsilon}_s = 7.26x10^{4}\left(\frac{E}{T}\right)\exp\left(\frac{2320\sigma}{E}\right)\exp\left(-\frac{215000}{RT}\right) \quad (10)$$

In Equation 10, $\sigma$ is the hoop stress and E is the elastic modulus (E = 1.145 x $10^{5}$-59.9T MPa). This equation assumes that $\sigma > 10^{-3}$ E which is likely only for values of T > 573 K (300°C).

Mayazumi and Onchi 1990a used a Larson-Miller parameter approach (P = [T + log $t_f$]) to develop an equation for the time to rupture for internally-pressurized Zircaloy-4 specimens at higher temperatures as follows:

$$t_f = 10^{\frac{\log\sigma - 5.024}{-0.000173T} - 20} \quad (11)$$

---

[2] Data at 577 K (304°C) were not used in developing the creep equations based on small strains on the order of 0.04 to 0.16% after 7,400 h testing.

where $t_f$ is the time to rupture in hours, $\sigma$ is the stress in MPa, and T is the temperature in Kelvin. Tests were conducted from 727 to 857 K (454 to 584°C) on unirradiated material to develop equation 11. Mayazumi and Onchi used these same tests to develop a creep strain equation covering transient and steady-state creep for this higher temperature range as follows:

$$\epsilon = 0.05\{1 - \exp(-10(\dot{\epsilon}_s t)^{0.51})\} + \dot{\epsilon}_s t \qquad (12)$$

The strain rate ($\dot{\epsilon}_s$) in equation 12 is calculated from the following equation:

$$\dot{\epsilon}_s = 1.02x10^5 (\frac{E}{T}) \exp(\frac{4060\sigma}{E}) \exp(-\frac{233000}{RT}) \qquad (13)$$

Strains predicted from equations 12 and 13 are not expected under disposal conditions because these equations are based on creep data obtained at substantially higher temperatures than expected at Yucca Mountain.

Murty et al. 1977 studied the creep behavior of Zircaloy-4 over the temperature range from 600 to 800°F (574 to 700 K) and hoop stress levels of 10 to 25 ksi (69 to 172 MPa). At the lowest temperature, steady-state creep was not achieved after 2000 hours. The experimental data at 650 to 800 F correlated well with an exponential stress dependence and the activation energy for creep was in good agreement with that for self diffusion. Climb of edge dislocations was thought to be the rate controlling step. The experimental results were fit to the following generalized steady-state creep equation:

$$\dot{\epsilon} = A \exp(B\frac{\sigma}{E}) \frac{Eb}{kT} D_o \exp(-\frac{Q}{RT}) \qquad (14)$$

where

| | |
|---|---|
| $\dot{\epsilon}$ | = steady state creep rate |
| $\sigma$ | = applied stress |
| E | = elastic modulus |
| b | = burger's vector |
| k | = Boltzmann constant, |
| T | = temperature (K) |
| Q | = activation energy (60 kcal/mole) |
| A, B | = constants |

Unfortunately, the paper does not provide values of the constants A and B to permit use of this equation in modeling nor does it quantify the magnitudes of the creep strains. It should be noted that Equation 14 is for steady-state creep and for values of $\sigma > 10^{3}E$. The activation energy for creep was determined to be 59.5 kcal/mole (249,000 J/mole). This energy value compares closely with the activation energy of 62 kcal/mole for self-diffusion in Zr-1.3% Sn determined by other investigators and suggests that, over the temperature range considered (i.e., 616 to 700 K), the creep process is controlled by a diffusion mechanism.

Matsuo 1987 conducted creep tests on cold-worked and stress relieved Zircaloy-4 over the temperature range from 603 to 693 K (330 to 420°C) at hoop stresses varying from 49 to 314 MPa for test durations of up to 3,000 hours. The results were analyzed using the same quasi-theoretical approach of Dorn as used by Mayazumi and Onchi and by Murty. For high stress levels (i.e., 78 to 314 MPa), Matsuo derived the following equation for the steady state creep rate ($s^{-1}$):

$$\dot{\epsilon} = 1.0x10^{9}\left(\frac{E}{T}\right)\exp\left(\frac{2400\sigma}{E}\right)\exp\left(-\frac{272000}{RT}\right) \qquad (15)$$

Since this equation was limited to "high" stress levels, it was modified as follows to include the full range of stresses evaluated (i.e., 49 to 314 Mpa):

$$\dot{\epsilon} = 4.36x10^{9}\left(\frac{E}{T}\right)\left[\sinh\left(1130\frac{\sigma}{E}\right)\right]^{2.1}\exp\left(-\frac{272000}{RT}\right) \qquad (16)$$

In equations 15 and 16, R is 8.3169 J/mole•K.

The modulus of elasticity was calculated using the same equation as used in Mayazumi and Onchi 1990b. As shown in Figure 3.7, the steady state creep rate developed in Matsuo 1987 is substantially lower than that in Mayazumi and Onchi 1990b, particularly at temperatures below 600 K (327°C). Matsuo also developed an equation for total strain using the same approach as Mayazumi and Onchi as follows:

$$\epsilon = \epsilon_{P}^{S}\left[1 - \exp\left(-52(\dot{\epsilon}_{S}t)^{0.5}\right)\right] + \dot{\epsilon}_{s}t \qquad (16a)$$

where $\epsilon_P^S$, the saturated primary creep strain, is defined as:

$$\epsilon_P^S = 0.0216(\dot{\epsilon}_{S,calc})^{0.109} \quad (16b)$$

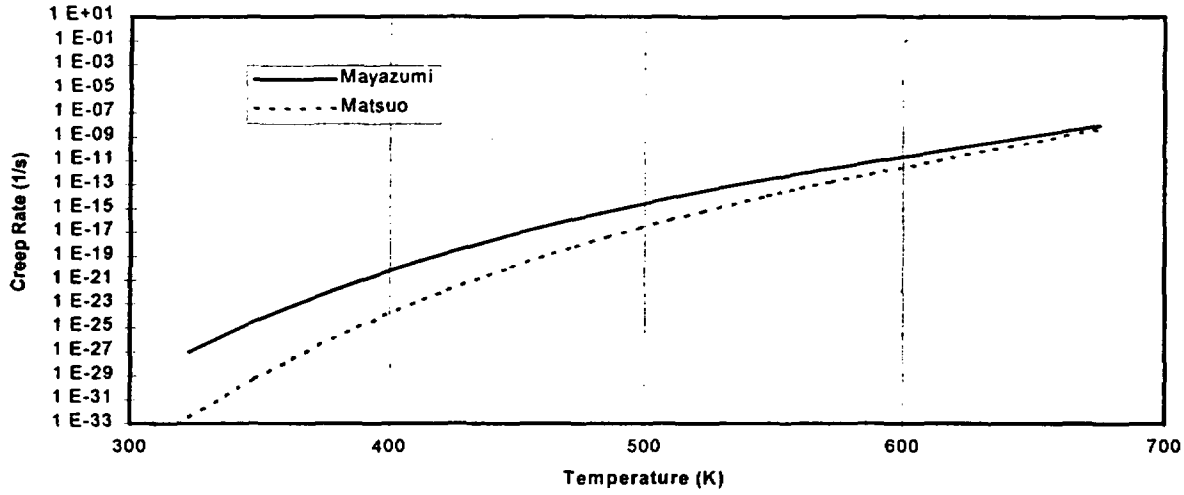


Figure 3.7 Steady state creep rates developed by Matsuo and Mayazumi and Onchi

In this equation, $\dot{\epsilon}_{S,calc}$ is calculated using equation 15.

The fact that the creep rate predicted from the work of Matsuo is substantially different from that predicted by Mayazumi and Onchi is puzzling. Although Matsuo modified his equations to use a *sinh* rather than an exponential term for the normalized stress, while Mayazumi and Onchi used an exponential term, this has little impact. The difference between using equations 15 and 16 to calculate the total strain is small. Both investigators used production cladding with the same outside dimensions (10.72 mm) and the same general thermal history (i.e. cold-rolled and stress relieved). Matsuo internally pressurized his specimens from an external pressure source connected to the specimens with Swagelok fittings while Mayazumi and Onchi sealed their specimens by welding the end plugs under various pressures. The fill pressure and the test temperature established the internal pressure (i.e., creep stress). The activation energy determined by Matsuo was about 272,000 J/mole while that determined by Mayazumi and Onchi was about 215,000 J/mole. This difference in activation energy is one of the major

contributors to the difference between the two studies. Additional details on the two experimental approaches are included in Appendix C.

Tests on irradiated Zircaloy-4 at temperatures ranging from 603 to 873 K (330 to 600°C) and at stresses ranging from 77 to 384 MPa are described in Mayazumi and Murai 1993. The test material was fuel element cladding from a 17 x 17 PWR bundle that had been irradiated at 47,000 MWd/MTU or 8-9 x $10^{21}$ n/cm$^2$ (≥1 Mev). The ratio of the post irradiation creep rate was reported to be a complex function of stress and temperature and varied from 0.02 to 0.6 that of unirradiated material. Some of the tests were taken to rupture. It was shown that rupture strains were smallest at low temperatures or high stresses but, in no case, did the rupture strain for the irradiated material fall below 3%. The authors noted that irradiated material ruptures at slightly higher temperatures or stresses or after slightly longer times than would be predicted by equation 11 above.

Experiments with irradiated Zircaloy-2[10] using specimens taken from a fuel bundle exposed to a burnup of 46,000 MWd/MTU are described in Saegusa et al. 1996. Tests were conducted at 663 and 693 K (390 and 420°C) and a hoop stress of 154 MPa (see Table 3.3 for comment on stress). These tests showed that the creep strain in unirradiated cladding is greater than in irradiated cladding at comparable test conditions but the irradiated cladding does not rupture even when the creep strain exceeds 1%. Based on this work, 1% creep strain was chosen as the acceptable limit for dry storage.

Data comparing the various creep tests discussed above are summarized in Table 3.5.

[3] This was identified in Figure 2 of the paper as Zircaloy-2, but based on references cited in the paper it is more likely that the material was Zircaloy-4. In fact, it is probably from the same source of material as described in Mayazumi and Murai 1993.

Table 3.5. Comparison of Experimental Ranges for Zircaloy Creep Test Data.

| Source | Alloy | Temperature (K) | Stress (MPa) | Condition | Time (h) |
|---|---|---|---|---|---|
| Seagusa et al. 1996 | Zr-2 | 663 & 693 | 154[a] | Irradiated 46,000 MWd/MTU | 2000 @ 663 K, 500 @ 693 K |
| | Zr-2 | 663 & 693 | 154[a] | Unirradiated | 1500 @ 663 K, 250 @ 693 K |
| Peehs et al. 1986a | Zr-4 | 523 to 673 | 150 & 200 | Unirradiated | up to 4000 |
| | Zr-4?? | 653/668 | 70 | Irradiated - $10^{20}$ n/cm$^2$ | 8000 |
| | Zr-4?? | 623 | 50 | Irradiated 0.5 to 1x$10^{22}$ n/cm$^2$ | 8000 |
| Murty et al. 1977 | Zr-4 | 574 to 685 | 69 to 172 | Unirradiated | up to 3020 |
| Mayazumi and Onchi 1990b | Zr-4 | 577 to 693 | 51 to 121 | Unirradiated | up to 7000 |
| Mayazumi and Onchi 1990a | Zr-4 | 727 to 857 | 64 to 150 | Unirradiated | up to 600 |
| Matsuo 1987 | Zr-4 | 603 to 693 | 49 to 314 | Unirradiated | up to 3000 |
| Mayazumi and Murai 1993 | Zr-4 | 603 to 873 | 77 to 384 | Irradiated 47,000 MWd/MTU (8-9 x$10^{21}$ n/cm$^2$) | up to 2000 |

a The paper cites a value of 19.6 MPa which is presumably the pressure. The stress listed in this table is based on the assumption the samples had the same geometry as those used in Mayazumi and Onchi 1990b (i.e., 10.72 mm o.d. by 0.66 mm wall thickness).

## 3.4 DELAYED HYDRIDE CRACKING (DHC)

An excellent survey of the conditions under which delayed hydride cracking occurs in Zircaloys is provided in Pescatore et al. 1990. Zirconium alloys can dissolve hydrogen during reactor operation. The solubility of hydrogen in alpha-Zr varies from 40 ppm at 260°C to 650 ppm at 550°C (Pescatore et al. 1990). Hydrogen which is soluble at reactor operating temperatures can precipitate as brittle zirconium hydrides at lower temperatures. In the absence of applied stress, the Zr-H platelets tend to align themselves circumferentially and, consequently, cladding properties are not seriously impaired. However, under certain conditions of stress, temperature, and fabrication history, the platelets can reorient into the radial direction with an attendant reduction in hoop strength. As described in Pescatore et al. 1990, the sequential steps in the process are as follows:

- Diffusion of hydrogen to a notch or crack tip

- Formation of a brittle hydride
- Application or continued existence of a tensile stress
- Cracking of the hydride and extension of the crack tip
- Repeat of the process at the new crack tip

For reorientation to occur, the hydrides must go into solution. Thus, at 300°C where the solubility is about 70 ppm, only about half the hydrides could be reoriented in a sample containing 140 ppm.

Conditions conducive to significant hydride reorientation include a hydrogen content of at least 100 ppm, a temperature of 300-350°C, and stresses of 175 to 200 MPa. This combination of conditions is unlikely during service, storage, or disposal. Limited reorientation (a few per cent) may occur at stresses as low as 50 MPa.

With the exception of some experimental rods, DHC failures have not been reported for any fuel rods during operation or storage (Pescatore et al. 1990). The rod which failed contained up to 90 ppm hydrogen and was internally pressurized to achieve a hoop stress of 145 MPa at 323°C. This stress is somewhat lower than expected for DHC based on the conditions cited above for unirradiated Zircaloy and raises questions as to the role of neutron fluence on this phenomenon.

A threshold stress intensity factor is also required for the onset of DHC. For Zr-2 this is about 10 MPa•$m^{0.5}$ (Puls et al. 1982, as cited in Pescatore et al. 1990). Another author cites the critical threshold stress for initiating DHC in Zircaloy-2 and -4 at 350 and 525 K (77 and 252°C) as 14 MPa•$m^{0.5}$ for materials with notches ≥0.2 mm (Cheadle et al. 1987). In similar tests at 290 and 525 K (17 and 252°C) on materials with smooth surfaces or notches ≤0.1 mm, no cracking was noted.

Pescatore and Cowgill 1994 quoted the NRC position on delayed hydride cracking (developed in the safety evaluation report for the Castor V/21 dry spent fuel storage cask) as follows:

> "...the hoop stresses in the cladding are not expected to be high enough to cause a radial orientation of the hydride and consequent crack initiation. It is remotely possible that pre-existing cracks under stress can induce diffusion of hydrogen to the crack tips where substantially higher concentrations could precipitate hydride in a manner that would encourage crack extension."

The Yucca Mountain project has considered DHC in its cladding degradation model (Siegmann et al. 1996) based on work by Einziger and Kohli 1984. The growth of a crack of depth W (m) is given by the expression:

$$W=22.1(t\exp(\frac{-2.291x10^4}{T}))^{0.5} \quad (17)$$

where t is the time (y) and T is the absolute temperature (K). The crack depth is used to calculate a stress concentration factor, $K_I$ (MPa•$m^{0.5}$), as follows:

$$K_I=\sigma\sqrt{W\frac{\pi}{2}} \quad (18)$$

where σ is the stress (MPa). For this report the critical or threshold stress concentration factor ($K_{IH}$) for DHC in Zircaloy is assumed to be 10 MPa•$m^{0.5}$ based on Pescatore et al. 1990. Shi and Puls 1994 have stated that the critical stress concentration factor in the Zr-2.5Nb alloy used in CANDU reactor pressure tubes has a mean value of 8.2 MPa•$m^{0.5}$ with 95% confidence that all values lie between 4.3 and 12 MPa•$m^{0.5}$. The stated range is based on physical observations.

## 3.5 MECHANICAL FAILURE

This conceptual failure model involves mechanical rupture of the fuel rods due to rocks from the roof of the drift falling on the fuel and causing a number of pins to shear. The current DOE scenario involves the following sequence of events (DOE 1998):

- The waste package is breached and becomes filled with water
- The waste package internals corrode allowing fuel bundles to settle to the bottom of the waste package
- The drift degrades, allowing rocks to fall onto the top of the waste package. The rocks' size distribution is based on rock joint studies with the median diameter being 0.5 m.
- The waste package corrodes allowing the rocks to fall from the upper surface onto the fuel bundles causing a number of rods to shear

In this model DOE assumes that between 3.4 and 35% of the fuel pins in the WP fail, with the expected value being 5%. DOE conjectures that failures occur linearly with the log of time over period from 30,000 to 500,000 years. The process cannot occur until the structural support characteristics of the waste package have been destroyed by massive corrosion.

This mechanism is irrelevant if the regulatory horizon is limited to 10,000 years.

## 3.6 LONG TERM CORROSION

Once the waste package has been breached either by some juvenile failure mechanism or by corrosion, the contents will be exposed to humid air and steam or water depending on the local cladding temperature. Since the fuel rods in the waste packages are subject to both radial and axial temperature gradients, a variety of localized environments are possible. For example, if fuel cladding temperatures are above 100°C, the cladding will be exposed to a steam environment. Dissolved salts may precipitate from evaporating solutions on the rods exposed to steam providing sites where the localized surface chemistry could promote pitting over time. As the cladding temperature drops, the radial and axial temperature gradients may lead to a situation where water pools in the bottom of the waste package while, above that, the hotter central rods are still exposed to steam. When the cladding temperature throughout the waste package has dropped below 100°C, the waste package can fill with water.

DOE is expected to postulate in the TSPA-VA that some unidentified long-term corrosion mechanism will exist after the Zircaloy fuel cladding becomes immersed in water. Possible mechanisms include pitting and crevice corrosion. In lieu of experimental evidence, DOE assumes in the TSPA-VA that the cladding is 100 times more corrosion resistant than C-22 (the corrosion resistant liner of the waste package). The corrosion rate for C-22 at 100°C, based on expert elicitation, varies from $1 \times 10^{-7}$ mm/y (0th percentile) to $2 \times 10^{-2}$ mm/y (at the 100th percentile) with the median value being $4 \times 10^{-5}$ mm/y (McNeish in DOE 1998a). If the corrosion resistance of Zircaloy is 100 times better than C-22, then, for 0.6 mm fuel pin cladding, penetration would be expected in 1.5 million years based on the median corrosion rate and in 3,000 years based on the maximum rate[11]. Assuming that the Zircaloy corrosion

[11] This would occur 4,000 years after disposal based on a juvenile failure time of 1,000 years for one waste package. Based on a failure rate of 17 additional WP per 10,000 years (Andrews in DOE 1998d), a total of 18

rates are log uniformly distributed, and that the waste package failure distribution is as described on page 36 of DOE 1998d, then about 1,600 fuel rods would be subject to corrosion failures in a 10,000-year regulatory time frame. This would be a small contribution to the radionuclide source term compared to 29,500 initially failed Zircaloy rods (based on a 0.1% failure rate). The derivation of this failure value is as follows:

> If the cladding is penetrated after 3,000 years of exposure to water at a corrosion rate of $2 \times 10^{-4}$ mm/y, then the cladding would be penetrated in 9,000 years (i.e., 10,000 years after disposal) at a corrosion rate of $6.7 \times 10^{-5}$ mm/y. Based on a log uniform distribution, the range of log corrosion rates is -9 to -3.7, and the 10,000-year corrosion rate is -4.18. Thus, there is a 9% probability that the corrosion rate would be sufficient to cause penetration in 10,000 years ([4.18-3.7]/[9-3.7] x 100). This rate would apply only to waste packages which have been breached (i.e., which see seeps).

This possibility will decrease as the time of waste package penetration increases from 1,000 years after disposal. When the time of package penetration exceeds 7,000 years, cladding penetration as a result of the generic corrosion mechanism will not occur within the 10,000-year regulatory time frame.

This calculation is conservative since it ignores the several hundred years required to fill a breached waste package and inundate all the fuel rods.

---

waste packages would have failed during a 10,000-year regulatory time frame.

# 4.0 MODELING APPROACH

This section presents information which can be used to model the performance of the fuel cladding as an engineered barrier and provides various illustrative calculations. The potential cladding failure mechanisms discussed in the section include creep, delayed hydride cracking, fuel side stress corrosion cracking, cladding oxidation and fuel oxidation. Except for the oxidation processes, all of the mechanisms can occur regardless of whether the waste package is breached or not. Cladding and fuel oxidation require ingress of air into the waste package and fuel oxidation requires that the fuel rod cladding be breached, as well.

## 4.1 FUEL ELEMENT DESIGN

The design of commercial nuclear reactor fuel elements is summarized in Appendix A (Appendix B, Table B.1, NUREG/CR-3950, Vol. 9). For modeling purposes, the ABB CENF 16x16 PWR fuel rod array was chosen based on the assumption that, since these fuel rods were filled with He at pressures up to 450 psig, the hoop stresses at comparable levels of fission gas release would be greater than in designs with lower fill pressures. BWR fuel rods use thicker cladding and lower fill gas pressures. Consequently, basing modeling on PWR designs is conservative. Design fuel burnups for the various fuel elements are also listed in Appendix A.

## 4.2 TEMPERATURE DISTRIBUTION

One of the most critical issues in modeling the behavior of the cladding is the temporal and spatial temperature distribution. For this analysis, the temperature profiles developed in the Advanced Conceptual Design Report (ACD 1996) are used. These profiles are reproduced in Figures 4.1 and 4.2 (Figures 6.3-1 and 6.3-2 from ACD 1996). The temperature profiles are based on a thermal loading of 83 MTU/acre, an initial areal power density of 94.4 kw/acre, a waste package spacing of 19.5 m, and a drift spacing of 22.5 m. The design basis PWR fuel is assumed to be 10 years old with a burnup of 48,000 MWd/MTU and an initial thermal power generation rate of 850 watts. For the design-basis PWR fuel, only 2.15% of the fuel subassemblies initially generate more than 850 watts per assembly (ibid, p. 5-5). The waste package is assumed to be a helium-filled 21 PWR UCF WP[12] container. Peak cladding

[4] A 21 PWR UCF WP is a waste package (WP) which contains 21 pressurized water reactor (PWR) spent fuel elements as uncanistered fuel (UCF).

temperatures on based on the "conservative" Wooten-Epstein model and the "best estimate" smeared-k model. Peak cladding temperatures occur five to eight years after disposal and are 263°C for the conservative case and 241°C for the best estimate.

The smeared thermal conductivity approach considers the fuel assembly as a smeared solid with internal volumetric heat generation. The volumetric heat loadings were multiplied by an axial peaking factor "...to approximate the axial center of the waste packaage with a two-dimensional model" (ACD 1996). The more conservative Wooten-Epstein correlation, which is based on the highest steady state temperature in the waste package, has been used as the primary tool in the past for transportation/storage cask calculations and has been accepted by the NRC. Both models were benchmarked against experimental data obtained from a Westinghouse 15 x 15 fuel assembly. Peak cladding temperatures calculated by the two models and the measured cladding temperature are as follows (ACD 1996):

- Measured/calculated test data - 215°C
- Smeared k - 221°C
- Wooten-Epstein correlation - 248°C

The calculated temperatures were developed using volumetric heat generation rates adjusted for axial heat peaking factors.

For comparison, an earlier temperature distribution developed for Yucca Mountain Site Characterization Plan is included as Figure 4.3 (Pescatore et. al, 1990). It can be seen that the peak fuel (i.e., peak cladding) temperature is 320°C as compared to 263°C in Figure 4.1. After 1000 years the cladding has dropped to 130°C as compared to 150°C in Figure 4.1. Figure 4.3 is based upon a lower local power density (57 kw/acre), a closer waste package spacing (5 m) than the 21 PWR UCF in Figure 4.1, and vertical emplacement.

Rothman described the temperature distribution for 10-year old waste with a power generation of 3.05 kw/package and an areal power density of 82 kw/acre as decreasing from a peak value of 345°C soon after emplacement to 180°C at 1,000 years (Rothman 1984).

For preliminary calculations in this report, the following temperatures were estimated from Figure 4.1:

- 0-10 years - 250°C
- 11-100 years - 225°C
- 101-1000 years - 175°C
- 1001-10,000 years - 125°C

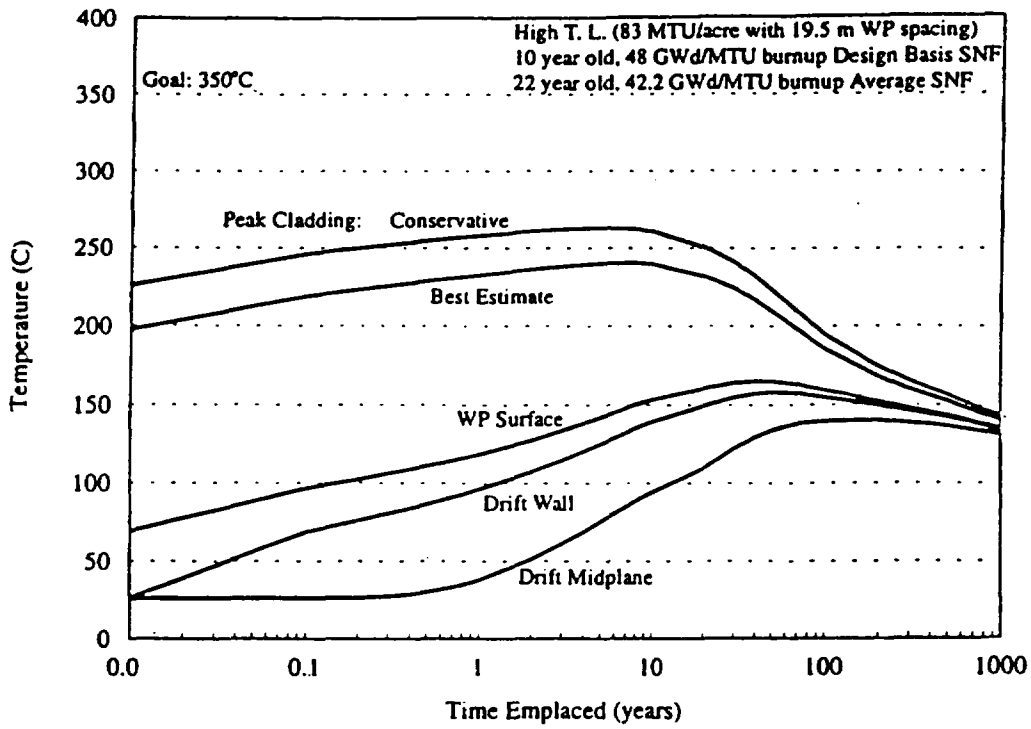


Figure 4.1. Repository Temperature Profiles For 21 PWR UCF Waste Package as Function of Time After Emplacement (conservative - Wooten-Epstein; best estimate - smeared k).

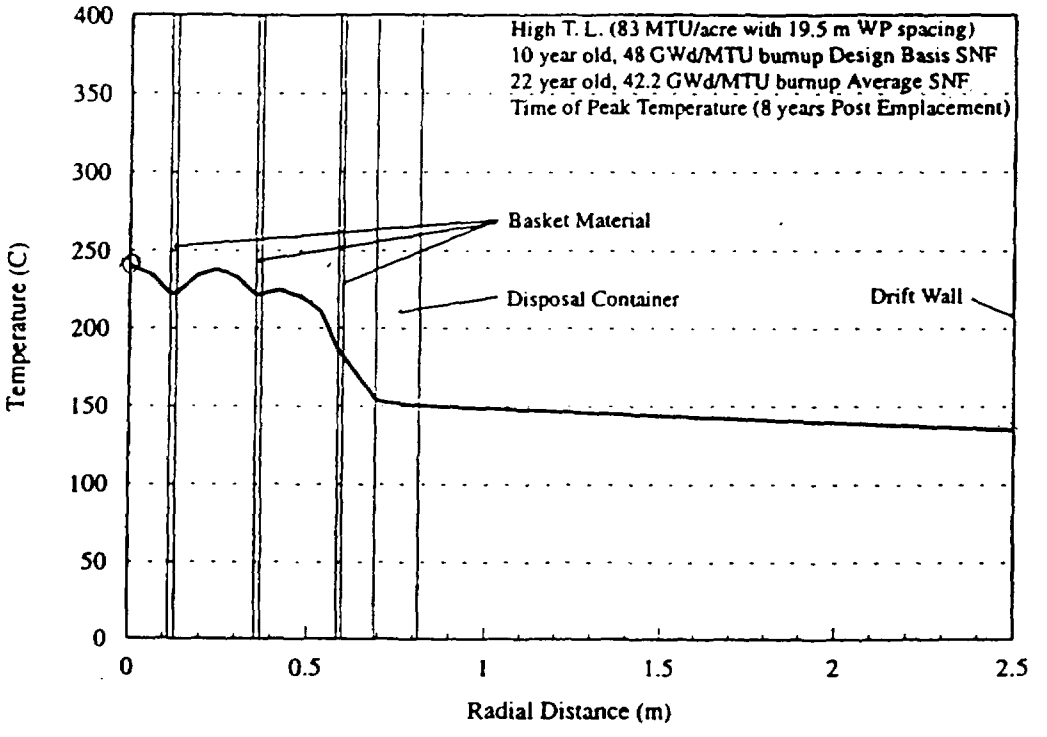


Figure 4.2. Radial Temperature Profile for 21 PWR UCF at Peak Time (8 years) After Emplacement

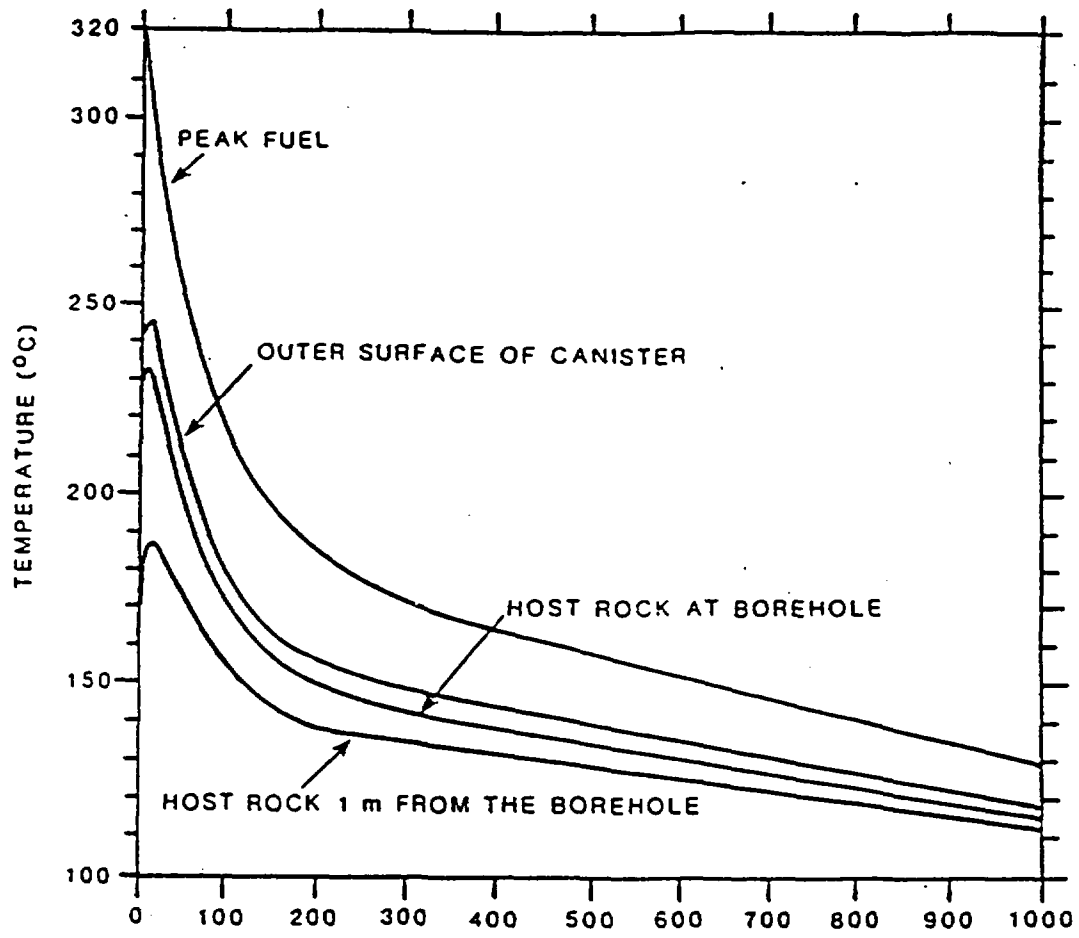


Figure 4.3. Temperature History of Repository Based on Site Characterization Plan ("Peak fuel" is the peak cladding temperature.)

For the period 10 to 10,000 years these data can be approximated by the equation:

$$T = 285 - 45 \log t \quad (19)$$

where T is the temperature (°C) and t is the time (y).

The fuel cladding temperatures as a function of time discussed above are for the maximum axial temperature in a fuel rod. There is a significant axial gradient as shown in Figure 4.4 where the non-dimensional cladding temperature ($[T - T_{surf}]/[T_{max} - T_{surf}]$) is estimated for various dry storage cask conditions (McKinnon and Doherty 1997). This axial temperature gradient is not of any significance for most of the failure mechanisms discussed here except possibly clad unzipping.

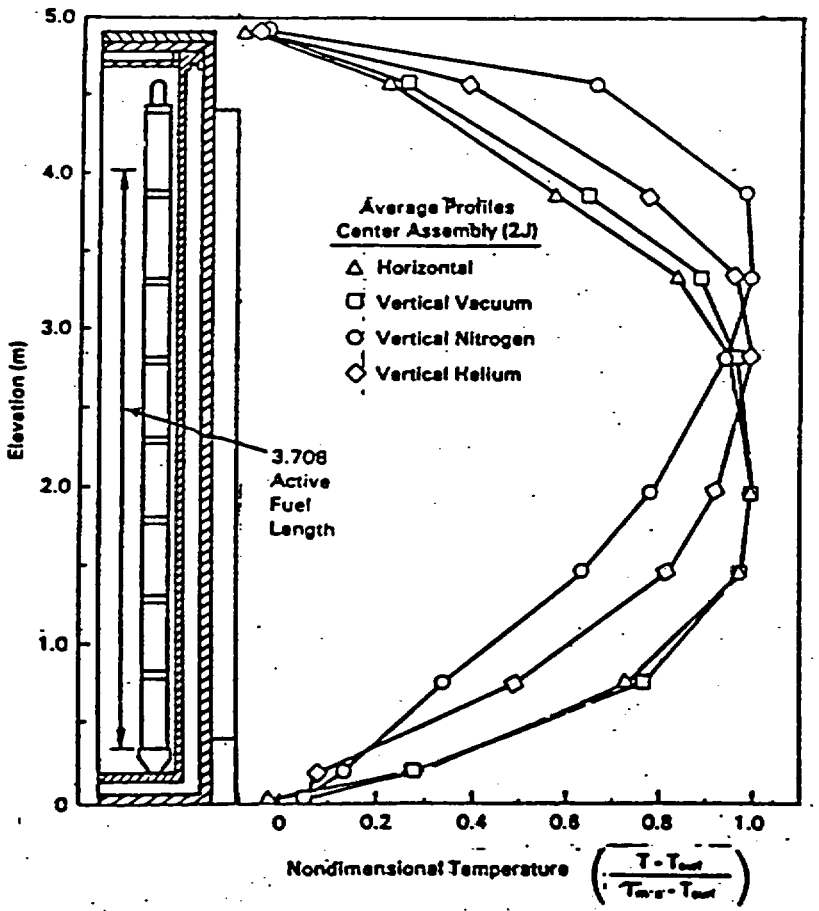


Figure 4.4. Axial temperature profile for spent fuel under various dry storage options.

## 4.3 CREEP FAILURE

Numerous authors have proposed that the primary failure mechanism for fuel rods in the disposal facility is creep rupture due to the internal pressure in the fuels rods (e.g., Einziger 1994, Pescatore et al. 1990, Pescatore and Cowgill 1994). The internal pressure is generated by the initial fill gas (He) plus gaseous fission products released from the $UO_2$ fuel pellets and helium produced by the decay of actinide elements. The gas pressure produces a tensile hoop stress in the cladding which, conceptually, at stresses below the ultimate tensile strength of the Zircaloy cladding, can develop creep strains of sufficient magnitude to cause rupture. Potential for occurrence of creep is independent of whether or not the waste package wall has been penetrated.

### 4.3.1 Internal Pressure

Values for internal pressure at 25°C in irradiated fuel rods, taken from Blackburn et al. 1978, are as follows:

- PWR - 3.8 MPa typical, 7.7 MPa design
- BWR - 0.2 MPa typical, 1.8 MPa design

The PWR design estimate was based on the assumption that at reactor operating temperatures the internal pressure would not exceed the external pressure (2250 psia) while the PWR typical condition was based on end-of-life estimates of 1.7 to 3.8 MPa for prepressurized PWR fuel (Johnson 1977). The BWR design estimate was based on the assumptions that the fission gas generation rate was $1.35 \times 10^{-3}$ gram-moles/MWd, that the maximum fission gas release in the highest power density rod was 20%, and that the rods were initially filled with He at 0.1 MPa pressure. The typical condition was based on estimates by Johnson 1977.

A summary of internal pressure estimates by various investigators was included in Pescatore et al. 1990. Values at 25°C are presented in Table 4.1.

Table 4.1 Internal Pressures (MPa) at 25°C in Spent Fuel Rods.

| Pressure (MPa) | Comments | Reference |
|---|---|---|
| PWR FUEL RODS | | |
| 1.4 - 2.8 | Average | Locke 1975[a] |
| 1.7 -3.8 | Average | Johnson 1977[a] |
| 5.5 | 99% <5.5 MPa | Rothman 1984 |
| 5.8 | Maximum | RESAR3S 1975[a] |
| 6.5 | Maximum | Cunningham 1987 |
| 8.3 | Atypical[b] | Johnson 1977[a] |
| BWR FUEL RODS | | |
| 1.4 - 2.0 | Average | Johnson 1977[a] |
| 1.83 | Average | Blackburn et al. 1978 |

a - Referenced in Rothman 1984

b - Pescatore et al. 1990, note that this value was measured for Maine Yankee fuel rods which were improperly fabricated with too large a pellet/cladding gap resulting in high fission gas releases. According to Rothman 1984, "the Yankee reactor fuel rods constitute well under 1% (likely much less than 0.1%) of all spent fuel anticipated at present."

The pressure, p(T), at any temperature T can be related to the pressure at 25°C, $p_{25}$, with the ideal gas law:

$$p(T) = p_{25}\left(\frac{T}{298}\right) \tag{20}$$

Equation 19 assumes the internal volume in the fuel rod is the same at 298 K (25°C) and at T. Insofar as the thermal expansion of the cladding is greater than that of the $UO_2$, the assumption is conservative (i.e., p(T) will be overstated). Relative thermal expansion can be rigorously addressed in modeling if desired.

The amount of fission gas generated is a function of fuel burnup. As commercial reactors have gained more operating experience and as fuel rod designs have been improved, the burnup has been extended to about 60,000 MWd/MTU as shown in Table 4.2 (NRC 1994). Rothman (*op. cit.*) states that the fission gas production rate is 31 $cm^3$/MWd (@ 1 atm and 0 °C) (ANS 1982).

For the calculations presented here, the internal pressure in the fuel rods was based on an initial fill pressure of 465 psia (3.2 MPa), a fuel burnup of 60,000 MWd/MTU, an assumed gaseous fission product yield of 31 $cm^3$/MWd (at 273 K and 1 atm), and a fractional fission gas release of 0.2 (Rothman 1984).

An extensive analysis of fission gas release from $UO_2$ subjected to high burnup was done under the aegis of the High Burnup Effects Program (HBEP) managed by Batelle Pacific Northwest Laboratories for an international consortium (Barnes et al., 1992). In this program, fission gas release was measured on 79 rods or rodlets simulating typical BWR and PWR geometries, as well as several non-standard designs. Peak pellet burnups ranged from 22.6 to 74.1 MWd/kgM. Some of the rods were subjected to "power bumping" subsequent to commercial irradiation. Power bumping was designed to simulate end-of-life power transients. This is not representative of typical operating procedures, but rather was intended to examine the effects of subjecting the rods to high linear heat generation rates (LHGRs) at the end of life.

Table 4.2. Highest Burnup Achieved by Vendors in 1991 (NRC 1994)

| Vendor | Plant or Test | Type | Burnup GWd/MTU) | Comments |
|---|---|---|---|---|
| ABB | ANO-2 | PWR | 46.5 | Batch Average |
| CENF | Calvert Cliffs-2 | PWR | 43.0 | Batch Average |
| CENF | St. Lucie-2 | PWR | 41.5 | Batch Average |
| GE | | BWR | >45.0 | Bundle Average |
| GE | | BWR | 60.0 | Peak Pellet Exposure |
| SPC | R.E. Ginna | PWR | 52.1 | Assembly Average |
| SPC | Big Rock Point | BWR | 45.1 | Assembly Average |
| W | Zion-1 | PWR | 55.0 | 4-Assembly Average |
| W | North Anna-1 | PWR | 58.0 | 4-Assembly Average |
| W | | PWR | >58.0 | Lead Assembly Average |
| BWFC | | | | No Information Provided |

Of the rods not subjected to power bumping, the maximum observed fission gas release was 26%. Six of 64 specimens exhibited fission gas release fractions exceeding 10%. Fission gas releases in the power bumped rods ranged from 2.6 to 55.8% with 11 of 15 rods exceeding 20% release. The fission gas release associated with power bumping was determined to be a

linear function of the linear heat generation rate. Fission gas releases of $<10\%$ were associated with LHGRs of $<30$ kw/m while fission gas releases of $>40\%$ were associated with LHGRs of 40-50 kw/m. The authors note that, with PWR-design rods, 22 of 49 had fractional fission gas releases of $>4\%$ compared to observed values of $<4\%$ in commercially irradiated full length rods exposed to burnup levels of 56 MWd/kg M. The difference is attributed to the higher LHGRs in the HBEP rods as compared to the commercial rods. As described in Appendix A, the average LHGR for PWRs is 18-22 kw/m, axial peak LHGRs in an average rod are 21-28 kw/m, and maximum peak LHGRs are 43 to 62 kw/m.

EPRI developed a model for fission gas release based on a population of 51 spent fuel rods from PWRs (EPRI 1989). The population includes fuels rods with exposures of up to 57,500 MWd/MTU and a maximum fission gas release of 24%. There was approximately a 98% probability of having fission gas release of less than 24%. This observed distribution was modified to account for possible transient reactor operating effects by ignoring the 24% data point and instead assuming a 1% probability that the fission gas release would be 50%. This curve is reproduced as Figure 4.5. It can be seen that the probability of fission gas release exceeding 10% is less than 0.15. The probability index, $-\ln(1-\phi)$, is the same as the probability ($\phi$) over the range shown.

Rothman pointed out that, although the cooling of the fuel rods reduces the internal pressure over time, this effect is partially offset by the generation of helium, particularly from decay of actinides. He noted that 19.35 moles of He per MTU are generated over 10,000 years after a burnup of 36 MWd/kg U (Rothman 1984). Marschke (SCA 1997) has developed additional data on helium generation as a function of burnup and time using a PC version of the ORIGEN2 computer code. Details are presented in Table 4.3.

Table 4.3. Helium Generation in Irradiated $UO_2$ (moles/MTU)

| Time (y) | Burnup (MWd/MTU) | |
|---|---|---|
| | 33,000 | 60,000 |
| 0 | 0.05 | 0.23 |
| 5 | 0.15 | 0.4 |
| 10 | 0.2 | 0.65 |
| 100 | 1.2 | 2.8 |
| 1000 | 6.2 | 10 |
| $10^4$ | 17.2 | 23.4 |
| $10^5$ | 37.2 | 46.9 |
| $10^6$ | 62.2 | 88.8 |

The value for 10,000 years and a burnup of 33,000 MWd/MTU is in good agreement with the value reported by Rothman. In the absence of any other information it could be conservatively assumed that all He in the $UO_2$ matrix is released. However, it is more likely that He will be released from the $UO_2$ by diffusion in much the same manner as other noble gases. Measurements of He diffusivity in $UO_2$ are reported in Belle 1961. Assuming a temperature of 600 K (327°C) , and an equivalent sphere with a radius of 0.01425 cm, the fractional He release by diffusion is only 0.0003 indicating that, if the release is indeed diffusion controlled, He can be neglected. For perspective, if all of the He from alpha decay was released over 10,000 years into a fuel pin with an initial fill pressure of 465 psia, and 20% fission gas release, the internal pressure would be 25% higher than if this component of the gas mixture were ignored. It should also be remembered that more than half of the He from alpha decay will be generated when the cladding is below 150°C (i.e., after 1,000 y). Post-disposal He release is therefore expected to be insignificant as a factor affecting cladding failure.

According to Peehs and his co-workers, releases of Cs and I during irradiation are similar to releases of fission gases into the fuel rod void space, which are typically 1 to 4 % of inventory even at burnups as high as 56 GWd/MTU. Measurement of transient releases of Cs and I during heating of spent fuel to temperatures of up to 800°C resulted in fractional releases of $<0.01\%$ of the inventory (Peehs et al., 1986a).

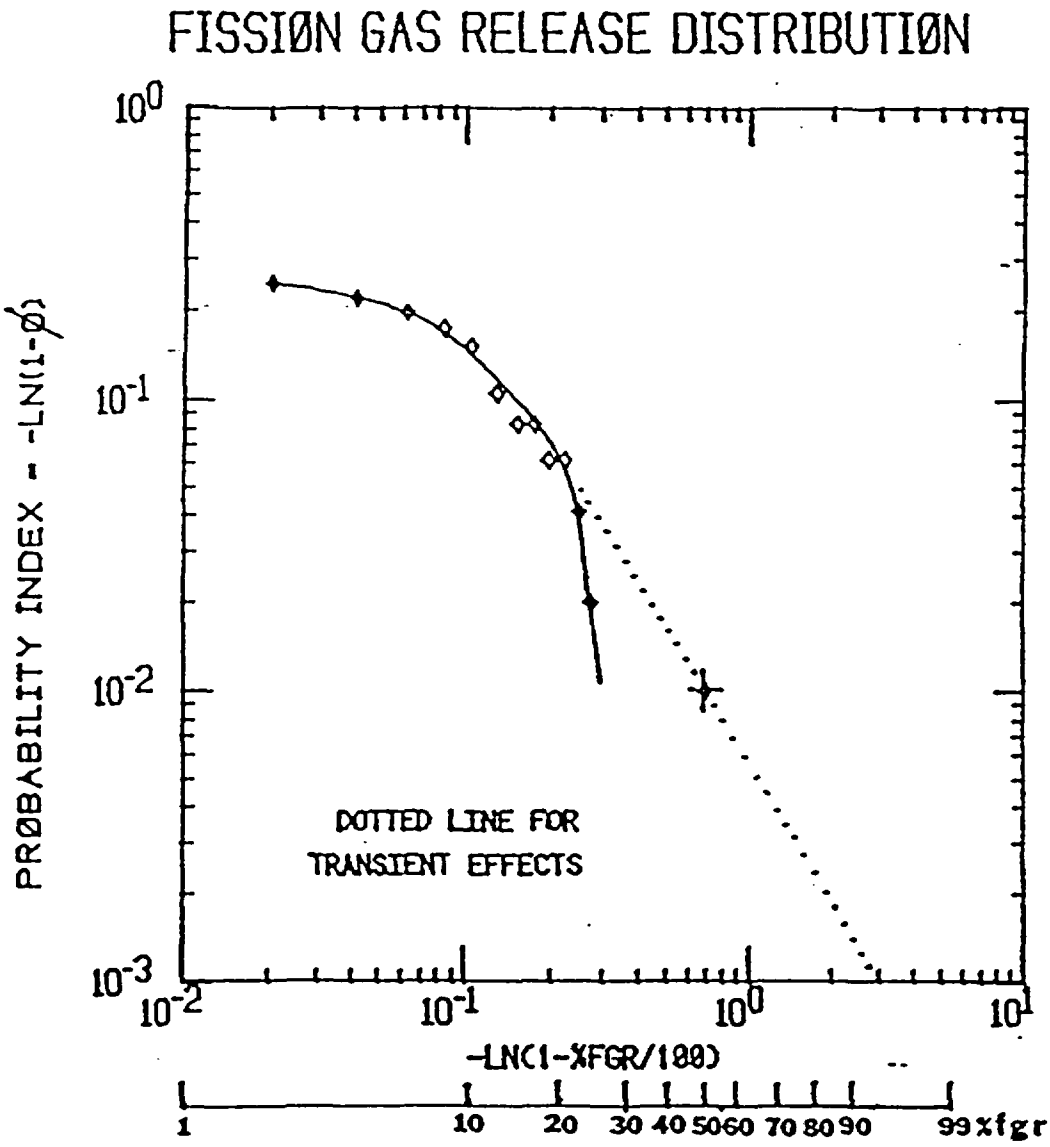


Figure 4.5. Fission Gas Release Probability Distribution Based on Prepressurized Pwr Fuel Rods (EPRI 1989).

Since uncertainty exists as to the actual fission gas release, a probability distribution should probably be assigned to this parameter with the upper limit set at about 50%. The approach used by EPRI seems appropriate and consistent with other data (EPRI 1989).

### 4.3.2 Cladding Stress

The tangential or hoop stress ($\sigma_\theta$) in a thick-walled cylinder subject to internal pressure $p_i$ and external pressure $p_o$ is given by the expression:

$$\sigma_\theta = -\frac{a^2 b^2 (p_o - p_i)}{b^2 - a^2}\frac{1}{r^2} + \frac{p_i a^2 - p_o b^2}{b^2 - a^2} \tag{21}$$

where a is the inner radius, b is the outer radius and r is the radial position in the cylinder wall (ASME 1953). At the inner wall where the tangential stress is greatest, equation 20 reduces to:

$$\sigma_\theta = (p_i - p_o)\frac{(a^2 + b^2)}{(b^2 - a^2)} - p_o \tag{22}$$

and, when the external pressure is either small relative to the internal pressure or zero, equation 21 becomes:

$$\sigma_\theta = p_i \frac{(b^2 + a^2)}{(b^2 - a^2)} \tag{23}$$

If the thickness of the tube is small compared to the radius ($t/r < 0.1$)(Pescatore and Cowgill 1994), the hoop stress can also calculated by the formula for thin-walled pressure vessels:

$$\sigma_\theta = p_i \frac{a}{b-a} = p_i \frac{a}{h} \tag{24}$$

where h is the cladding thickness. Use of the membrane formula will result in hoop stresses approximately 8% lower than calculated with equation 22. If the average radius [(a+b)/2] is used in the membrane formula, the difference is reduced to approximately 1% for typical fuel element geometries. For the calculations presented here, the average radius was used to determine the hoop stress.

### 4.3.3 Creep Models

#### 4.3.3.1 Empirical Models

Application of the Peehs Model as described in equation 6 yields the temperature-strain relationship shown in Table 4.4. The values presented are based on 10,000 years at each temperature/stress level. Because of the functional relationship for time in equation 6, the strain is not significantly different at 1,000,000 years. In any case, one is dealing with unprecedented extrapolations from short term data. Extrapolations practiced in today's engineering designs are typically tens of years at most. The calculated creep strains even at temperatures as high as 573°K are well below the 1% strain limit originally proposed by Peehs. According to Pescatore and Cowgill 1994, this strain limitation is traceable to Peehs and Fleisch 1986 but that document is apparently not the source for the assumption. The 1% strain limit is mentioned during the Q&A session associated with Peehs et al. 1986b. In fact, in Pescatore and Cowgill 1994, Appendix A, stress-rupture performance data for irradiated Zr-2 and Zr-4 are cited which show several specimens with rupture strains below 1% and in one case as low as 0.01%.[13] (See Appendix B for details.) However, even if the strain limit is set at 0.1%, creep failures are unlikely for the expected temperature and stress regimes.

[13] As described in Yaggee et al. 1980, the specimen which failed at 0.01% strain had a peculiar history. The tubular specimen was initially tested for 50.6 h at 275 MPa and 325 °C without iodine and then 25 mg of iodine was introduced into the sample. Failure occurred almost immediately (i.e., 0.03 h). It is likely that the prior testing had created a crack or enlarged an existing crack and that failure was an example of iodine stress corrosion cracking and not creep rupture. This test should be excluded from any creep rupture database.

Table 4.4 Tensile Creep Strain in Zircaloy Tubing after 10,000 Years
(based on Peehs et al. 1986b)

| Temperature (K) | Hoop Stress (MPa) | Creep Strain (%) |
|---|---|---|
| 323 | 43.1 | 0.002 |
| 348 | 46.4 | 0.003 |
| 373 | 49.7 | 0.004 |
| 398 | 53.1 | 0.006 |
| 423 | 56.4 | 0.009 |
| 448 | 59.7 | 0.013 |
| 473 | 63.1 | 0.020 |
| 498 | 66.4 | 0.033 |
| 523 | 69.7 | 0.056 |
| 548 | 73.1 | 0.103 |
| 573 | 76.4 | 0.208 |

Einziger reported the results of creep tests on irradiated fuel rods from the Turkey Point Unit 3 reactor at 323°C and a hoop stress of 145 MPa for up to 2101 h. The maximum measured strain was 0.157% (Pescatore and Cowgill 1994). Under these conditions, the Peehs equation (i.e., equation 6) would have predicted 0.18% strain. In another test by Einziger at 482°C and 49.5 MPa for 4,652 hours, the measured hoop strain was 1.65% while the strain calculated from equation 6 was 1.85%. This is surprisingly good agreement considering that the metallurgical histories of the samples were not identical.

Times to rupture based on Mayazumi and Onchi's Larson-Miller correlation (equation 11) are presented in Table 4.5. It can be seen that even at cladding temperatures of 573°K, rupture times are in excess of one million years. This is qualitatively consistent with the Peehs formulation where calculated strains are on the order of 0.29% over the same time period and the fact that failure strains are expected to be $>1\%$.

Table 4.5. Predicted Creep Rupture of Unirradiated Zircaloy-4[a]

| Temperature (K) | Hoop Stress (MPa) | Rupture Time (y) |
|---|---|---|
| 373 | 49.7 | 4E+27 |
| 398 | 53.1 | 9E+23 |
| 423 | 56.4 | 6E+20 |
| 448 | 59.7 | 9E+17 |
| 473 | 63.1 | 3E+15 |
| 498 | 66.4 | 2E+13 |
| 523 | 69.7 | 2E+11 |
| 548 | 73.1 | 2E+9 |
| 573 | 76.4 | 6E+7 |

a - Based on Mayazumi and Onchi's Larson-Miller correlation (Equation 11).

Mayazumi and Onchi's creep strain data (equation 10) are compared with Peehs' creep strain data (equation 6) and Matsuo's creep strain data (equation 16) in Figure 4.6. From this figure it can be seen that for temperatures of up to about 480 K (207°C), the Peehs correlation is more conservative (i.e., predicts higher strains than does Mayazumi and Onchi's or Matsuo's model), but in any case the strains are small. Above 480 K, Mayazumi and Onchi equation 10 predicts substantially higher creep strains. The Matsuo equation predicts the lowest total strain.

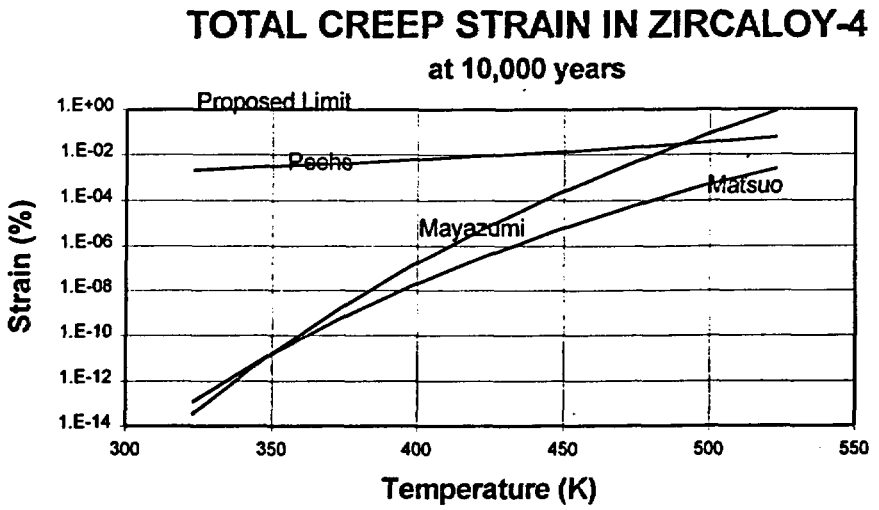


Figure 4.6. Creep Strain in Zircaloy Fuel Rod Cladding after 10,000 Years as a Function of Temperature.

Given the above, it is expected that creep failures (based on a 1% strain limit) will not occur during disposal if the cladding temperature does not exceed about 525°K (252°C) for the most conservative creep model (i.e., Mayazumi and Onchi, equation 10).

To illustrate the sensitivity of the creep rate to possible uncertainties in various experimentally derived parameters, the activation energy (272,000 J/mole), the stress multiplier in the *sinh* term (1130) and the exponential in the *sinh* term (2.1) in equation 16 from Matsuo 1987 were each decreased 25% from the values in the equation developed by the author. The results, presented in Figure 4.7, indicate that the creep rate is highly sensitive to the value of the activation energy while reductions in other parameters contribute only small changes in the creep rate.

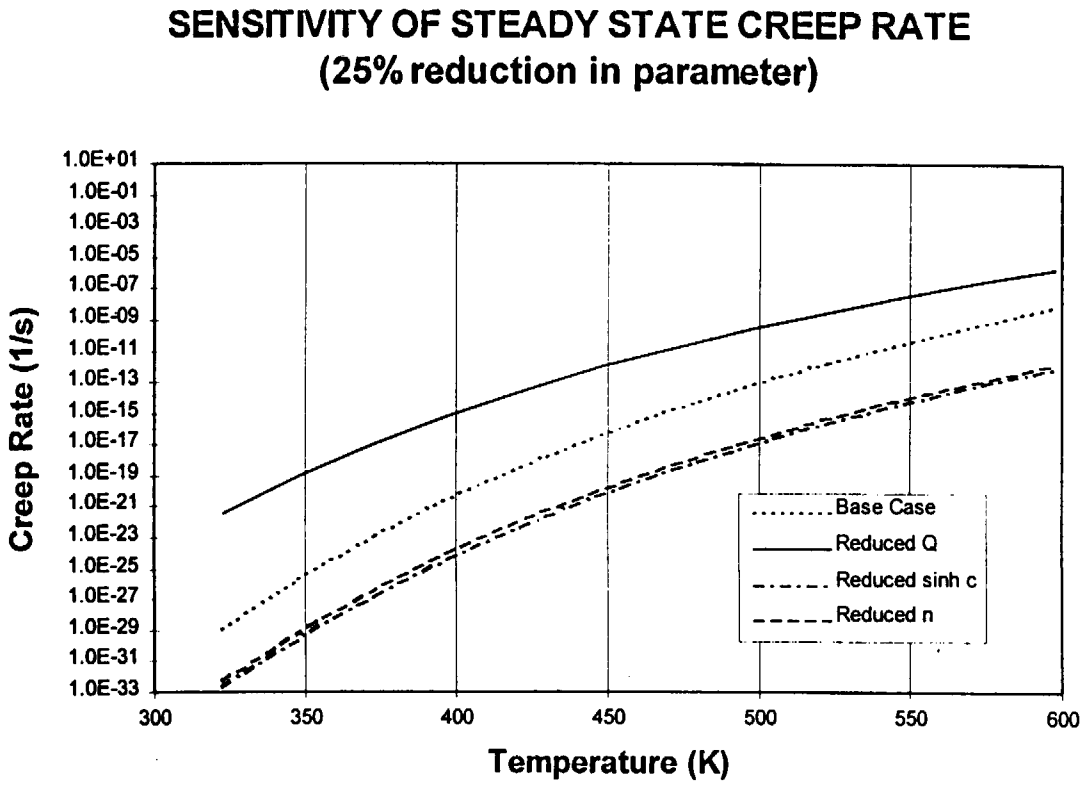


Figure 4.7. Effect of Parameter Reductions on Creep Rate Derived by Matsuo.

### 4.3.3.2 Mechanistic Models

As discussed in Section 3.3.1, grain boundary sliding is the dominant creep deformation mechanism predicted by Chin et al. This ultimately causes rupture by diffusion-controlled cavity growth of voids (DCCG) at the grain boundaries for the range of temperatures and stresses expected in spent fuel elements. Pescatore et al. 1990 and McCoy and Doering 1994 have pointed out that DCCG is particularly sensitive to cavity spacing ($\lambda$). Changing $\lambda$ from $5 \times 10^{-6}$ m to $1.25 \times 10^{-5}$ m increased the time for 15% grain boundary decohesion from two years to more than 100 years. Table 4.6 and Figure 4.8 compare the time to failure for DCCG based on model parameters from Chin and Gilbert 1989 and from McCoy and Doering 1994 as summarized in Table 4.7. The Chin parameters are less conservative than those used by McCoy, although in either case the failure times are greater than about $10^5$ years below 473 K (200°C). Using the temperature distribution described in Section 4.2 above, the fractional life based on the Chin parameters is 0.0011 and based on the McCoy parameters is 0.0092.

Table 4.6. Creep Failure Times for Diffusion Controlled Cavity Growth as Predicted by Chin and Gilbert and by McCoy and Doering

| Temperature (K) | Hoop Stress (MPa) | Time to Failure (y) | |
|---|---|---|---|
| | | Chin | McCoy |
| 323 | 43.1 | 1.39E+15 | 4.98E+11 |
| 348 | 46.4 | 1.28E+13 | 1.50E+10 |
| 373 | 49.7 | 2.23E+11 | 7.20E+08 |
| 398 | 53.1 | 6.44E+09 | 5.07E+07 |
| 423 | 56.4 | 2.83E+08 | 4.89E+06 |
| 448 | 59.7 | 1.76E+07 | 6.12E+05 |
| 473 | 63.1 | 1.47E+06 | 9.53E+04 |
| 498 | 66.4 | 1.57E+05 | 1.79E+04 |
| 523 | 69.7 | 2.09E+04 | 3.95E+03 |
| 548 | 73.1 | 3.33E+03 | 9.98E+02 |
| 573 | 76.4 | 6.23E+02 | 2.85E+02 |

Table 4.7. Comparison of Parameters Used by Chin and McCoy to Estimate Failure Times Based on DCCG

| Parameter | Chin | McCoy |
|---|---|---|
| C (or n)-constant | $2.525 \times 10^{-3}$ | $2.355 \times 10^{-3}$ |
| l (or $\lambda$)-average cavity spacing (m) | $2.6 \times 10^{-6}$ | $10 \times 10^{-6}$ |
| Grain boundary diffusion coefficient ($m^2/s$) | $3.89 \times 10^{-6} \exp(-175000/RT)^a$ | $5.9 \times 10^{-6} \exp(-131000/RT)^a$ |
| $\delta$-grain boundary width (m) | $1.6 \times 10^{-8}$ | $9.69 \times 10^{-10}$ |
| m-non-dimensional microstructural factor | 1 | 0.164521 |

a - activation energy in J/mole

A note on the grain boundary diffusion coefficient in Table 4.7 is in order. The value chosen by McCoy and Doering was the most conservative of the several values quoted in their paper. At 300°C (573 K), the diffusivity used by Chin et al. is 15,000 times greater than that used by McCoy and Doering. The grain boundary diffusion coefficient used by McCoy is taken from a publication by Garde, et al., 1978. Garde et al. noted that the activation energy for self-diffusion in alpha-Zircaloy reported by others ranged from approximately 218 to 282 kJ/mole near 840°C. They concluded that the lower activation energy for zirconium diffusion (based on work by Lyashenko et al.) was more appropriate for material undergoing plastic deformation. They then adjusted this value (i.e. 218 kJ/mole) by a factor of 0.6 to convert from volume (lattuce) diffusion to grain boundary diffusion. This resulted in the diffusion coefficient quoted by McCoy in Table 4.7.

Use of the Chin mechanistic model with either set parameters results in substantially shorter creep lives than would be predicted by any of the empirical models discussed above.

Additional discussion on the modeling of Zircaloy creep is provided in Appendix D.

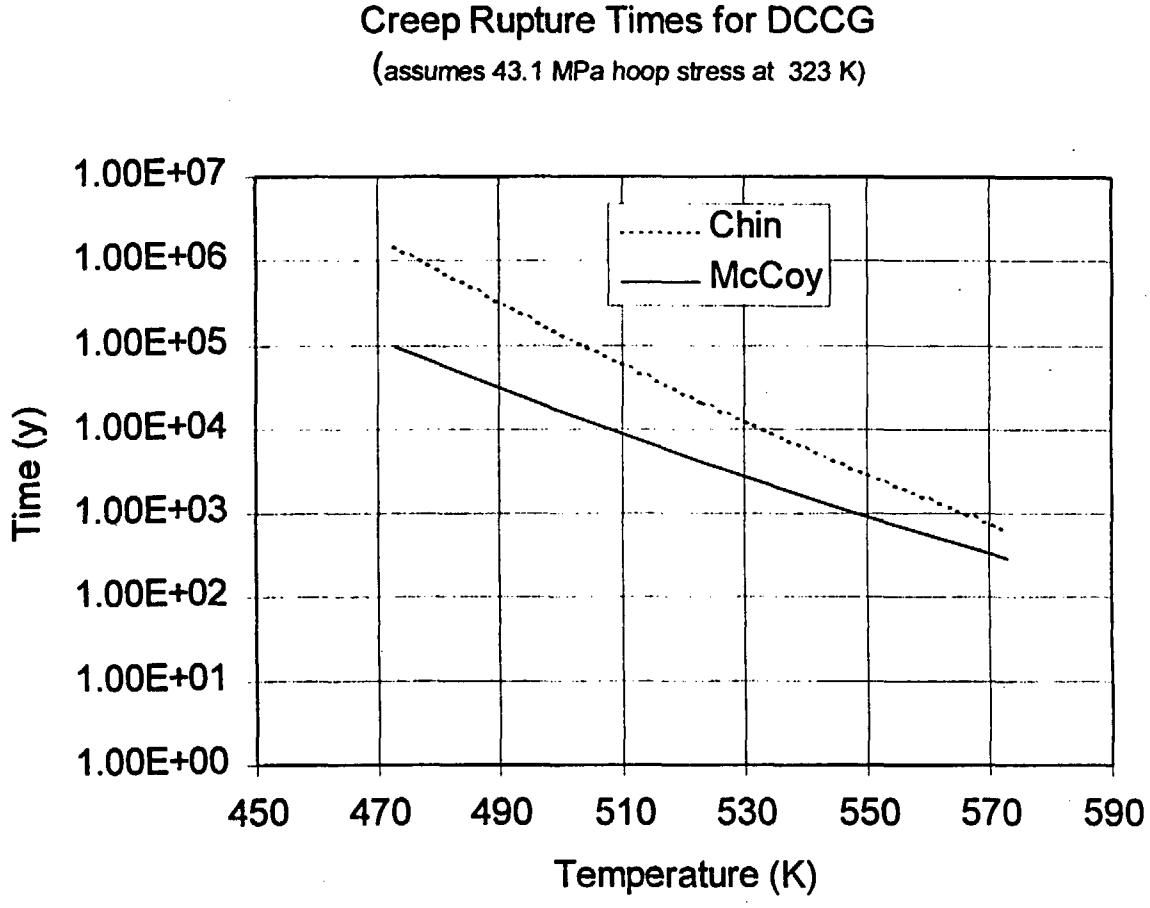


Figure 4.8. Creep Rupture Times for Dccg Based on Input Parameter Assumptions in Table 4.7.

## 4.4 DELAYED HYDRIDE CRACKING

The occurrence of delayed hydride cracking (DHC) is independent of whether or not the waste package wall has been penetrated. Also, DHC failure will not occur in rods with previously-penetrated cladding because internal pressure will already have been relieved.

Based on the approach outlined in Section 3.4, the crack depth (W) and the stress concentration factor ($K_I$) were calculated for various times and temperatures. Results are summarized in Table 4.8. It can be seen that in every case the calculated values of $K_I$ are well below the critical stress concentration factor of 10 Mpa•$m^{0.5}$ proposed by Puls, et.al. ig82.. This situation does not change appreciably even if the times are extended to $10^6$ years and the temperatures to 623 K (350°C).

Table 4.8. Predicted Crack Depths and Stress Concentration Factors for Delayed Hydrogen Cracking in Zircaloy Cladding (Critical Stress Concentration = 10MPa•$m^{0.5}$)

| T (K) | Sigma (MPa) | Crack Depth (m) | | | Stress Concentration (MPa.$m^{0.5}$) | | |
|---|---|---|---|---|---|---|---|
| | | 100y | 1000y | 10000 y | 100y | 1000y | 10000y |
| 323 | 43.1 | 8.76E-14 | 2.77E-13 | 8.76E-13 | 1.6E-05 | 2.84E-05 | 5.06E-05 |
| 348 | 46.4 | 1.12E-12 | 3.54E-12 | 1.12E-11 | 6.15E-05 | 0.000109 | 0.000195 |
| 373 | 49.7 | 1.02E-11 | 3.21E-11 | 1.02E-10 | 0.000199 | 0.000353 | 0.000628 |
| 398 | 53.1 | 6.99E-11 | 2.21E-10 | 6.99E-10 | 0.000557 | 0.00099 | 0.00176 |
| 423 | 56.4 | 3.83E-10 | 1.21E-09 | 3.83E-09 | 0.001384 | 0.002461 | 0.004376 |
| 448 | 59.7 | 1.74E-09 | 5.49E-09 | 1.74E-08 | 0.003119 | 0.005546 | 0.009862 |
| 473 | 63.1 | 6.71E-09 | 2.12E-08 | 6.71E-08 | 0.006478 | 0.01152 | 0.020486 |
| 498 | 66.4 | 2.26E-08 | 7.16E-08 | 2.26E-07 | 0.01252 | 0.022264 | 0.039592 |
| 523 | 69.7 | 6.8E-08 | 2.15E-07 | 6.8E-07 | 0.022773 | 0.040497 | 0.072015 |
| 548 | 73.1 | 1.85E-07 | 5.84E-07 | 1.85E-06 | 0.039363 | 0.069998 | 0.124475 |
| 573 | 76.4 | 4.6E-07 | 1.45E-06 | 4.6E-06 | 0.064908 | 0.115425 | 0.205258 |

Stress concentrations at 10,000 years were more than an order of magnitude below the assumed critical stress of 10 MPa•$m^{0.5}$ at a temperature of 573 K (300°C). Since the calculated stress concentrations decrease with decreasing temperature, even if there is a two order of magnitude uncertainty in the critical stress concentration, DHC will not occur in 10,000 years at temperature

below 523 K (250°C). Based on the profiles presented in Figures 4.1, and 4.3, the hottest fuel rods in a waste package should fall below this temperature in 10 years or less.

The crack depth equation (equation 17) has an experimentally determined constant in the exponential function. The uncertainty associated with the exponential constant in that equation (i.e., 2.291 x$10^4$) is unknown, but if it is less than ±20%, the crack depth (W) would not exceed the wall thickness and actual stress concentration ($K_I$) would not exceed the critical stress concentration ($K_{IH}$) in 10,000 years at 573 K (300°C).

Based on these considerations it does not appear that delayed hydride cracking will be a significant factor in determining the time at which cladding fails or the amount of fuel exposed over time even when the relevant uncertainties are considered.

## 4.5 FAILURE LEVELS PRIOR TO DISPOSAL

Based on the information in sections 3 and 4 above, it appears unlikely that significant failure mechanisms will be active after disposal which will cause fuel rods to breach for the first 10,000 years of storage. Thus, releases to the accessible environment will in large measure be governed by number of breached rods initially placed in the waste packages. Of course, no releases will occur until pitting corrosion violates the integrity of the waste package. Based on the information developed in Section 2, the following failure levels are expected for commercial reactor fuel rods at the time of disposal:

- In-Service Failures (all types) - <0.05% (Section 2.2)
- In-Service Failures (stainless steel) - 0.2% of total stainless steel, 0.003% of all types (Section 2.2.1)
- Pool Storage Failures - 0 (Section 2.3.1)
- Dry Storage Failures - 0.03% (Section 2.3.2)
- Consolidation Failures - 0.005% (Section 2.4.1)
- Other Handling Failures - 0.0003% (Section 2.4.2)

Consolidation failures can be eliminated since this burnup enhancement process is not currently practiced.

A failure level of 0.1% at the time of disposal would appear to embrace the observed failure with a margin of safety for unanticipated causes. This parameter can be assigned a probability distribution.

To predict the risks associated with initial rod failures, it is also necessary to estimate whether the failed rods are randomly distributed throughout the waste packages. In the case of the stainless steel rods, the total population of 397,048 rods involves 2,179 fuel assemblies. It was estimated in Section 2.2.1 (see Tables 2.13 and 2.14) that a maximum of 342 fuel assemblies will contain defective rods. Since Yucca Mountain plans to use 7,586 waste packages (based on 63,000 MTU of commercial fuel weight and about 9 MTU per waste package), the expected probability of that a waste package contains one stainless steel fuel assembly is 0.29 (*i.e.*, 2179/7586) and the probability that the waste package contains a stainless steel fuel assembly with initially failed fuels rods is 4.5% (*i.e.*, 342/7586). Using 0.3 as the probability that percolation water seeps will intercept a waste package (Andrews in DOE 1998a), the probability that the seeps will intercept a waste package with stainless steel rods is about 9% (0.29 x 0.3) and the probability that the seeps will intercept a waste package with initially-failed stainless steel rods is 1.3% (0.045 x 0.3).

In the case of the Zircaloy rods with an expected initial failure level of 0.1%, about 29,500 rods could have failed prior to disposal. On average, each waste package (WP) would contain about 4.2 failed rods. Assuming a Poisson model[14], the probability of finding various numbers of failed fuel rods in a waste package is shown in Table 4.9.[15] From this table it can be seen that there is 1.5% probability that a particular waste package contains no failed rods and there is 99.6% probability that no more than 10 failed Zircaloy rods are in a particular waste package.

[14] It is mathematically more rigorous to assume a hypergeometric distribution, but the use of the binomial distribution and its derivative, the Poisson distribution is a reasonable approximation if the number of trials (4212) is less than 5% of the total (29.5 million) (Freund and Williams 1977)

[15] The Poisson rate constant in Table 4. 8 was based on 7,000 waste packages containing 29.5 million Zr clad rods. Based on recent information the rate constant should be revised slightly to one based on 29.1 million Zr rods in 7,586 waste packages.

Table 4.9. Poisson Process for Number of Failed Fuel Rods per Waste Package

| Assumptions: 0.1% initial failure level and 7000 WP, $\lambda$=29.5E06*0.001/7000=4.213, Prob(x)=$\lambda^x$exp(-$\lambda$)/x! where x is no. of failed rods per WP | | |
|---|---|---|
| **x** | **Prob(x)** | **Cum. Prob(x)** |
| 0 | 0.0148 | 0.0148 |
| 1 | 0.0624 | 0.0772 |
| 2 | 0.1314 | 0.2086 |
| 3 | 0.1845 | 0.3930 |
| 4 | 0.1943 | 0.5873 |
| 5 | 0.1637 | 0.7511 |
| 6 | 0.1149 | 0.8660 |
| 7 | 0.0692 | 0.9352 |
| 8 | 0.0364 | 0.9716 |
| 9 | 0.0170 | 0.9887 |
| 10 | 0.0072 | 0.9958 |
| 11 | 0.0028 | 0..9986 |
| 12 | 0.0010 | 0.9996 |

## 4.6 FUEL SIDE STRESS CORROSION CRACKING

The occurrence of fuel side stress corrosion cracking (FSSCC) is independent of whether or not the waste package wall has been penetrated. It will not occur in fuel rods with previously-penetrated cladding because internal pressure will already have been relieved.

From Figures 4.1 and 4.3, one can observe that the peak cladding temperature falls below 200°C (473 K) after about 100 years. Based on the EPRI analysis summarized in Figure 3.4, FSSCC failures can occur at this temperature/time juncture only if cracks in the cladding exceed about 15% of the wall thickness. The EPRI model assumes 50% fission gas release but EPRI 1989 does not provide sufficient detail as to how this fission gas release level is

converted to a cladding stress, σ. (As shown in Figure 3.4, σ (MPa) = 0.155 T (K), but the basis for the equation is not provided in the source document for the figure.) At 473 K (200°C), the calculated stress using the EPRI equation is 73 MPa. For the present study, assuming a typical PWR fuel rod geometry, an initial He fill pressure of 3.2 MPa, and a burnup of 60,000 MWd/MTU, the calculated fission gas release to generate this stress value is 27%. Taken at face value, the EPRI model would appear to be non-conservative in that it apparently underestimates the stress for a given fission gas release level. However, if one assumes a value of 3 MPa•$m^{½}$ as the threshold stress intensity factor (Pescatore and Cowgill 1994), and applies Equation 18 for a crack with a depth that is 15% of a $0.635x10^{3}$ m thick cladding, a stress of 245 MPa would be required to cause failure. The maximum expected stress based on the Figure 4.1 "Best Estimate" temperature profile is 70 MPa.

It is also noteworthy that there is only a 4% probability that fission gas release will exceed the 27% level as determined from the model presented in Figure 4.5. Thus, it appears that FSSCC should not be a significant contributor to post-disposal failures based on expected fission gas releases and a threshold stress intensity factor of 3 Mpa•$m^{½}$ and the assumed temperature profile.

## 4.7 CLADDING AND FUEL OXIDATION

Oxidation of the cladding cannot begin until the waste package is breached. If the waste package is breached immediately (i.e., a juvenile failure occurs at time zero) the maximum cladding temperature, based on Figure 4-1 ("Best Estimate" ), is about 250°C. At this temperature, 2,800 years would be required to oxidize 25% of the cladding thickness under isothermal conditions (see Table 3.1). Since the temperature is constantly decaying, this estimate is clearly bounding. If the initial juvenile waste package failure occurs after 1,000 years, as is proposed in the 1998 Viability Assessment, then the temperature will have already decayed to about 150°C before breach and, therefore, cladding oxidation virtually ceases.

Oxidation of the fuel cannot occur until the waste package and the fuel cladding are breached. The worst case would be one where waste package breach occurs at time zero and the breached waste package contains fuel pins with pinhole defects. Under these circumstances, and assuming the "Best Estimate" temperature distribution from Figure 4.1, a crack would be initiated and the

cladding would unzip as is indicated in Table 3.2. Based on the information in Table 4.9, there is a 99.5% probability that the waste package would contain no more than 10 initially failed rods. If waste package breach does not occur until 1,000 years, the peak cladding temperature (Fig. 4.1) will have fallen to about 150°C. At that temperature, crack initiation due to $UO_2$ oxidation will not occur in less than 30,900 years (see Table 3.2).

## 4.8 PROPOSED CONCEPTUAL MODEL FOR CLADDING PERFORMANCE

Based on the information presented here, the following conceptual model is proposed for assessing the role of cladding as a long-term barrier to radionuclide release.

1. The repository contains 4,604 PWR waste packages with 21 assemblies and 4,851 fuel rods per waste package and 2,982 BWR waste packages with 44 assemblies and 2,400 fuel rods per waste package.

2. Creep, delayed hydride cracking, and fuel side stress corrosion cracking are potential cladding failure mechanisms regardless of whether or not the waste package has been breached. The extent, if any, to which these processes occur depends on the cladding temperature profile. Cladding corrosion, cladding oxidation, fuel oxidation, and mechanical rupture due to rock falls can occur only after the waste package fails. As modeled here, cladding corrosion and mechanical rupture are not dependant on the cladding temperature, but cladding and fuel oxidation are.

3. No releases can occur until the waste package is breached. The time at which this occurs depends on assumptions as to the timing juvenile failures and rate of corrosion penetration.

4. It is unlikely that any releases can occur until a fuel pin becomes immersed in water. (Gaseous fission products such as I-129 will, of course, be released from any defective fuel pins when the waste package is breached.) Some sort of vapor phase transport might also be postulated but that is not considered here.

5. If all the cladding in the failed waste package is below 100°C, then any failed rods can fill with water as soon as they become inundated. Complete inundation can only occur if penetration of the package occurs near the top. If failure occurs at some lower point on the circumference, gravity will prevent all of the rods from becoming inundated. Thus, for any significant radionuclide leaching from the fuel to occur, a bath tub model should be employed.

6. Waste package penetration can occur near the end of the waste package where the fuel rod cladding is below 100 °C even though, based on the axial temperature gradient, fuel near the center will have a cladding temperature above the boiling point of water. In this case, the interior of the waste package can fill with water provided that the rate of influx is greater than the rate of evaporation. If the rate of influx is not greater than the rate of evaporation, it is still possible for some portion of the rods near the bottom of the waste package to become inundated.

7. Even if some or all of the rods become inundated, water will not necessarily enter a defective fuel rod if local temperature at a defect exceeds the boiling point. Most proposed post-disposal failure mechanisms are highly temperature- and stress-sensitive. If any failures occur, they will be located at the hottest point on the fuel rods. Failure will relieve the internal pressure eliminating the driving force for further failure. Boiling will prevent ingress of water through such defects until the local temperature falls below 100 °C even though the fuel rods are inundated.

8. Even though the cladding temperature at the defect falls below 100°C, water could have difficulty entering the fuel pin and leaching radionuclides from the $UO_2$ (or its transformation products) until the $UO_2$ surface temperature has dropped below 100 °C, as well. When the $UO_2$ surface cools to below 100 °C, it will be accessible to leaching. Conceptually, not all of the $UO_2$ surface will immediately be available for leaching. Even though the outer surface of the hottest pellets has cooled to less than 100°C, the interior fracture surfaces will be at higher temperatures for some fraction of the pellets due to volumetric heat generation, thereby potentially limiting the surface area available for leaching. However, based on an initial heat output of 0.98 kW/MTU for 26-year-old fuel irradiated to 39 GWd/MTU for a 21-assembly PWR package (per TSPA 95) and 9 MTU per waste package, the thermal gradients across the fuel cladding and within the $UO_2$ are less than 1°C. As such, it is reasonable to assume that, once the cladding has cooled to 100 °C, all of the available $UO_2$ surface will also be at the same temperature.

9. The situation with pre-disposal breaches is likely to be different for some fraction of the rods. Many pre-disposal defects are the result of debris induced fretting which typically occurs at the relatively cool bottom ends of the fuel pins. Assuming that the fuel in this region is below 100° C at the time of waste package inundation, water can immediately enter through the defect and travel along the fuel inside the pin to an extent limited by the axial fuel temperature gradient.

10. Fuel assemblies (not fuel rods) with initial failures are randomly distributed throughout the repository. However, the sensitivity of results to other inventory management schemes should be examined.

11. Transport of radionuclides out of the failed rods with pinhole defects or hairline cracks is by diffusion. Transport of radionuclides from failed rods with gross defects is by advection. All the available surface area in a failed rod is subject to leaching if the maximum cladding temperature is less than 100 °C. Rods with gross defects include (*inter alia*) some of the failed stainless steel rods from LaCrosse and Haddam Neck plus any Zircaloy rods where defect propagation and unzipping occur after disposal.

12. The initial failure level for Zircaloy clad fuel rods is 0.1%. These failure are distributed over 94,838 PWR and 130,875 BWR assemblies. The failures are primarily pinholes or hairline cracks. Based primarily on the author's judgement, it is proposed that 90% of the rods have pin holes or hairline cracks and should be analyzed for radionuclide transport using a diffusion model. The balance of the rods are assumed to larger defects where advection is the proposed transport mechanism.

13. Cladding stresses in BWR fuel rods are a factor of two lower than in PWR assemblies.

14. The Mayazumi and Onchi creep equations for Zircaloy (Equation 10) will be used with a 1% strain limit to estimate the potential for creep failure.

15. The repository will contain 2,179 stainless steel assemblies comprised of 397,048 fuel rods. Of these, 333 are BWR assemblies containing a total of 32,588 fuel rods. There are 239 PWR assemblies containing 652 failed rods and 103 BWR assemblies containing 188 failed rods (54 assemblies with sipping failures containing one failed rod per assembly, 31 assemblies with visible cracks containing two failed rods per assembly and 18 assemblies with gross failures containing four failed rods per assembly).

# 5.0 DOE MODELING APPROACH

In TSPA 1995 (see pp. 5-20 through 5-22) DOE did not take any credit in performance assessment (PA) for retardation of radionuclide release due to the sustained integrity of the fuel rod cladding after disposal. DOE presented the mechanistic equations for deformation and fracture developed by Chin and his co-workers (Chin and Gilbert 1989; Kahn, Madsen, and Chin 1985; Santanum, Ragahaven and Chin 1992; Chin, Khan, and Tarn 1986) but did not use these equations in its PA modeling. The so-called reduced form equations listed in TSPA 1995 contained several numerical errors and were incorrectly stated to calculate rupture times in years (rather than in seconds).

Subsequently, in the 1996 Performance Allocation (TRW 1996) credit for cladding was considered. A Monte Carlo sampling procedure was used to estimate the amount of spent fuel which is exposed as a function of time, based on the following assumptions:

- Log normal distributions were assumed for pin properties and initial conditions
- Clad temperature across the waste package and as a function of time were derived from heat conduction models
- Stress was modified by temperature, helium production, clad oxidation, and creep strain
- The Peehs model was used to estimate creep strain (Peehs, et al. 1986b)
- Allowable creep strain was set at 1%
- Delayed hydrogen cracking was included
- Clad tearing (unzipping) based on Einziger 1994 was used for defective pins exposed to oxidizing conditions
- Waste package failure distributions were taken from TSPA 1995

In TSPA 1995, spent fuel waste package failures were distributed into eight bins each containing 893 packages with discrete bin failure times varying from 2,400 to 7,260 years (i.e. the time at which all waste packages in a bin fail) for the first six bins. Packages in the

seventh bin fail at much later times and packages in the eighth bin never fail. Based on the six bins, the fraction of cladding pins unzipped is summarized in Table 5.1. In these studies, the median initial center fuel rod[16] temperature was either 276 °C or 325°C and was log normally distributed with an error factor (EF) of 1.4 where the EF is the ratio of the 95th quartile to the median[17]. This EF is conservative since the suggested EF for the heat transfer calculations was 1.14 which was then adjusted upward to account for uncertainties in decay heat, humidity, etc. (Siegmann, et al. 1996). This assumed distribution resulted in center fuel rods as hot as 386°C for the lower assumed median temperature and 455°C for the higher assumed median temperature.

Table 5.1. Pin Failure Rate in 1996 Performance Allocation Studies

| Waste Package Group | Median Waste Package Failure Time (y) | Pins Unzipped (%) | |
|---|---|---|---|
| | | 276°C | 325°C |
| 1 | 2399 | 0.62 | 4.83 |
| 2 | 2890 | 0.56 | 4.50 |
| 3 | 3300 | 0.52 | 4.25 |
| 4 | 3760 | 0.44 | 3.65 |
| 5 | 4290 | 0.38 | 3.02 |
| 6 | 7260 | 0.17 | 1.21 |

Based on 83 MTU/acre, no backfill, 0.3 mm/y infiltration rate

Inclusion of the cladding as a barrier resulted in a two-order of magnitude reduction in the mass of Tc-99 released and the cumulative mass of combined radionuclides released as compared to the base case where no cladding barrier was assumed (TRW 1996). However, the cumulative mass of Np-237 released is reduced by less than a factor of 10 because the lower

[16] The center fuel rod is the rod at the center of the waste package, i.e. the hottest rod.

[17] Only the lower median temperature results were actually included in the Performance Allocation.

Np solubility slows its release in the base case even though more fuel is exposed to dissolution. Doses associated with Tc-99 and Np-237 were reduced similarly to the masses released.

DOE has developed a modified approach for the Viability Assessment (VA). Although the details are still evolving as of this date, it appears, based on material presented to the Expert Elicitation Panel in December 1997, that a strain failure analysis will be used assess early failures and a mechanical failure analysis based on rock falls puncturing the waste packages will be used for late times (Siegmann 1997).

For the early strain failures, a statistical model calculates the fraction of a 42,000-pin sample that becomes perforated and is subject to unzipping of the cladding. Boundary conditions are established for each waste package bin based on type, repository location, and percolation rate. Assumptions and modeling procedures to be used in the strain failure analysis include:

- Pins are analyzed for temperature distribution across the waste package
- Pins are Westinghouse 17x17 design with average burnup
- Creep is based on Matsuo 1987 with a 4% strain limit
- Zircaloy surface oxidation after waste package failure is based on Einziger 1994
- $UO_2$ oxidation to $U_3O_8$ to cause splitting of the cladding is based on Einziger 1994[18]
- Error factors (ratio of median to 95th quartile) used to establish uncertainty distributions are:
  - temperature - 1.25
  - strain correlation - 2
  - clad oxidation and unzip - 1.75
  - power history - 1.91
  - stress - 1.4
  - strain failure criterion - 10
  - waste package failure time - 1.5

Based on these considerations, for the design basis (hot) waste package (WP), 3.1% of the pins become perforated and, for the average case, no pins are perforated. In neither case does the cladding unzip as long as the waste package failure time is greater than 100 years. As shown

[18] Later documentation (i.e., DOE 1998) states that $UO_2$ oxidation modeling is based on O'Connell 1997 which is described as similar to Einziger 1994.

in Figure 5.1, the center pin in the design base WP reaches a peak cladding temperature of 327°C within a few years after closure and drops to about 170°C in 200 years; center fuel pin in the average WP reaches a peak of 237°C and declines to about 125°C after 200 years. Backfill is not included in the TSPA-VA reference design (DOE 1998b).

The late-term mechanical failure model assumes than blocks of rubble fall from the roof of the repository, punch holes through fully-degraded waste packages, and rupture fuel rods. Various block sizes and various punch geometries are included. For example, a circular punch could break 21% of the fuel rods but expose only 0.49% of the fuel.

Updated information relative to VA assumptions was presented by Siegmann at the DOE/NRC Technical Exchange held in San Antonio TX on March 17-19, 1998 (DOE 1998). For the TSPA abstraction, the cladding degradation code (CLAD-DEG) calculates the amount of exposed fuel at any time which is input into the RIP code to calculate the radioactive mass flux exiting the waste package. Cladding credit is not included in the base case but will be included in the sensitivity analyses. The fraction of fuel exposed after 10,000 years is between 0.01 and 0.02. The CLAD-DEG code assumes that juvenile cladding failures for Zircaloy fuel pins varies from 0.01 to 3% with the expected value being 0.1%. All of the stainless steel pins (1.15% of the total) are conservatively assumed to have failed prior to disposal. Zircaloy fuel pin hoop stresses are 58 MPa for the hottest rods in an average waste package and 68 MPa for the hottest rods in the design waste packages based on a burnup of 40,000 Mwd/MTU. Creep failures occur in the first 50 years after disposal before the temperature has decayed to levels where creep is no longer an issue. Fuel pins fail only in extreme cases when the temperature exceeds 350°C. However, the fuel pins are not exposed to air until after 8,000 years when WP failure begins (except for those WPs which have experienced juvenile failure.) Creep failures range from 0.01 to 1.5% of the pins with 0.15% being the expected value.

Mechanical failures associated with rock falls do not occur before 30,000 years presumably due the structural integrity of the WP prior to that time. When they do occur, 3.4 to 35% of the pins are assumed to have ruptured with the expected value being 5% ruptures.

Delayed hydride cracking of the Zircaloy cladding was also considered. However, this type of failure should not occur since actual stress intensity factors are less than 1.4 $MPa \bullet m^{0.5}$ as compared to a threshold stress intensity factor of 6.7 $MPa \bullet m^{0.5}$ (DOE 1998).

At the DOE/NRC Technical Exchange of March 1998, crevice corrosion was not included in the cladding degradation model but DOE noted that such a process should not be dismissed without further tests and analyses. As will be described subsequently, DOE has since modified the cladding model to include some form of corrosion degradation.

Cladding credit reduces the dose from all pathways at 20 km by about a factor of 10 as compared to the base case after 100,000 years as shown in Figure 5.2. The dose after 10,000 years is negligible (i.e., $< 10^{-3}$ mrem/y) for both the base case and the cladding credit case. It is presumed that these results (RIP Version 5.18.22, March 4, 1998) did not include juvenile failures since there are no releases in less than 10,000 years. Dose rates are driven by Np-237 releases.

In a subsequent presentation to the Nuclear Waste Technical Review Board Performance Assessment Panel on April 23-24 in Albuquerque NM, DOE described further refinements to the cladding degradation model (DOE 1998a). Juvenile waste package failures are to be included (one package at 1,000 years) as is corrosion of the cladding using a "corrosion model similar to C-22 corrosion."[19] As noted earlier, creep is modeled using the strain versus time equations developed by Matsuo and a 4% strain limit. To select this particular model, DOE conducted a variance analysis of all available data (presumably including Matsuo, Mayazumi and Onchi, Peehs et al., and Einziger et al.) and found that the Matsuo creep equation provided the best fit to all the data. Creep failure was described as not contributing significantly to the exposed fuel area. The revised model is summarized in Figure 5.3. It is apparent that, with the latest modeling approach, the fraction of fuel exposed does not increase significantly until about 100,000 years. The expected dose rate for the base case and the alternative case where cladding is not included are shown in Figure 5.4 (based on RIP Version 5.19). (Note that the base case in Figure 5.4 includes cladding credit whereas the base case in Figure 5.2 assumes

[19] The corrosion is determined by scaling Zircaloy corrosion under similar conditions. The Zircaloy is assumed to be 100 times more corrosion resistant than the C-22 (DOE 1998b). This approach is being used as a placeholder until experimental corrosion data can be developed (Stahl 1998).

no cladding credit) At 10,000 years the cladding credit reduces the dose rate by about two orders of magnitude. This differential is reduced to about one order of magnitude after 100,000 years as corrosion failures accelerate (see Figure 5.3). Comparing Figure 5.2 with Figure 5.4 for case which includes cladding credit, it can be seen that the dose rates are comparable (i.e., about 0.1mrem/y) at 20,000 years. This suggests that inclusion or exclusion of juvenile failures has little effect for times greater than this.

Further modeling changes associated with TSPA-VA Rev. 01 were described at the DOE/NRC Quarterly Technical Meeting on June 18, 1998. Although details were not presented, the

expected initial failures were quoted as 1.25% and the expected failures at 100,000 years were quoted as 3.3% (DOE 1998c).

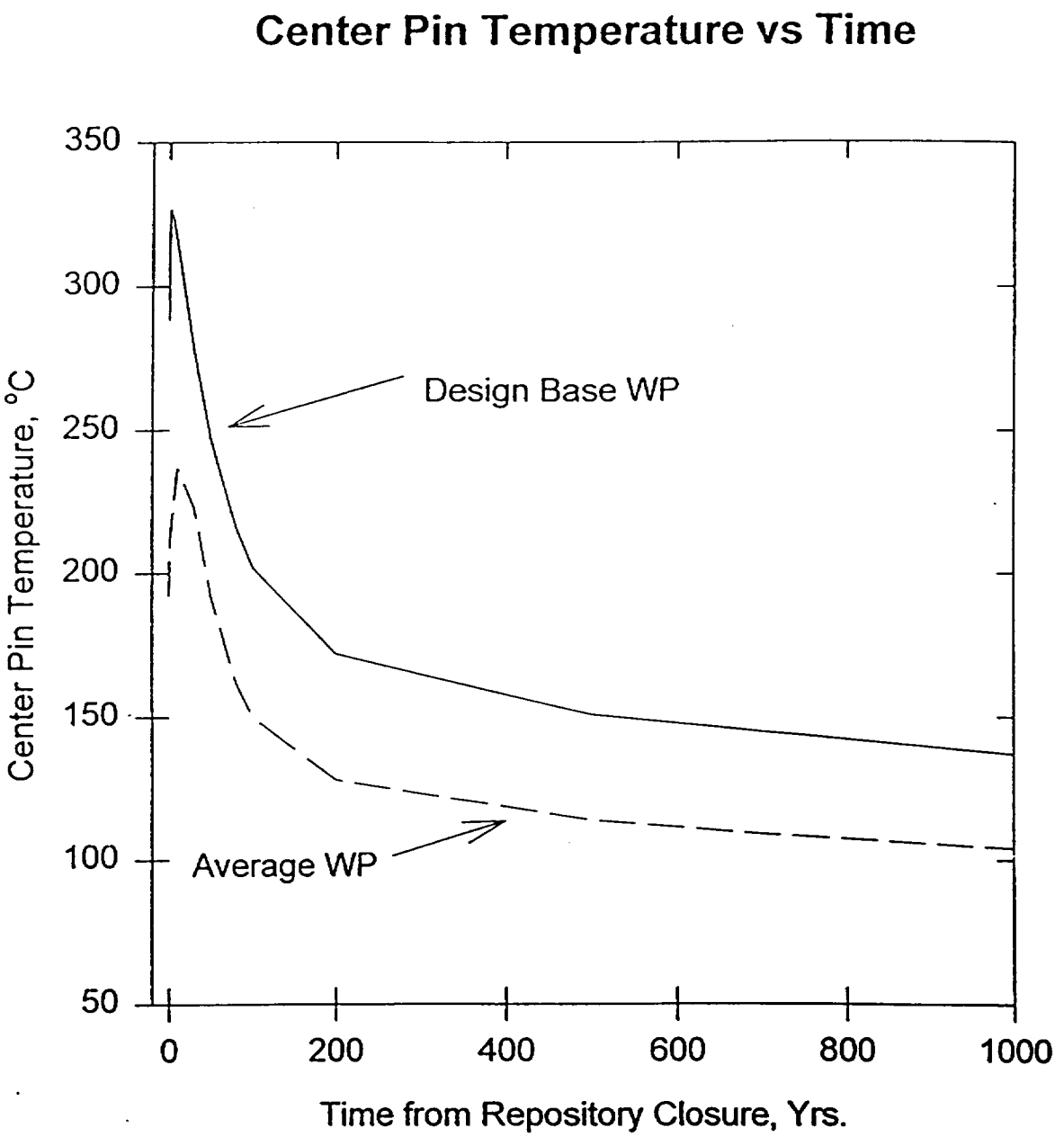


Figure 5.1. TSPA-VA Center Pin Temperature Profiles for Design Base and Average Waste Packages.

# Cladding Credit Case
# 100,000-yr Expected-Value Dose-Rate History

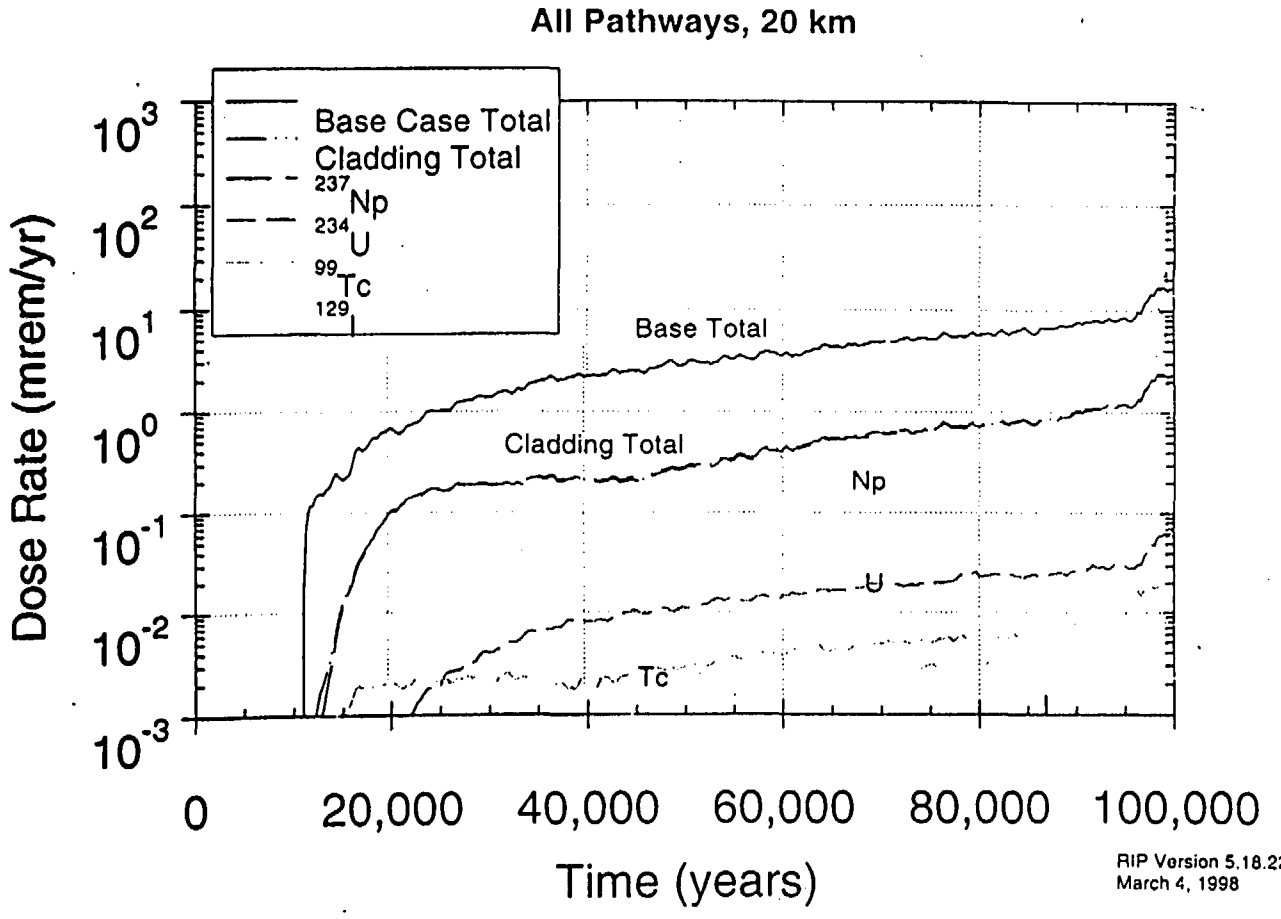


Figure 5.2. Expected Tspa-va Dose Rates for Base Case and for Cladding Credit Case (No Juvenile Failures Included).

# Cladding Degradation

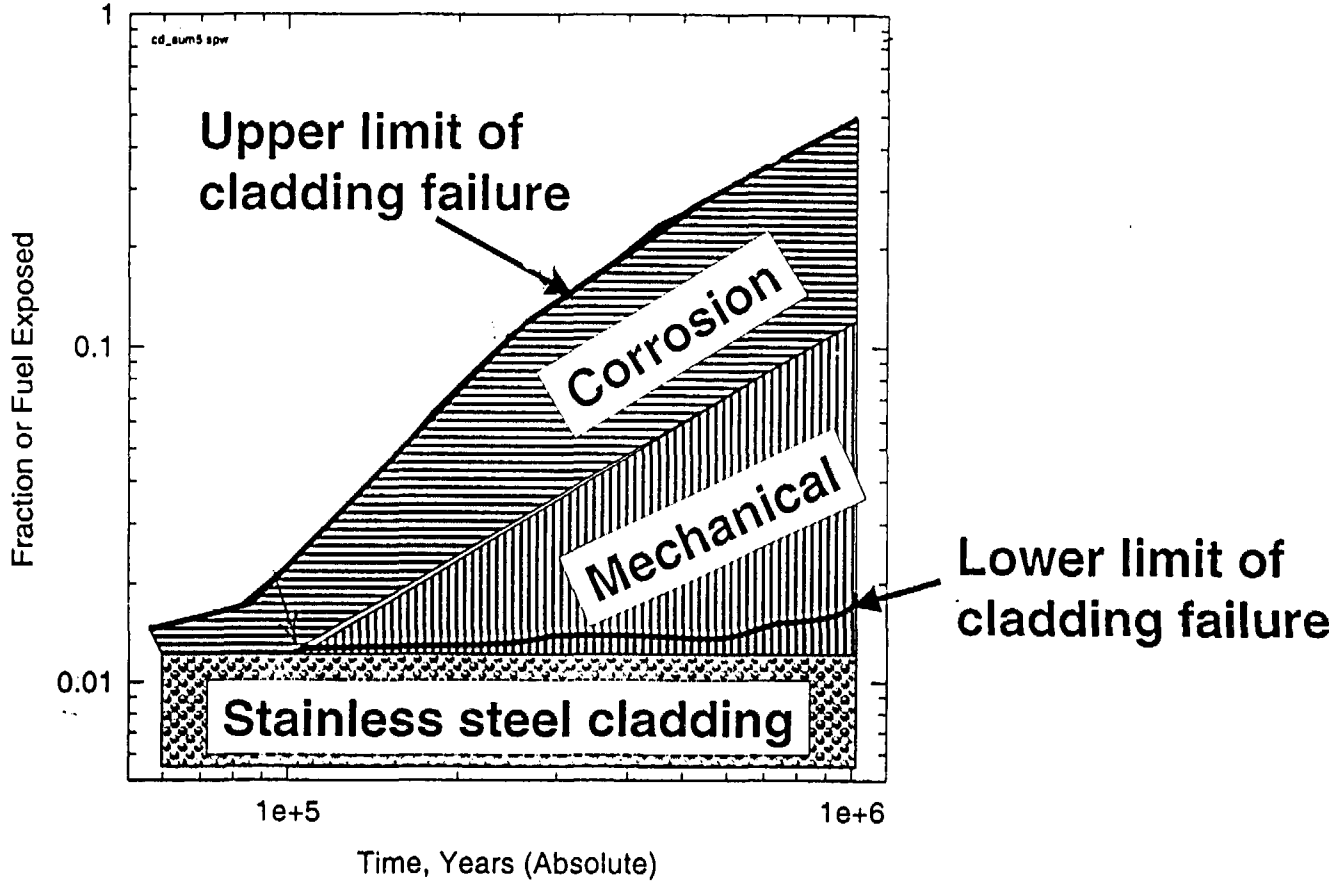


Figure 5.3. Current Tspa-va Cladding Degradation Model.

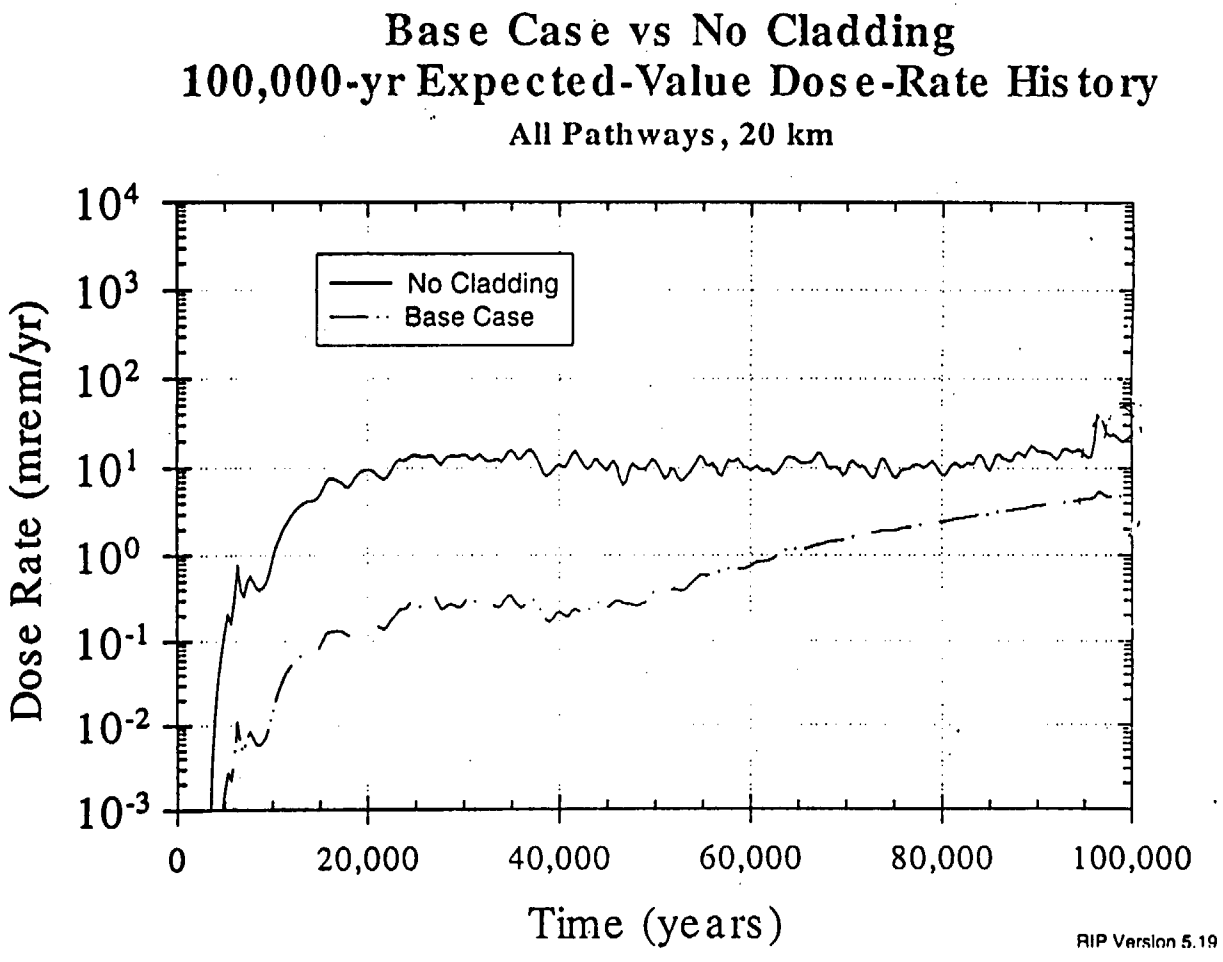


Figure 5.4. Expected Tspa-va Dose Rates for Base Case and Case Where No Cladding Credit Is Assumed (Juvenile Failure Included)

# 6.0 SOURCES OF UNCERTAINTY

As a supplement to discussion of uncertainty in prior sections, additional discussion of the major sources of uncertainty in cladding behavior is provided in this section. Comments on the sensitivity of results to certain parameter variations are also provided.

## 6.1 CREEP PROPERTIES

As shown in Figure 6.1, total creep strains after 10,000 years based the experimental studies and derived creep equations of Peehs et al. (equation 6), Mayazumi and Onchi (equation 10), and Matsuo (equation 16) vary by about one order of magnitude at 500 K (227°C) and about five orders of magnitude at 400 K (127°C). Divergence of model predictions also increases above 500 K (227°C). All three models include contributions from both primary and secondary creep. The creep equation derived by Peehs *et al.* is strictly empirical and the temperature dependency of the creep rate is very flat. Available technical reports do not provide comprehensive documentation of the Peehs experimental approach and detailed results. The creep equations derived by both Mayazumi and Onchi and by Matsuo are based on Dorn's quasi-theoretical model coupled with experimental data.

To develop insight into the uncertainty introduced by each of these three experimentally based creep models, failure levels were estimated for each. Using the time-temperature function (equation 19) presented in Section 4.2 for a population of 10,000 rods and assigning a standard deviation of 0.133 to this function[20], no rods exceeded 1% strain based on the Matsuo creep equation, 5 rods exceeded 1% strain based on the Peehs equation, and 225 rods exceeded 1% strain based on the creep equation of Mayazumi and Onchi (SCA 1997a).

[20] The three-sigma value is 1.4 times the value predicted by Equation 19.

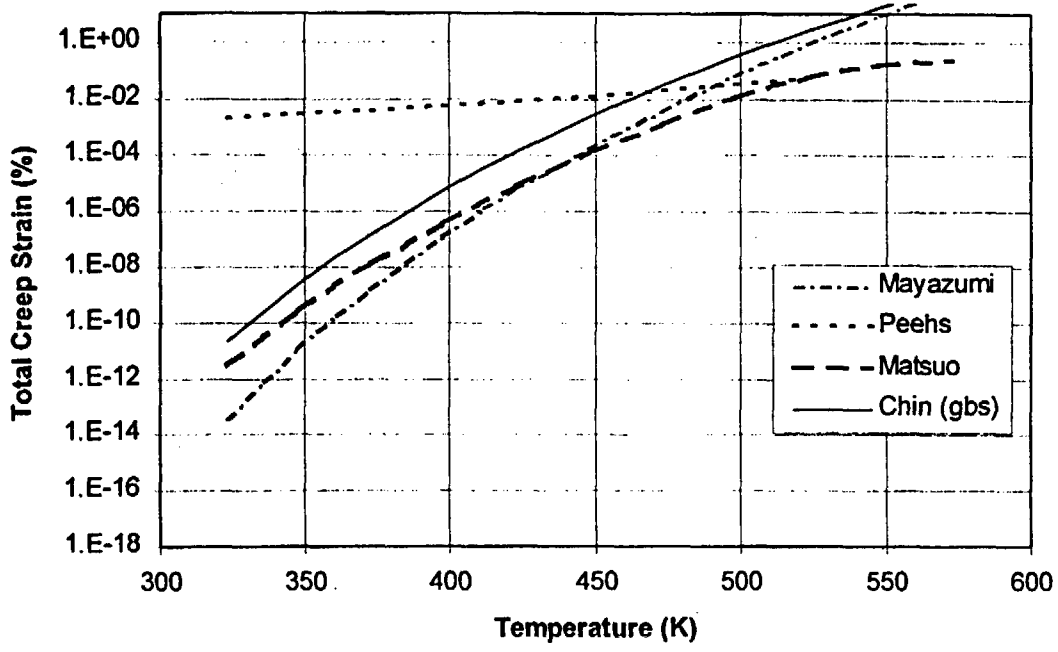


Figure 6.1. Estimated Total Creep Strain in Zircaloy at 10,000 Years Based on Various Empirical and Mechanistic Models.

As discussed in Section 3.3.1 a different approach was taken by Chin and his co-workers who developed a Zircaloy deformation map based on theoretical considerations which assume that different creep mechanisms are dominant under differing stress and temperature conditions. Creep equations (for steady state creep only) are developed for each creep mechanism shown in Figure 3.5. Figure 6.1 also includes the total creep strain based on Chin's model for grain boundary sliding driven by grain boundary diffusion -- the expected creep mechanism under repository storage conditions (i.e., $3.3 < T_m/T < 5.9$ and $-6.94 < \ln(\sigma/E) < -7.68$).[21] The Chin model yields higher creep strains than the experimentally-based correlations developed by Matsuo and by Mayazumi and Onchi for all temperatures considered here. The Chin model also predicts higher creep strains above about 470 K (197°C) than does the Peehs model.

Figure 6.2 compares the steady state creep rates as a function as a function of temperature based on the work of Chin et al,. of Matsuo, and of Mayazumi and Onchi. Peehs and his coworkers did not provide an equation for steady state creep rate but only total strain (i.e., equation 6). Differentiation of Equation 6 to obtain a creep rate results in a complex time-dependent function of questionable physical reality. From Figure 6.2, it can be seen that, at 350 K (77°C), there are about eight orders of magnitude difference between the lowest creep rate (Matsuo) and the highest creep rate (Chin). The difference decreases as the temperature increases and is about two orders of magnitude at 550 K (277°C).

Although grain boundary sliding appears from the deformation map in Figure 3.5 to be the dominant mechanism, the expected conditions of stress and temperature lie close to the boundary defining other mechanisms such as low temperature climb and high temperature climb. These alternative mechanisms are compared in Figure 6.3. From this figure it can be seen that up to about 623 K (350°C), grain boundary sliding produces the maximum creep rate but above that temperature, high temperature climb is dominant.

---

[21] Chin and Gilbert 1989 indicate in Table 2 of that paper that the constant $A_{GBS}$ in the deformation equation for grain boundary sliding has a value of $8.85 \times 10^6$. In Santanum et al. 1992, the value of this constant is quoted as $8.81 \times 10^2$. In none of this series of papers is an adequate source of the parameters used in Tables 3.4 and 3.4 of the present report provided. Discussion with one of the authors and other involved with the work shed no light on the reason for the drastically different values cited for $A_{GBS}$. In the present work, the value of $8.85 \times 10^6$ was used based the assumption that no significant work was done after 1989 and this value appears in other documents prior to that date (e.g. Chin et al. 1986).

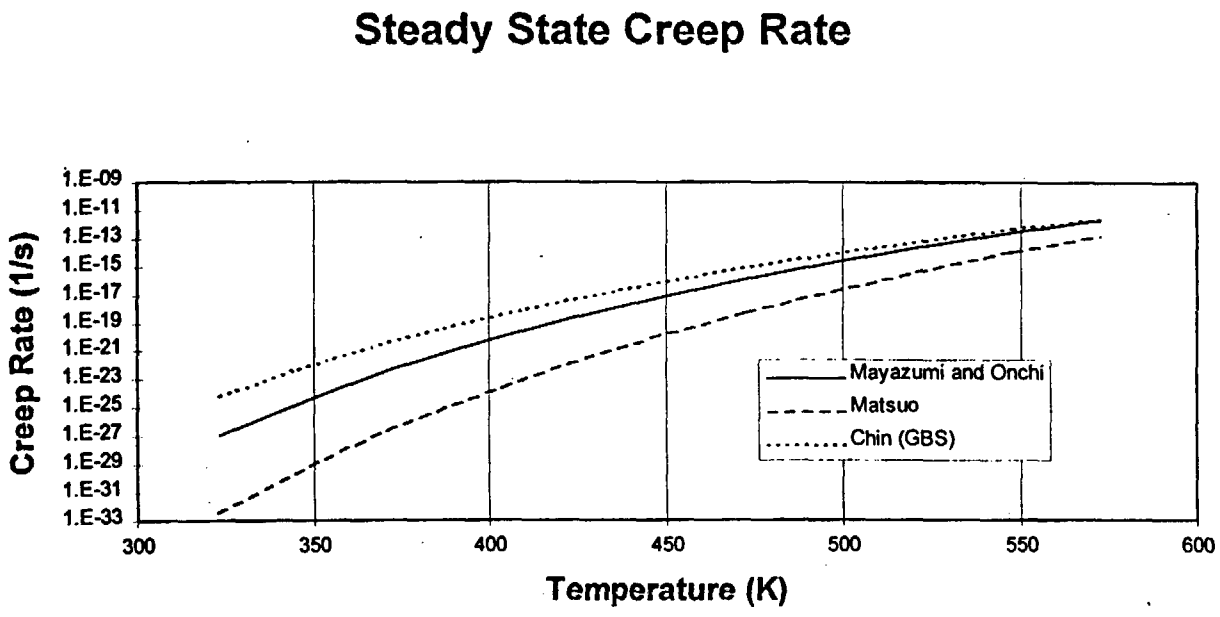


Figure 6.2 Steady state creep rates for Zircaloy as determined by various researchers.

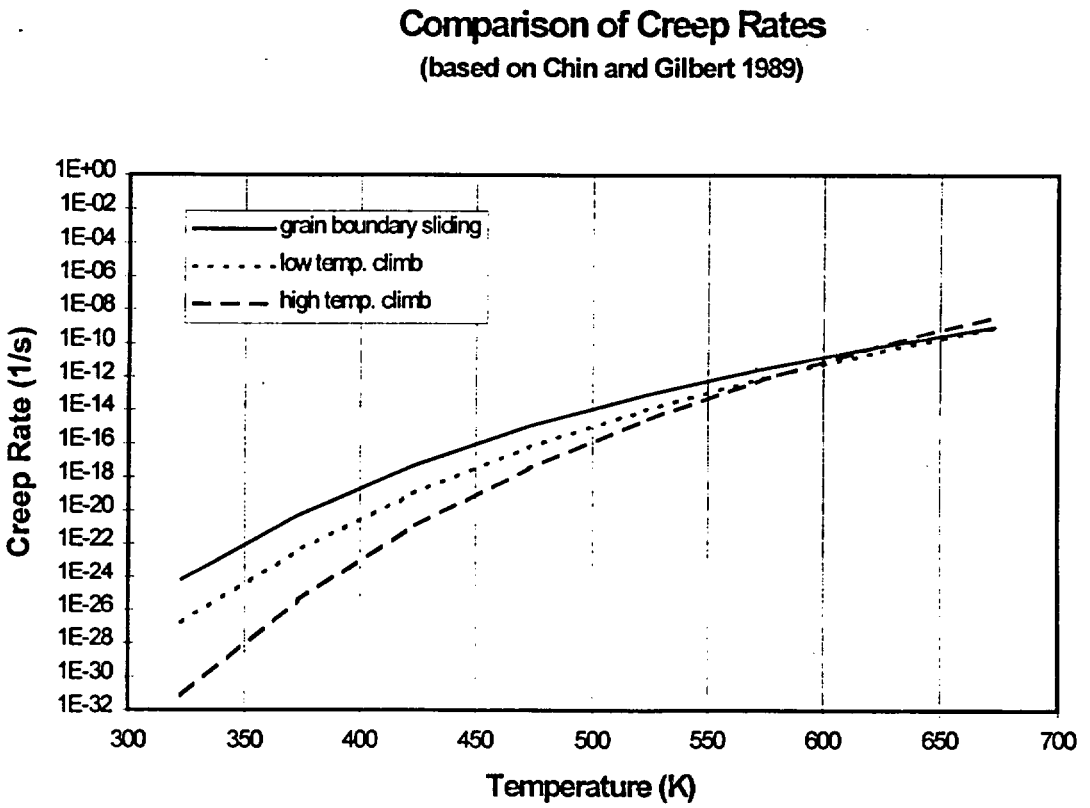


Figure 6.3 Steady state creep rates for various deformation models (based on Chin and Gilbert 1989)

One of the problems with using the quasi-theoretical equations of Matsuo or Mayazumi and Onchi for modeling cladding degradation is that the experimental data were obtained under temperature and stress conditions different from those expected during repository disposal (see Appendix D for additional discussion of this issue). The consequence of this is that the dominant creep mechanism(s) for the range of experimental conditions will be different from the dominant mechanism under disposal conditions. For example, the Matsuo data were obtained under conditions where, according to Chin's Zircaloy deformation map (Figure 3.5), the expected deformation mechanisms are low-temperature and high-temperature climb of dislocations while Mayazumi and Onchi's data were obtained under conditions where high-temperature climb is dominant. Figure 6.4 here shows the experimental temperature ranges and creep strains for these

two investigations and compares the experimentally-predicted strains in one year with those calculated using Chin's model for these two deformation mechanisms. From this figure it can be seen that the Chin high-temperature climb model is in reasonable agreement with the Mayazumi and Onchi experimental results over the experimental temperature range from 577 to 693 K (304 to 420°C). The difference is less than an order of magnitude with the experimental data being higher than the model data. Below 577 K, the Mayazumi and Onchi data show a better correlation with Chin's low-temperature climb predictions, although as noted above, this is not the expected deformation mechanism under the experimental conditions. Comparison of the Matsuo data with the two Chin models over the experimental temperature range of 603 to 693 K (330 to 420°C) shows increasing divergence with increasing temperature.

Since extrapolation of the creep data to lower temperatures where the deformation mechanisms are different from those that existed in the experimental regime is necessary, the selection of the appropriate data set is judgmental and subject to considerable uncertainty. Careful review of the technical papers of Matsuo and of Mayazumi and Onchi suggests that both studies used similar materials, similar experimental methods, and similar data reduction methods (see Appendix C for additional discussion of this comparison). There is no obvious basis to judge that one creep correlation is superior to the other. In the case of the Peehs data, the experimental program is not as transparent and the empirical creep equation has a surprisingly limited temperature dependence. If the Peehs model is rejected for these reasons, the more conservative approach up to about 600 K (327°C) would be to use creep equations based on the Matsuo data set. Above this temperature the Mayazumi and Onchi equations yield more conservative results. As shown in Figure 5.1, the hottest fuel rod in the design WP in the TSPA-VA has a peak clad temperature of 600 K. The cladding would have to remain at this temperature for about 18 years to reach a 1% creep strain based on the Mayazumi and Onchi creep equations. Thus, creep failures assuming a 1% strain limit criterion are likely to involve a very small number of rods.

The number of failed rods will depend on the uncertainty assigned to the cladding temperature of the hottest fuel rod in the design waste package. As discussed in Section 5, DOE has assigned an error factor of 1.25 (ratio of mean to 95th quartile) to this parameter to reflect temperature uncertainty. Based on this assumption, 5% of the hottest fuel rods in the design waste package could have peak temperatures exceeding 750 K (477°C). From the information in Figure 6.3, these rods would fail in less than one year. It is not known what fraction of the total fuel rods

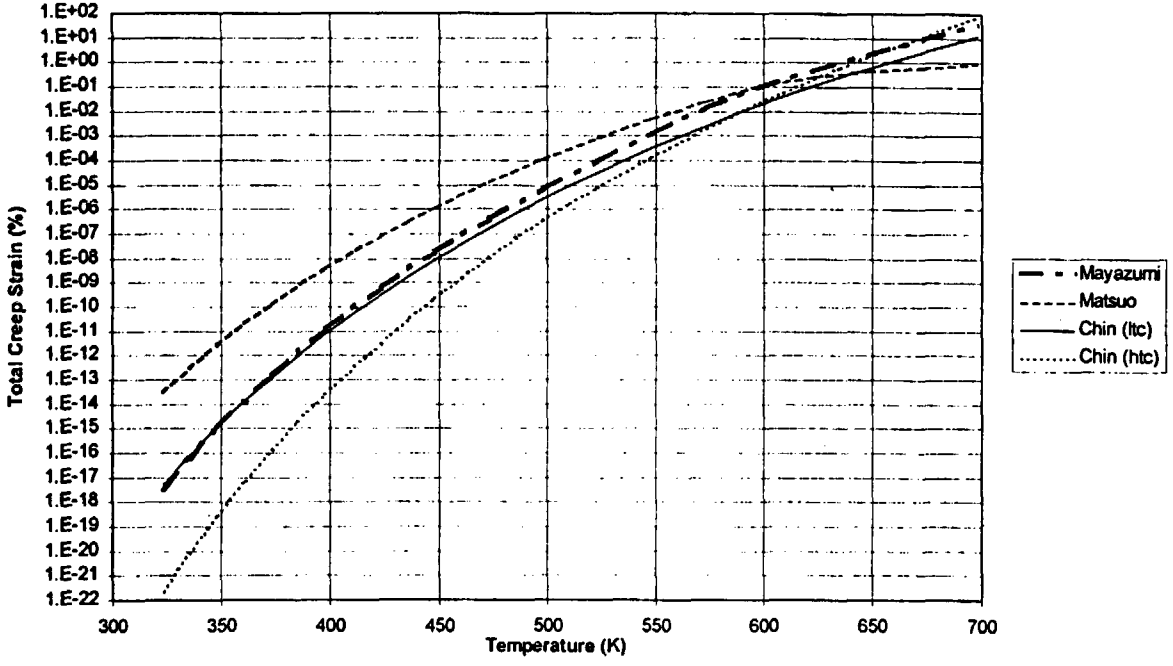


Figure 6.4. Total Creep Strain in One Year Based on Various Creep Models.

would be exposed to such a condition. Applying the same reasoning to the average waste package where the peak temperature of the hottest rod is 510 K (237°C), 5% of the hottest rods in the average waste package could have temperatures exceeding 638 K (365°C). In these rods, a 1% strain limit would be reached in about 1 year based on the Mayazumi and Onchi correlation.

The preceding discussion has assumed that the creep strain limit is fixed at 1%. This value has been suggested by various investigators *(e.g.*, Saegusa *et al.* 1996, Pescatore *et al.* 1990). DOE has proposed a 4% strain limit for the TSPA-VA (see Section 5). Pescatore and Cowgill 1994 have summarized rupture strains in irradiated Zircaloys at temperatures ranging from 565 to 633 K (292 to 360°C) (see Appendix B). Strains at rupture ranged from 0.4 to 11% (neglecting one sample with a peculiar history as discussed in Section 6.4 below). Mayazumi and Murai 1993 conducted post-irradiation creep rupture tests at 633 to 873 K (360 to 600°C) on Zircaloy-4 samples taken from a fuel bundle with a burnup of 47,000 MWd/MTU. Measured rupture strains for the temperature range between 633 and 693 K (360 and 420°C) varied between 3% and 16% and generally increased as the test temperature was increased. It should be noted that the data reported by Pescatore and Cowgill were obtained at high stresses (200 to 550 MPa). There is some information in Mayazumi and Murai which suggests that the rupture strain increases as the stress is reduced. The allowable strain criterion is clearly subject to uncertainty. To reflect uncertainty in this parameter, one can assign it a probability distribution or select a lower limiting strain (say, 0.1%). The Yucca Mountain Project currently uses the former approach and assigns an error factor of 2.0 to this parameter (Siegmann et al., 1996).

As summarized in Table 6.1, the most important uncertain variables affecting creep failure are the creep model, the spatial and temporal temperature distribution and the allowable creep strain.

It should also be noted that the cladding hoop stress in spent BWR fuel rods is substantially lower than in PWR fuel rods at the same fractional fission gas release. Comparing GE BWR/2,3 8X8 fuel assemblies with ABB CENF PWR 16X16 assemblies (see Appendix A for relevant parameters), the stress in the BWR fuel rods is more than a factor of two lower than in PWR fuel rods at the same burnup, cladding temperature, and fractional fission gas release.

Table 6.1. Uncertain Variables Affecting the Creep Failure Incidence of Zircaloy Fuel Rods

| Uncertain Variable | Expected Value | Maximum Value | Minimum Value | TSPA VA Value |
|---|---|---|---|---|
| Allowable Strain | 1% | 16% @ 693 K | 0.4% @ 598 K | 4% |
| Creep Strain Model | Mayazumi and Onchi | Peehs(<470 K); Chin-gbs (>470K) | Matsuo(>430 K); Mayazumi and Onchi (<430K) | Matsuo |
| Clad Temperature (hottest fuel rod) | 585 K[a] | | | Avg. WP - 510 K (±1.25 EF); Design WP - 600 K (±1.25 EF) |

a - SCA 1997b, Appendix G, Fig. 4.1-3 and 4.1-7 (includes effect of backfill)

In the Matsuo creep equations, the strain rate is a function of $\sinh(A\sigma)^{2.1}$. Thus, a decrease in the stress, $\sigma$, by a factor of 2 would reduce the steady state creep rate by a factor of about 4.6. Alternatively, using the Mayazumi and Onchi creep equations where the strain rate is a function of $\exp(B\sigma)$, a two-fold stress reduction would reduce the steady state creep rate by a factor of 2.85. Clearly, creep will be significantly reduced for BWR fuel rods which constitute about 25% of the total fuel rod population scheduled for disposal at Yucca Mountain.

On a more general note, the extrapolation of creep data to thousands of years is unprecedented in engineering analyses.

## 6.2 FISSION GAS RELEASE

Typical fission gas release values measured in commercial fuel elements are less than 10% (EPRI 1989). However, fission gas release of about 50% was observed in some experimental rods subjected to power bumping. Based on these considerations the curve presented in Figure 4.5 is proposed to reflect the uncertainty in this parameter.

## 6.3 FUEL BURNUP

Peak burnups based on 1991 information ranged from approximately 40 to 60 GWd/MTU as shown in Table 4.2. Obviously the mean burnup will be substantially less than this. A rough estimate of the peak to average burnup can be derived from the axial temperature profiles presented in Figure 4.4.

As noted in Section 4.3.1, fission gas production and, hence, fuel cladding stress is a linear function of burnup assuming that fission gas release is independent of burnup. In addition, higher burnup can incrementally alter the creep strength of the cladding. This effect is discussed in Section 6.4 below.

## 6.4 EFFECTS OF IRRADIATION

As discussed in section 3.3.2, Peehs and his co-workers found, in one set of tests at 70 MPa and 380/395°C after exposure to neutron fluences on the order of $10^{20}$ n/cm$^2$, that the creep strain in irradiated material was about half that in unirradiated material while in a second set of tests at 50 MPa and 350°C, after exposure to a neutron fluence of 0.5 to 1 x $10^{22}$ n/cm$^2$, the creep strain for irradiated and unirradiated material was the same at a given time.

Mayazumi and Murai 1993 tested Zircaloy-4 irradiated at neutron fluences of 8-10 x $10^{21}$ n/cm$^2$ at temperatures of 603 to 873 K (330 to 600°C). The creep rate was 0.02 to 0.6 that of unirradiated material but in no case was the rupture strain less than 3%. Irradiation caused rupture to occur at slightly higher temperatures or stresses or slightly longer times than predicted using equations developed for unirradiated material.

Appendix B includes rupture strain data for irradiated Zircaloys as summarized by Pescatore. All these tests were conducted at high stress levels. While the rupture strains generally exceeded 0.4% in one instance a pinhole failure developed at a strain of 0.01%. However, this specimen had a peculiar history (Yaggee et al., 1980). It was first exposed to a stress of 275 MPa at 325°C for 50.6 hours and then 0.79 mg/cm$^2$ of iodine was added to the pressurizing gas to study stress corrosion cracking effects. The specimen ruptured almost immediately. It is likely that a preexisting crack or a crack formed during initial stressing was

responsible for the failure. A companion specimen tested without the initial iodine-free exposure failed after a substantially longer period (500 X) at a strain of 0.1%.

## 6.5 CLADDING TEMPERATURE

Temperature is probably the single most important variable in defining the long-term integrity of the cladding. All of the possible identified failure mechanisms are highly temperature dependent. In order to properly estimate failure rates, the time-dependent spatial temperature distribution within a waste package and throughout the repository must be known. DOE publications on Yucca Mountain offer a variety of temperature distributions. For purposes of this study the waste package temperature history shown in Figures 4.1 and 4.2 taken from the Performance Allocation is used assuming the smeared conductivity model. These curves are based on an areal loading of 83 MTU/acre. As noted in Section 4.6, DOE currently assumes an error factor (EF) of 1.4 for the temperature distribution where the EF is the ratio of the 95th quartile to the median.

## 6.6 INITIAL FUEL ROD FAILURES

The number of failed rods which are initially sealed in the waste packages can affect the rate and quantity radionuclides released to the UZ. Presumably gaseous and volatile fission products will have been released from the defective rods prior to their being sealed in the waste packages. These rods will not be further affected until the waste package is breached by corrosion. Once the waste package is breached, air can diffuse into any defect and begin the oxidize the $UO_2$ fuel pellets. Such oxidation will occur only if the fuel is above 100°C (see Section 3.1). If the temperature is above 100°C, a crack in the cladding may form over time and eventually result in splitting of the cladding along the entire fuel rod length exposing all the fuel in the rod to possible mobilization and transport from the waste package.

As discussed in Section 4.5, the expected failure level for commercial fuel rods is less than 0.1%. However, the number is uncertain. Any distribution should be assigned a reasonably large standard deviation to reflect this uncertainty.

Table 6.2 summarizes the various uncertain parameters relating to initially failed fuel rods and their ranges of values based on the preceding discussion and SC&A estimates. Values proposed by DOE for TSPA-VA are also included.

Table 6.2. Summary of Uncertain Parameters Relating to Initially Failed Fuel Rods

| Uncertain Parameter | Expected Value | Maximum Value | Minimum Value | TSPA-VA |
|---|---|---|---|---|
| Number of Failed Zr rods [a] | 0.1% | 1% | 0.01% | 0.1% (0.01-3% range) |
| Number of Failed SS rods [a] | 0.003% | 1.4% | 0.003% | 1.15% |
| Initial fraction of fuel exposed in Zr rods[b] | | 100% | 0 | 100% |
| Initial fraction of fuel exposed in S.S. rods[b] | | 100% | 0 | 100% |
| Distribution of failed Zr rods in waste packages | 4.2/WP | ≤10/WP (P=99.6%) | 0/WP (P=1.5%) . | 4.2/WP |
| Distribution of failed S.S. rods in waste packages | In 4.3% of all WP | In 4.5% of all WP | In 4.0% of all WP | Unknown |
| Time for crack initiation at 408K | 2.5E05 y | 8.5E07 y | 7.1E02 y | 2.5E05 y |

a - Per cent of 29.5 million total rods.

b - Only about 30% of the waste packages are intercepted by seeps in TSPA-VA

The significance of this uncertainty will vary depending on the results of calculations of the number of fuel pins which fail during storage. If fraction which fail during storage is large relative to the number of initial failures, then uncertainty in the number of initial failures will not be important.

# 7.0 SUMMARY AND CONCLUSIONS

It has been postulated that the cladding of the spent fuel disposed of at the proposed Yucca Mountain repository would provide a significant barrier to the release of radionuclides, which in turn would result in low post-emplacement, off-site exposures. This can be true only if the cladding is initially intact and remains intact for a significant portion of the evaluation duration. Towards this end, an extensive review of the literature has been performed to gather in formation which would allow spent fuel cladding performance to be characterized and modeled, and thereby included in off-site exposure performance assessment of the proposed Yucca Mountain repository, and would also allow for an evaluation of the validity of such models developed by others. The investigation included the characterization of cladding failures prior to the fuel being emplaced in the repository, and post-emplacement failure mechanisms, as well as an attempt to describe the magnitude of the failure (e.g., pin holes, hairline cracking, gross failure, unzipping), and to quantify when these failures would occur. For the purpose of this review the post-emplacement time period was limited to the proposed 10,000 year regulatory horizon — detailed characterization of cladding failures which may occur after this time period was not performed.

The preceding sections have presented a detailed description and discussion of the information that was gathered during this literature review, while a summary description of the main conclusions of the review is presented below.

1. Based on the assumption that Yucca Mountain will be limited to 63,000 tonnes of commercial SNF, the repository will contain 29,490,804 fuel rods in 7,586 waste packages. All but 1.3% of these fuel rods will have Zircaloy cladding with the balance being stainless steel. The initial fuel rod failure level for Zircaloy clad fuel pins is expected to be 0.1% or less. This is based on the following estimates:

- In-service failures - <0.05%
- Pool storage failures - 0
- Dry storage failures - 0.03%
- Consolidation failures - 0.005%
- Other handling failures - 0.0003%

The repository will contain 2,179 stainless steel assemblies comprised of 397,048 fuel rods. Of these, 333 are BWR assemblies containing a total of 32,588 fuel rods. There are 239 PWR

assemblies containing 652 failed rods and 103 BWR assemblies containing 188 failed rods (54 assemblies with sipping failures containing one failed rod per assembly, 31 assemblies with visible cracks containing two failed rods per assembly and 18 assemblies with gross failures containing four failed rods per assembly).

2. Failure mechanisms for Zircaloy cladding examined in this report include:

- Creep (stress) rupture
- Fuel side stress corrosion cracking (FSSCC)
- Delayed hydride cracking (DHC)
- Oxidation
- Crack extension and unzipping due to fuel oxidation
- Mechanical failure due to rock falls
- Aqueous corrosion

The last two mechanisms on the list are being considered by DOE in the 1998 TSPA Viability Assessment but have been excluded from detailed consideration here because the mechanisms have little or no effect within a 10,000-year regulatory horizon. All of these mechanisms are highly sensitive to the temporal and spatial temperature distributions within the waste packages.

3. Based on the expected temperature history described in Section 4.2, cladding oxidation should not be significant. Oxidation cannot occur until a waste package is breached and approximately 10,000 years (after breach) are required to oxidize 25% of the cladding thickness under isothermal conditions at 498 K (225°C). The cladding temperature will have decayed to below this value in less than 100 years.

4. If a pinhole cladding defect exists (or forms after disposal), the $UO_2$ can oxidize once the waste package is breached. When the oxidation product is $U_3O_8$, the cladding can become stressed as a result of a 30% volume increase and cause a pinhole defect to develop into a crack. The fuel oxidation can proceed to such an extent that the cladding unzips (i.e., splits) along much of its length. Occurrence of clad cracking and unzipping appears to be unlikely based on the Section 4.2 temperature history. The processes will not occur if the fuel temperature is below 373 K (100°C) because the end product of the reaction is $U_4O_9$ which does not have an associated volume increase. A cladding crack can form after 10,000 years under isothermal conditions at approximately 430 K (157°C) but the temperature should fall below this value in about 1,000 years.

5. Delayed hydride cracking requires that a critical stress concentration factor of approximately 10 $MPa \cdot m^{0.5}$ be exceeded. Calculated stress concentration factors are more than an order of magnitude below the critical value after 10,000 years for temperatures below

300°C, the maximum investigated. Even if there is a two order of magnitude uncertainty in the critical stress concentration factor, DHC will not occur in 10,000 years at temperatures below 523 K (250°C).

6. Fuel side stress corrosion cracking is not expected to be a significant post-disposal mechanism based on a threshold stress concentration of 3 $MPa \cdot m^{0.5}$. A cladding hoop stress of 245 MPa would be required for a crack 0.000095 m deep (15% of the wall thickness) to exceed the threshold value. Since the expected stress at 573 K (300°C) (the peak estimated cladding temperature) is 70 MPa and decreases as the temperature decreases, the actual stress concentrations should be well below the critical value.

7. Creep of the Zircaloy is possible due internal fuel rod pressure from initial gas pressurization plus fission gas release. Allowable post-disposal creep is a function of such uncertain factors as the creep model selected, the time-temperature function, the cladding stress (which is related to temperature and fission gas release), and the allowable strain. The mechanistic creep and stress rupture models based on the work of Chin and his co-workers were reviewed as were the empirical models of Peehs, of Mayazumi and Onchi, and of Matsuo. The creep model based on the experimental work of Mayazumi and Onchi is recommended as a conservative approach for future modeling activities. A strain limit of 1% is also recommended. With these recommendations and assuming that the standard deviation for the time-temperature function described in Section 4.2 is 0.133, 225 fuel rod failures could occur in a population of 10,000 fuel rods.

8. One of the problems with all of the creep models based on experimental data is that the data are obtained under conditions where the extant creep mechanism(s) is not the same as that expected under disposal conditions. For example, based on the work of Chin and his co-workers, the expected creep mechanism after disposal is grain boundary sliding driven by grain boundary diffusion. The experimental work of Mayazumi and Onchi was conducted in a temperature/stress regime where the dominant deformation mechanism is high-temperature dislocation climb. This adds an additional element of uncertainty to the creep modeling.

9. Most cladding defects tend to be small -- typically characterized as pinholes or hairline cracks. Transport of radionuclides from these failed fuel rods can be analyzed as diffusion controlled. In a limited number of fuel rods, larger defects are produced by cracking from pellet/clad interaction, unzipping and the like. Transport of radionuclides from such rods can be treated as an advectively controlled process.

10. A detailed conceptual model which can be used to describe the effects of fuel rod cladding as a barrier to radionuclide release has been developed. The model focuses on initial failure

levels and post-disposal failure by creep. Inundation of the fuel rods is necessary for transport of radionuclides from the waste packages.

11. DOE did not consider cladding credit in TSPA 1995. However, the efficacy of this engineered barrier was considered in the 1996 Performance Allocation. The Peehs empirical relationship was used model creep and 1% creep strain was the assumed failure criterion. Inclusion of a cladding barrier resulted in two orders of magnitude reduction in the dose from Tc-99 and less than a factor of 10 reduction in the dose from Np-237. In the 1998 TSPA VA, DOE plans to use the Matsuo creep model and a 4% strain limit. The strain is treated as an uncertain variable with an error factor of 10. The modeling will also consider aqueous corrosion by some generic long-term mechanism and the impact of rock falls after the waste packages have lost their physical integrity.

## 8.0 REFERENCES

Bailey 1987. "Categorization of Failed and Damaged Spent LWR Fuel Currently in Storage," PNL-5882, Pacific Northwest Laboratory, November 1987.

Bailey, W.J. *et al.* 1992. "Fuel Performance Annual Report for 1989," NUREG/CR-3950, Vol. 7, Pacific Northwest Laboratory, June 1992.

Bailey, W.J. and S. Wu 1990. Fuel Performance Annual Report for 1988," NUREG/CR-3950, vol.6, (PNL-5210), Pacific Northwest Laboratory, May 1990.

Bailey, W.J. *et al.* 1991. "Recent GE BWR Fuel Experience," *Proceedings of International Topical Meeting on LWR Fuel Performance*, American Nuclear Society and European Nuclear Society, Avignon, France, April 21-24, 1991.

ACD 1996. "Advanced Conceptual Design Report," B00000000-01717-5705-00027 REV 00, Vol. III, March 1996.

ANS 1982. "Background and Derivation of ANS-5.4 Standard Fission Product Release Model," NUREG/CR-2507, American Nuclear Society Working Group 5.4, January 1982.

ASME 1953. *Metals Engineering Design.* American Society of Mechanical Engineers. McGraw-Hill Book Company.

Bailey, W.J. and D.C. Langstaff 1980. "Experience with Fuel Damage from Abnormal Conditions in Handling and Transport," *6th International Symposium on Packaging and Transportation of Radioactive Materials,* PATRA 80, West Berlin, November 10-14, 1980.

Barnes, J.O, et al., 1992. "Evaluation of Fission Gas Release in High-Burnup Light Water Reactor Fuel Rods," in *Nucl. Technol.*, v. 102, pp 210-231, May 1992.

Belle, J. ed. 1961. *Uranium Dioxide: Properties and Nuclear Applications*, U.S. Atomic Energy Commission.

Blackburn, L.D. et al. 1978. "Maximum Allowable Temperature for Storage of Spent Nuclear Reactor Fuel," HEDL-TME 78-37, Hanford Engineering Development Laboratory, May 1978.

Cheadle, B.A., C.E. Coleman, and J.F.R. Ambler 1987. "Prevention of Delayed Hydride Cracking in Zirconium Alloys," in Zirconium in the Nuclear Industry, Seventh International

Symposium, ASTM STP 939, American Society for Testing Materials, Philadelphia, PA, pp. 224-240.

Chin, B.A., M.A. Khan and J.C.L. Tarn 1986. "Deformation and Fracture Map Methodology for Predicting Cladding Behavior During Dry Storage," PNL-5998, Pacific Northwest Laboratory, September 1986.

Chin, B.A. and H.J. Gilbert 1989. "Prediction of Maximum Allowable Temperatures for Dry Storage of Zircaloy-clad Spent Fuel in Inert Atmosphere," in *Nucl. Technol.* 85:57-65.

DOE (U.S. Department of Energy) 1987. "Characteristics of Spent Fuel, High-Level Waste, and Other Radioactive Wastes Which May Require Long-Term Isolation," DOE/RW-0184, Vol. 1, Office of Civilian Radioactive Waste Management, December 1987.

DOE (U.S. Department of Energy) 1995. "Total System Performance Assessment - 1995: An Evaluation of the Potential Yucca Mountain Repository," B00000000-01717-2700-00136, Rev. 01, Management and Operating Contractor, November 1995.

DOE (U.S. Department of Energy) 1996. "Description of Performance Allocation," B00000000-01717-2200-00177, Rev. 00, Management and Operating Contractor, August 15, 1996.

DOE (U.S. Department of Energy)1997. "First Interim Report - Total Systems Performance Assessment Peer Review Panel," June 20, 1997.

DOE (U.S. Department of Energy) 1998. "DOE/NRC Technical Exchange on Total System Performance Assessment Viability Assessment," San Antonio Tx, March 17-19, 1998.

DOE (U.S. Department of Energy) 1998a. "Evaluation of EBS Processes: Near-field geochemical environment, Waste form degradation/immobilization, EBS transport," presentation by J.A. McNeish to NWTRB Performance Assessment Panel, Albuquerque NM, April 23-24, 1998.

DOE (U.S. Department of Energy) 1998b. "Basic Structure, Conceptual Model, and Results of the TSPA-VA," presentation by R.W. Andrews to NWTRB Performance Assessment Panel, Albuquerque NM, April 23-24, 1998.

DOE (U.S. Department of Energy) 1998c. "Total System Performance Assessment - Viability Assessment: Rev. 00 to Rev. 01 Changes in the TSPA-VA Base case," presentation by A. Van Luik to DOE/NRC Quarterly Meeting, Las Vegas, NV, June 18, 1998.

DOE (U.S. Department of Energy) 1998d. "Viability Assessment Total System Performance Assessment - Summary of Results and Sensitivity Analyses," by Robert W. Andrews to the Nuclear Waste Technical Review Board, June 24, 1998.

EIA (Energy Information Administration, U.S. Department of Energy) 1996. "Spent Nuclear Fuel Discharges from U.S. Reactors - 1994," SR/CNEAF/96-01, February 1996.

Einziger, R.E. et al., 1992 "Oxidation of Spent Fuel in Air at 175° to 195°C." in *High-Level Radioactive Waste Management - Proceedings of the Third International Conference*, Las Vegas, NV, April 12-16, 1992.

Einziger, R.E. 1994. "Preliminary Spent Fuel Oxidation Source Term Model," in *High Level Radioactive Waste Management - Proceedings of the Fifth Annual International Conference*, vol. 2, pp.554-559.

Einziger, R.E. 1997. Submittal to TSPA-VA Abstraction/Testing Workshop, Livermore CA, February 19-21, 1997.

Einziger, R.E. and R. Kohli 1984. "Low-Temperature Rupture Behavior of Zircaloy-Clad Pressurized Water Reactor Spent Fuel Rods Under Dry Storage Conditions," in *Nucl. Technol.* 67:107-123.

EPRI 1989. "Estimates of Zircaloy Integrity During Dry Storage of Spent Nuclear Fuel," EPRI NP-6387, Project 2062-9, Electric Power Research Institute, May 1989.

EPRI 1996. "Yucca Mountain Total System Performance Assessment, Phase 3," EPRI TR-107191, Electric Power Research Institute, December 1996.

EPRI 1997. "The Technical Basis for the Classification of Failed Fuel in the Back End of the Fuel Cycle," EPRI TR-108237, Robert H. Jones for Electric Power Research Institute, July 1997.

Freund, J.E. and F.J. Williams 1977. *Elementary Business Statistics, The Modern Approach,* Third Edition, Prentice-Hall Inc.

Garde, A.M., H.M. Chung and T.F. Kassner 1978. "Micrograin Superplasticity in Zircaloy at 850°C," in *Acta Metallurgica.* 26, pp. 153-166.

Goncarovs, G. 1991. "Debris Induced Fretting and Coolant Radiochemistry During Connecticut Yankee Cycle 15," *Proceedings of International Topical Meeting on LWR Fuel*

*Performance*, American Nuclear Society and European Nuclear Society, Avignon, France, April 21-24, 1991.

Graves, Richard H. 1979. Letter from Connecticut Yankee Atomic Power Company to Boyce Grier, U.S. Nuclear Regulatory Commission, Region 1, Licensee Event Report for Reportable Occurrence LER79-01/1T, February 28, 1979.

IAEA 1982. "Storage of Water Reactor Spent Fuel in Water Pools," Technical Report Series No. 218, International Atomic Energy Agency.

Johnson, A.B. Jr. 1977. "Behavior of Spent Nuclear Fuel in Water Pool Storage," BNWL-2256, September 1977.

Khan, M, N.H. Madsen, and B.A. Chin 1985. "Fracture Predictions in Zircaloy Fuel Cladding," in *Proc. 12th Int. Symp. Effects of Radiation on Materials*, ASTM Stp. 870, pp. 642-655, American Society for Testing Materials.

Kholi, R. et. al. 1985. "The Behavior of Breached Boiling Water Reactor Fuel Rods on Long-Term Exposure to Air and Argon at 598K," in *Nuclear Technology* v. 69, pp. 186-197, May 1985.

La Crosse 1979. Letter to James Keppler, U.S. Nuclear Regulatory Commission from Dairyland Power Cooperative dated April 19, 1979. Docket No. 50-409, Subject: Dairyland Power Cooperative La Crosse Boiling Water Reactor (LACBWR) Provisional Operating License No. DPR-45 Reportable Occurrences Nos. 79-05 and 79-06.

Limoges, C. 1998. Private communication with Charles Limoges, Unit #1, Indian Point, (914) 734-5184, June 29, 1998.

Maffei, D., 1998. Private communication with Donald Maffei, Unit #1 Project Manager, Indian Point, (914) 734-5880, June 26, 1998.

Matsuo, Y. 1987. "Thermal Creep of Zircaloy-4 Cladding under Internal Pressure," in *J. Nuc. Sci. and Tech.*, 24[2], pp. 111-119, February 1987.

Mayazumi, M. and T. Onchi 1990a. "Creep Deformation and Rupture Properties of Unirradiated Zircaloy-4 Nuclear Fuel Cladding Tube at Temperatures of 727 to 857 K," in *J. Nucl. Mat.* 175:135-142.

Mayazumi, M. and T. Onchi 1990b. "Creep Deformation of Unirradiated Zircaloy Nuclear Fuel Cladding Tube Under Dry Storage Conditions," in *J. Nuc. Mat.*, 171:383-388.

Mayazumi, M. and K. Murai 1993. "Post Irradiation Creep and Rupture of Irradiated PWR Fuel Cladding," in *Proceedings of 1993 International Conference on Nuclear Waste Management and Environmental Remediation*, vol. 1, pp. 607-612.

McCoy, Kevin 1998. "Design Basis Cladding Analysis," BBA000000-01717-0200-00054 REV 01, CRWMS/M&O, March 5, 1998.

McCoy, J.K. and T.W. Doering 1994. "Prediction of Cladding Life in Waste Package Environments," in *High Level Radioactive Waste Management-Proceedings of the Fifth Annual International Conference*, Las Vegas NV, pp. 565-572.

McKinnon, M.A., and A.L. Doherty 1997. "Spent Nuclear Fuel Integrity During Dry Storage - Performance Tests and Demonstrations," PNNL-11576, Pacific Northwest National Laboratory, May 1997.

Mitchell 1998. Private communication from David Mitchell, Framatome Technologies, Lynchburg, VA, July 2, 1998

Murty, K.L., G.S. Clevinger, and T.P. Papazoglou 1977. "Thermal Creep of Zircaloy-4 Cladding" in *Transactions of the 4th International Conference on Structural Mechanics*, San Francisco CA, August 15-19, 1977.

Myers, P. 1998. Private communication from Paul Myers, Southern California Edison Company, (949) 368-8256, July 28, 1998

Nuclear Regulatory Commission (NRC), 1990. "Fuel Performance Annual Report for 1988." NUREG/CR-3950, vol. 6. Pacific Northwest Laboratory. May 1990.

Nuclear Regulatory Commission (NRC), 1994. "Fuel Performance Annual Report for 1991." NUREG/CR-3950, vol. 9. Pacific Northwest Laboratory. August 1994

NRC 1996. "Information Digest - 1996 Edition," NUREG-1350, volume 8, U.S. Nuclear Regulatory Commission, July 1996.

Painter, C.L. *et al.* 1994. "Fuel Performance Annual Report for 1991," NUREG/CR-3950, vol.9, (PNL-5210), Pacific Northwest Laboratory, August 1994.

Pasupathi, V. and R.W. Klingensmith 1981. "Investigation of Stainless Steel Clad Fuel Rod Failures and Fuel Performance in the Connecticut Yankee Reactor," NP-2119, Battelle Columbus Laboratories, November 1981.

Peehs, M. and J. Fleisch 1986. "LWR Spent Fuel Storage Behavior," in *Journal of Nuclear Materials*, vol. 137, pp. 190-202, 1986, Elsevier Science Publications.

Peehs, M., R. Bockelmann and J. Fleisch 1986a. "Spent Fuel Dry Storage Performance in Inert Atmosphere," in *Proc. 3rd International Spent Fuel Storage Technology Symposium/Workshop*, vol. 1, pp. S-215 - S-230, USDOE-CONF-860417/UC-85.

Peehs, M., G. Kaspar and E. Steinberg 1986b. "Experimentally Based Spent Fuel Dry Storage Performance Criteria," in *Proc. 3rd International Spent Fuel Storage Technology Symposium/Workshop*, vol. 1, pp. S-316 - S-331, USDOE-CONF-860417/UC-85.

Pescatore, C., M.G. Cowgill, T.M. Sullivan, 1990. "Zircaloy Cladding Performance Under Spent Fuel Disposal Conditions - Progress Report May 1 - October 31, 1989," BNL 52235, Brookhaven National Laboratory.

Pescatore, C. and M. Cowgill, 1994. "Temperature Limit Determination for the Inert Dry Storage of Spent Nuclear Fuel," EPRI Report TR-1-3949, Electric Power Research Institute, May 1994.

Puls, M.A., L.A. Simpson and R. Dutton, 1982. "Hydride-induced Crack Growth in Zirconium Alloys," in *Fracture Problems and Solutions in the Energy Industry*, Pergamon Press, New York, pp.13-25.

Rafferty, S. 1998. Private communication with Seymour Rafferty, LaCrosse Boiling Water Reactor, (608) 689-2331. June 26, 1998.

Rothman, A.J. 1984. "Potential Corrosion and Degradation Mechanisms of Zircaloy Cladding on Spent Nuclear Fuel in a Tuff Repository," DE85003996, Lawrence Livermore National Laboratory, September 1984.

Saegusa, T., M. Mayazumi, C. Ito, and K. Shirai 1996. "Experimental Studies on Safety of Dry Cask Storage Technology of Spent Fuel," in *Journal of Nuclear Science and Technology*, vol. 33, no. 3, pp. 250-258, March 1996.

Sanders, *et al.*, 1992. "A Method for Determining the Spent-Fuel Contribution to Transport Cask Containment Requirements," SAND90-2406, Sandia National Laboratories, November 1992.

Santanam, L., S. Raghavan, and B. Chin 1992. "Zircaloy Cladding Rupture During Repository Storage," in *Nuclear Technology*, vol 97, pp. 316-322, March 1992.

SCA 1997. Private communication from S. Marschke, S. Cohen and Associates, May 1997.

SCA 1997a. Private communication from S. Marschke, S. Cohen and Associates, July 1997.

SCA 1997b. "Uncertainty in Performance Factors for a Potential Radioactive Waste Repository at Yucca Mountain," S. Cohen and Associates Inc., prepared for EPA under Contract 68D20155, Work Assignment 5-12, September 30, 1997.

Siegmann, E., J.H. Lee, and J.E. Atkins 1996. "Probabilistic Analysis of Cladding Degradation Incorporating Waste Package Degradation," M & O Contractor, September 30, 1996.

Siegmann, E.J. 1997. "Cladding Credit in the TSPA-VA," presentation to Expert Elicitation Panel, San Francisco, December 15-16, 1997.

Shi, S.Q, and M.P. Puls 1994. "Criteria for fracture initiation at hydrides in zirconium alloys," in *Journal of Nuclear Materials* v. 208, pp. 232-242, 1994.

Stahl, David 1998. Private communication with David Stahl, M&O contractor, June 1998.

TRW 1996. "Description of Performance Allocation," B00000000-01717-2200-00177, Rev. 00, TRW, August 15, 1996.

TSPA 1993. "Total System Performance Assessment for Yucca Mountain - SNL Second Iteration (TSPA-1993), SAND93-2675, Sandia National Laboratories, April 1994.

TSPA 1995. "Total System Performance - 1995: An Evaluation of the Potential Yucca Mountain Repository," B00000000-01717-2200-00146, Rev. 01, CRWMS M&O Contractor, November 1995.

Williams, R. 1998. Private communication with R. Williams, plant manager, Yankee Rowe, (413) 424-5261, June 25, 1998

Wilson. M.E. *et al.* 1994. "Total System Performance for Yucca Mountain - SNL Second Iteration (TSPA-1993)," SAND93-2675, Sandia National Laboratories, April 1994.

Yaggee, F.L., R.F. Mathas, and L.A. Neimark 1980. "Characterization of Irradiated Zircaloys: Susceptibility to Stress Corrosion Cracking," NP-1557, Argonne National Laboratories, October 1980.

Yang, R.L. *et al.* 1991. "Fuel Performance Evaluation for EPRI Program Planning," *Proceedings of International Topical Meeting on LWR Fuel Performance*, American Nuclear Society and European Nuclear Society, Avignon, France, April 21-24, 1991.

# APPENDIX A

## Typical Fuel Assembly Parameters
## (NUREG/CR-3950, Vol. 9)

# Appendix A - Typical Fuel Assembly Parameters (NUREG/CR-3950, Vol. 9)

| Vendor | ABB CENF | ABB CENF | B&W | B&W | B&W | B&W | B&W |
|---|---|---|---|---|---|---|---|
| Reactor Type | PWR | PWR | PWR | PWR | PWR | PWR | PWR |
| Reactor System | CE | CE | B&W | B&W | W | W | W |
| Fuel Rod Array | 14x14 | 16x16 | 15x15 | 17x17 | 15x15 | 15x15 | 17x17 |
| Version | CE | CE | Mark B[c] | Mark C | Haddam | Mark BW | Mark BW |
| Assemblies Per Core | 217 | 217 | 177 | 205 | 157 | 157 | 193 |
| Fuel Rod Positions per Assembly | 176 | 236 | 225 | 289 | 225 | 225 | 289 |
| Typical Number of Fuel Rods per Assembly | 164 | 224 | 208 | 264 | 204 | 204 | 264 |
| Rod Pitch, mm (in) | 14.7 (0.580) | 12.9 (0.506) | 14.4 (0.568) | 12.8 (0.502) | 14.3 (0.563) | 14.3 (0.563) | 12.6 (0.496) |
| System Pressure, MPA (psia) | 15.5 (2250) | 15.5 (2250) | 15.2 (2200) | 15.5 (2250) | 13.9 (2015) | 13.9 (2015) | 15.5 (2250) |
| Core Average power Density, kW/liter | 78.5 | 96.4 | 91.4 | 107.3 | 82.25 | 82.25 | 82.25 |
| Average LHGR,[a] kW/m (kW/ft) | 20.0 (6.09) | 18.2 (5.54) | 20.3 (6.20) | 18.8 (5.73) | 18.1 (5.53) | 18.4 (5.60) | 17.8 (5.43) |
| Axial Peak LHGR in an Average Rod, kW/m (kW/ft) | 24.0 (7.31) | 21.0 (6.41) | 24.4 (7.44) | 22.6 (6.88) | 25.1 (7.66) | 25.5 (7.76) | 27.6 (8.42) |
| Max. Peak LHGR, kW/m (kW/ft) | 53.5 (16.3) | 42.7 (13.0) | 53.0 (16.16) | 49.9 (15.20) | 47.6 (14.5) | 47.6 (14.5) | 42.7 (13.0) |
| Max. Fuel Temp., °C (°F) | 2140 (3890) | 1880 (3420) | 2340 (4244) | 2290 (4155) | 2149 (3900) | 2149 (3900) | 1927 (3500) |
| Core Average Enrichment wt% $^{235}U$ | 3.89 | 2.36 | 3.30 | 3.15 | 4.00 | 3.41 | 3.40 |
| Max. Local Exposure, GWd/MT | 50 | 55 | 55 | 55 | 55 | 55 | 55 |

| Vendor | ABB CENF | ABB CENF | B&W | B&W | B&W | B&W | B&W |
|---|---|---|---|---|---|---|---|
| Cladding Material[b] | Zry-4 | Zry-4 | Zry-4 | Zry-4 | 304SS | Zry-4 | Zry-4 |
| Fuel Rod Length, M (in.) | 3.71 (145.9) | 4.09 (161.0) | 3.904 (153.7) | 3.878 (152.7) | 3.218 (126.7) | 3.197 (125.9) | 3.848 (151.5) |
| Active Fuel Length, m (in.) | 3.47 (136.7) | 3.81 (150) | 3.602 (141.8) | 3.632 (143.0) | 3.061 (120.5) | 3.012 (118.6) | 3.658 (144.0) |
| Plenum Length, m (in.) | 0.22 (8.6) | 0.25 (10.0) | 0.298 (11.7) | 0.242 (9.5) | 0.122 (4.8) | 0.159 (6.3) | 0.164 (6.4) |
| Fuel Rod OD, mm (in.) | 11.18 (0.44) | 9.70 (0.382) | 10.92 (0.430) | 9.63 (0.379) | 10.72 (0.422) | 10.72 (0.422) | 9.50 (0.374) |
| Cladding ID, mm (in.) | 9.75 (0.384) | 8.43 (0.332) | 9.58 (0.377) | 8.41 (0.331) | 9.88 (0.389) | 9.35 (0.368) | 8.28 (0.326) |
| Cladding Thickness, mm (in.) | 0.711 (0.028) | 0.635 (0.025) | 0.673 (0.0265) | 0.610 (0.024) | 0.419 (0.0165) | 0.686 (0.027) | 0.610 (0.024) |
| Diametral Gap, [c] micron (mil) | 190.5 (7.5) | 178 (7.0) | 213.4 (8.4) | 198.1 (7.8) | 165 (6.5) | 178 (7.0) | 165 (6.5) |
| Fuel Pellet Diameter, mm (in.) | 9.56 (0.3765) | 8.26 (0.325) | 9.362 (0.3686) | 8.209 (0.3232) | 9.715 (0.3825) | 9.17 (0.361) | 8.115 (0.3195) |
| Fuel Pellet Length, mm (in.) | 11.43 (0.45) | 9.91 (0.39) | 11.05 (0.435) | 9.53 (0.375) | 11.63 (0.458) | 10.80 (0.425) | 10.16 (0.400) |
| Fuel Pellet Density, %TD[d] | 95 | 95 | 95 | 95 | 95 | 95 | 96 |
| Fill Gas and Pressure (psig) | He 300-450 | He 300-450 | He 415 | He 435 | He 40 | | |

[a] LHGR = linear heat generation rate
[b] Type 304 stainless steel (304SS), Zircaloy-4 (Zry-4), and Zircaloy-2 (Zry-2)
[c] Diametral gap = cladding ID - pellet diameter
[d] Theoretical density (TD) of stoichiometric $UO_2$ is 10.96 g/cm³
[e] Distinquishing Features:
Mark B4: Pressurized fuel
Mark B4Z: Mark B4 fuel with Zircaloy spacers
Mark B5: Revised end fitting
Mark B5Z: Mark B5 fuel with Zircaloy spacer
Mark B6: Zircaloy spacers, skirtless upper and spacer, removable top nozzle.
Mark BEB: Extended Burnup LTA
Mark Bgd: LTA with integral Gadolinia absorbers in the fuel
Mark B7: Mark B6 features plus shorter lower end fitting, longer fuel rod, increased plenum volume
Mark B8: Debris fretting resistant fuel rod design, reduced prepressurization

| Vendor | GE | GE | GE | GE | SNP | SNP | SNP | SNP | SNP | SNP |
|---|---|---|---|---|---|---|---|---|---|---|
| Reactor Type | BWR/2,3 | BWR/2,3 | BWR/4-6 | BWR/4-6 | BWR/2,3 | BWR/2,3 | BWR/2,3 | BWR/2,3 | BWR/4-6 | BWR/4-6 |
| Reactor System | GE | GE | GE | GE | GE | GE | GE | GE | GE | GE |
| Fuel Rod Array | 8x8 | 9x9 | 8x8 | 9x9 | 9x9 | 9x9 | 9x9 | 9x9 | 9x9 | 9x9 |
| Version | Barrier | GE-11 | GE-4a | GE-11 | JP-3 | 9-5 | 1X | 9X | JP-4,5 | 9-5 |
| Assemblies Per Core | 560 | | 560 | | 724 | | | | | |
| Fuel Rod Positions per Assembly | 64 | 81 | 64 | 81 | 81 | 81 | 81 | 81 | 81 | 81 |
| Typical Number of Fuel Rods per Assembly | 62 | 77 | 63 | 77 | 79 | 76 | 72 | 72 | 79 | 76 |
| Rod Pitch, mm (in) | 16.3 (0.640) | | 16.3 (0.640) | | 14.52 (0.572) | | 14.52 (0.572) | 14.52 (0.572) | 14.52 (0.572) | |
| System Pressure, MPA (psia) | 7.14 (1035) | | 7.14 (1035) | | 7.07 (1026) | | | | | |
| Core Average power Density, kW/liter | 49.15 | | 50.51 | | 46 | | | | | |
| Average LHGR,[c] kW/m (kW/ft) | 17.7 (5.38) | | 17.9 (5.45) | | 12.1 (3.68) | | | | | |
| Axial Peak LHGR in an Average Rod, kW/m (kW/ft) | 21.24 (6.99) | | 21.48 (7.09) | | 17.5 (5.34) | | | | | |
| Max. Peak LHGR, kW/m (kW/ft) | 44.0 (13.4) | | 44.0 (13.4) | | 37.7 (11.5) | | | | | |
| Max. Fuel Temp., °C (°F) | 1890 (3435) | | 1830 (3325) | | 2040 (3705) | | | | | |
| Core Average Enrichment wt% $^{235}U$ | 1.99 | | 2.54 | | 2.8 | | | | | |
| Max. Local Exposure, GWd/MT | 45 | | 40 | | 55 | | | | | |
| Cladding Material[d] | Zry-2 | Zry-2 | Zry-2 | Zry-2 | Zry-2 | Zry-2 | Zry-2 | Zry-2 | Zry-2 | Zry-2 |

| Vendor | GE | GE | GE | GE | SNP | SNP | SNP | SNP | SNP | SNP |
|---|---|---|---|---|---|---|---|---|---|---|
| Fuel Rod Length, M (in.) | 4.20 (165.4) | | 4.09 (161.1) | | 4.04 (159.07) | | | | 4.16 (163.84) | |
| Active Fuel Length, m (in.) | 3.81 (145.24) | | 3.71 (146) | | 3.68 (145.24) | | | | 3.81 (150.0) | |
| Plenum Length, m (in.) | 0.25 (9.48) | | 0.36 (14.0) | | 0.243 (9.580) | | | | 0.24 (9.578) | |
| Fuel Rod OD, mm (in.) | 12.27 (0.483) | | 12.52 (0.493) | | 10.76 (0.424) | | | | 10.76 (0.424) | |
| Cladding ID, mm (in.) | 10.64 (0.419) | | 10.80 (0.425) | | 9.25 (0.364) | | | | | |
| Cladding Thickness, mm (in.) | 0.813 (0.032) | | 0.863 (0.034) | | 0.76 (0.030) | | | | 0.76 (0.030) | |
| Diametral Gap, [c] micron (mil) | 229 (9.0) | | 229 (9.0) | | 190 (7.5) | | | | | |
| Fuel Pellet Diameter, mm (in.) | 10.41 (0.410) | | 10.57 (0.416) | | 9.05 (0.356) | | | | | |
| Fuel Pellet Length, mm (in.) | 10.41 (0.410) | | 10.67 (0.420) | | 10.41 (0.410) | | | | | |
| Fuel Pellet Density, %TD[f] | 95 | | 95 | | 94.5 | | | | 94.5 | |
| Fill Gas and Pressure (psig) | He 30 | | He 0 | | He 60 | | | | He 60 | |

[a] Gadolinia in fuel rods
[b] Bottom 42 inches of fuel rod is stainless steel
[c] LHGR = linear heat generation rate
[d] Type 304 stainless steel (304SS), Zircaloy-4 (Zry-4), and Zircaloy-2 (Zry-2)
[e] Diametral gap = cladding ID - pellet diameter
[f] Theoretical density (TD) of stoichiometric $UO_2$ is 10.96 g/cm$^3$

| Vendor | SNP | SNP | SNP | SNP | SNP | SNP | W | W | W |
|---|---|---|---|---|---|---|---|---|---|
| Reactor Type | BWR/4-6 | BWR/4-6 | PWR | PWR | PWR | PWR | PWR | PWR | PWR |
| Reactor System | GE | GE | ABB CE | W | W | W | CE | B&W | W |
| Fuel Rod Array | 9x9 | 9x9 | 14x14 | 14x14 | 15x15 | 17x17 | 14x14 | 15x15 | 17x17 |
| Version | 1X | 9X | ABB CE | Top Rod | W | W | WE | WE | Advantage 5 |
| Assemblies Per Core | | | | | 193 | 193 | | 193 | 193 |
| Fuel Rod Positions per Assembly | 81 | 81 | 176 | 196 | 225 | 289 | 176 | 225 | 289 |
| Typical Number of Fuel Rods per Assembly | 72 | 72 | 176 | 179 | 204 | 264 | 176 | 208 | 264 |
| Rod Pitch, mm (in) | 14.45 (0.569) | 14.45 (0.569) | 14.73 (0.580) | 14.12 (0.556) | 14.30 (0.563) | 12.60 (0.496) | 14.73 (0.580) | 14.3 (0.563) | 12.60 (0.496) |
| System Pressure, MPA (psia) | | | | | 15.5 (2250) | 15.5 (2250) | | 15.5 (2250) | |
| Core Average power Density, kW/liter | | | | | 98.1 | 104.7 | | 98.1 | |
| Average LHGR, kW/m (kW/ft) | | | 20.76 (6.34) | | 22.0 (6.60) | 17.8 (5.44) | | 22.0 (6.70) | |
| Axial Peak LHGR in an Average Rod, kW/m (kW/ft) | | | | | 26.40 (8.04) | 21.4 (6.53) | | 26.40 (8.04) | |
| Max. Peak LHGR, kW/m (kW/ft) | | | | | 51.9 (15.8) | 54.5 (16.6) | | 61.7 (18.8) | |
| Max. Fuel Temp., °C (°F) | | | | | 2200 (3997) | 1747 (3177) | | 2340 (4250) | |
| Core Average Enrichment wt% $^{235}U$ | | | 3.34 | | 2.55 | 3.65 | 3.00 | 2.80 | 3.42 |
| Max. Local Exposure, GWd/MT | | | | | 47.5 | 52 | | 50 | |

| Vendor | SNP | SNP | SNP | SNP | SNP | SNP | W | W | W |
|---|---|---|---|---|---|---|---|---|---|
| Cladding Material | Zry-2 | Zry-2 | Zry-4 | Zry-4 | Zry-4 | Zry-4 | Zry-4 | Zry-4 | Zry-4 |
| Fuel Rod Length, M (in.) | | | 3.72 (146.4) | 3.86 (152.0) | 3.86 (152.0) | 3.86 (152.0) | 3.72 (146.4) | 3.80 (149.7) | 3.87 (152.3) |
| Active Fuel Length, m (in.) | 3.81 (150.0) | 3.81 (150.0) | 3.40 (134.0) | 3.65 (144.0) | 3.65 (144.0) | 3.65 (144.0) | 3.47 (136.7) | 3.66 (144) | 3.65 (144.0) |
| Plenum Length, m (in.) | | | | 0.18 (7.28) | 0.17 (6.80) | 0.18 (7.26) | | 0.21 (8.2) | 0.18 (7.41) |
| Fuel Rod OD, mm (in.) | (0.431) | (0.431) | 11.17 (0.440) | 10.59 (0.417) | 10.76 (0.424) | 9.14 (0.360) | 11.17 (0.440) | 10.72 (0.422) | 9.14 (0.360) |
| Cladding ID, mm (in.) | | | | | 9.25 (0.364) | 7.87 (0.310) | | 9.48 (0.373) | |
| Cladding Thickness, mm (in.) | (0.025) | (0.029) | 0.78 (0.031) | 0.74 (0.029) | 0.76 (0.030) | 0.63 (0.025) | 0.66 (0.026) | 0.62 (0.024) | 0.58 (0.023) |
| Diametral Gap, micron (mil) | | | | | 190 (7.5) | 177.8 (7.0) | | 190 (7.5) | |
| Fuel Pellet Diameter, mm (in.) | 9.49 (0.374) | 9.47 (0.373) | 9.39 (0.370) | | 9.05 (0.356) | 7.69 (0.303) | 9.68 (0.381) | 9.29 (0.366) | 7.85 (0.309) |
| Fuel Pellet Length, mm (in.) | | | 10.80 (0.425) | | 6.93 (0.273) | 8.84 (0.348) | 15.24 (0.600) | 15.24 (0.600) | 12.95 (0.510) |
| Fuel Pellet Density, %TD[0] | 96.26 | 94.5 | 94 | 94 | 94 | 94 | 95 | 95 | 95 |
| Fill Gas and Pressure (psig) | | | He 375 | He 305 | He 290 | He 290 | He 275-400 | He | He |

# APPENDIX B

## Stress-Rupture Observations on Irradiated Zircaloys (Pescatore and Cowgill 1994)

## Appendix B - Stress-Rupture Observations on Irradiated Zircaloys (Pescatore and Cowgill 1994)

| Material | Temp. (°C) | Stress (MPa) | Strain (%) | Failure Mode | Spec. ID | Reference |
|---|---|---|---|---|---|---|
| Zr-2 (SR) | 325 | 337 | 0.4 | S? | 165AE4B | Chung, 1987 |
| Zr-2 (SR) | 325 | 344 | 0.8 | D | 165AE4A | Chung, 1987 |
| Zr-2 (SR) | 325 | 384 | 1 | P? | 165AG10 | Chung, 1987 |
| Zr-2 (SR) | 325 | 514 | 1 | D | 165W21 | Chung, 1987 |
| Zr-4 (SR) | 292 | 498 | 1 | S? | 217B4B | Chung, 1987 |
| Zr-4 (SR) | 292 | 545 | 2 | D | 217B4B | Chung, 1987 |
| Zr-4 (SR) | 292 | 552 | 11 | D | 217A2G | Chung, 1987 |
| Zr-4 (SR) | 325 | 275 | 0.01 | P | 155BC9 | Yagee, 1980 |
| Zr-4 (SR) | 325 | 315 | | S? | 217C4B | Chung, 1987 |
| Zr-4 (SR) | 325 | 315 | | S? | 217A4B | Chung, 1987 |
| Zr-4 (SR) | 325 | 469 | 2 | S? | 217C2B | Chung, 1987 |
| Zr-4 (SR) | 360 | 200 | 0.4 | S | 155BD4 | Yagee, 1979 |

Notes

(SR) - stress-relieved.
D - ductile rupture; S - axial split; P - pinhole leakage.
All strains of 1 % or greater approximated to whole numbers.

# APPENDIX C

## Comparison of Matsuo 1987 and Mayazumi and Onchi 1990 Creep Tests

# APPENDIX C
# COMPARISON OF MATSUO 1987 AND MAYAZUMI AND ONCHI 1990 CREEP TESTS

This appendix presents a comparison of the Zircaloy-4 creep tests of Matsuo 1987 (subsequently abbreviated as Matsuo) and Mayazumi and Onchi 1990 (subsequently abbreviated as Mayazumi). As described in Sections 3 and 4 of this report, the two data sets produce creep strains differing by about two orders of magnitude at 450 to 500 K (177 to 227°C) (see, for example, Figure 4.6). The original papers were carefully reviewed in an attempt to identify any differences between the two sets of experimental data.

Both investigators used Zr-4 tubing that was cold-worked and stress relieved. The tubing was referred to as manufactured by the "normal production process" (Mayazumi) and the "usual mass production process" (Matsuo). Tubing in both cases was 10.72 mm o.d. The wall thickness was slightly greater with Mayazumi (0.66 mm) than with Matsuo (0.62 mm).

## Specimen Chemistry

Specimen chemistries are compared in Table C-1 indicating that the test specimens are quite similar and meet ASTM Specification B 811 for nuclear fuel cladding .

Table C-1. Composition of Creep Test Specimens

| Element (wt %) | ASTM B 811-90 | Mayazumi (specimen) | Matsuo (ingot) |
|---|---|---|---|
| Sn | 1.20 to 1.70 | 1.51-1.57 | 1.43-1.52 |
| Fe | 0.18 to 0.24 | 0.18-0.21 | 0.20-0.21 |
| Cr | 0.07 to 0.13 | 0.10-0.12 | 0.10-0.11 |
| Fe + Cr | 0.28 to 0.37 | 0.28-0.33 | 0.30-0.32 |
| O (ppm) | 900 to 1600 | 1260-1380 | 1300 (1280-1350)[a] |
| C (ppm) | 270 max. | 120-130 | 80-150 |
| H (ppm) | 25 max. | <6 | 14-16[a] |
| N (ppm) | 80 max. | 22-23 | 48-56[a] |

a - specimen analysis

Strength Properties

Tensile tests were conducted at 658 K (385°C) by both investigators and results are summarized in Table C-2. Again the properties are very similar.

Table C-2. Tensile Properties of Zr-4 at 658 K

| Property | Mayazumi | Matsuo |
|---|---|---|
| Ultimate tensile strength (MPa) | 472 | 453/456 |
| 0.2% yield strength (MPa) | 341 | 397/395 |
| Elongation (%) | 20.7 | 22.2/21.3 |

Mayazumi also did a burst test at room temperature and found that the bursting pressure was 132 MPa (or 1006 MPa hoop stress) and the circumferential strain at failure was 8%.

Test Procedures

In both investigations, tubular samples had Zircaloy end plugs welded into both ends of the specimen. In the case of Mayazumi, the second end plug was welded into the specimen in a glove box where the He pressure was varied from 3.43 to 6.86 MPa depending on the desired internal pressure at the creep test temperature. In the case of Matsuo, one end plug was connected with a Swagelok fitting to a pressurizing system which controlled the internal pressure to $\pm 0.5\%$ during creep testing.

Conclusion

There are no obvious procedural or material differences which account for the differences in observed creep behavior.

# APPENDIX D

## Additional Comments on the Creep Behavior of Zircaloy Fuel Cladding

# APPENDIX D
# ADDITIONAL COMMENTS ON THE CREEP BEHAVIOR OF ZIRCALOY FUEL CLADDING

The creep data described in this report were based primarily on three sets of experimental data reported by Matsuo, 1987, by Mayazumi and Onchi, 1990, and by Peehs. *et al.*, 1986. The theoretical modeling approach of Chin and his co-workers was also described. To use the experimental data in the Yucca Mountain context, it is necessary to extrapolate the creep equations to lower temperatures and much longer times than embraced by the experimental conditions.

The deformation map developed by Chin and his co-workers, reproduced from Chin and Gilbert, 1989 as Figure D-1, shows the experimental ranges covered by the various researchers and the range of conditions expected for the stored Yucca Mountain spent fuel. As discussed in Section 4.2, the peak cladding temperature is expected to be around 260 to 320°C and this will decline so that by 1000 years the temperature will be 100 to 150°C. Expected cladding stresses based on fission gas pressure buildup will range from about 50 to 90 MPa. From this figure it can be seen that the experimental work was in the regions dominated by low-temperature and high-temperature diffusion-controlled climb of dislocations while, for the conditions expected at Yucca Mountain, grain boundary sliding is the dominant deformation mechanism.

Two different mechanisms for grain boundary sliding have been proposed -- one in which grain boundary diffusion is the rate limiting process and one in which lattice diffusion is the limiting process. Typically, the activation energy for lattice diffusion is higher than for grain boundary diffusion. In Chin and Gilbert 1989 values of 250 kJ/mole for lattice diffusion (Q) and 175 kJ/mole for grain boundary diffusion ($Q_{gb}$) are proposed. As noted in Langdon and Vastava 1982, the ratio of $Q_l/Q_{gb}$ for a number of metals generally lies in the range 0.6 to 1. (Chin's ratio is 0.7.) For Yucca Mountain stress and temperature conditions, grain boundary diffusion

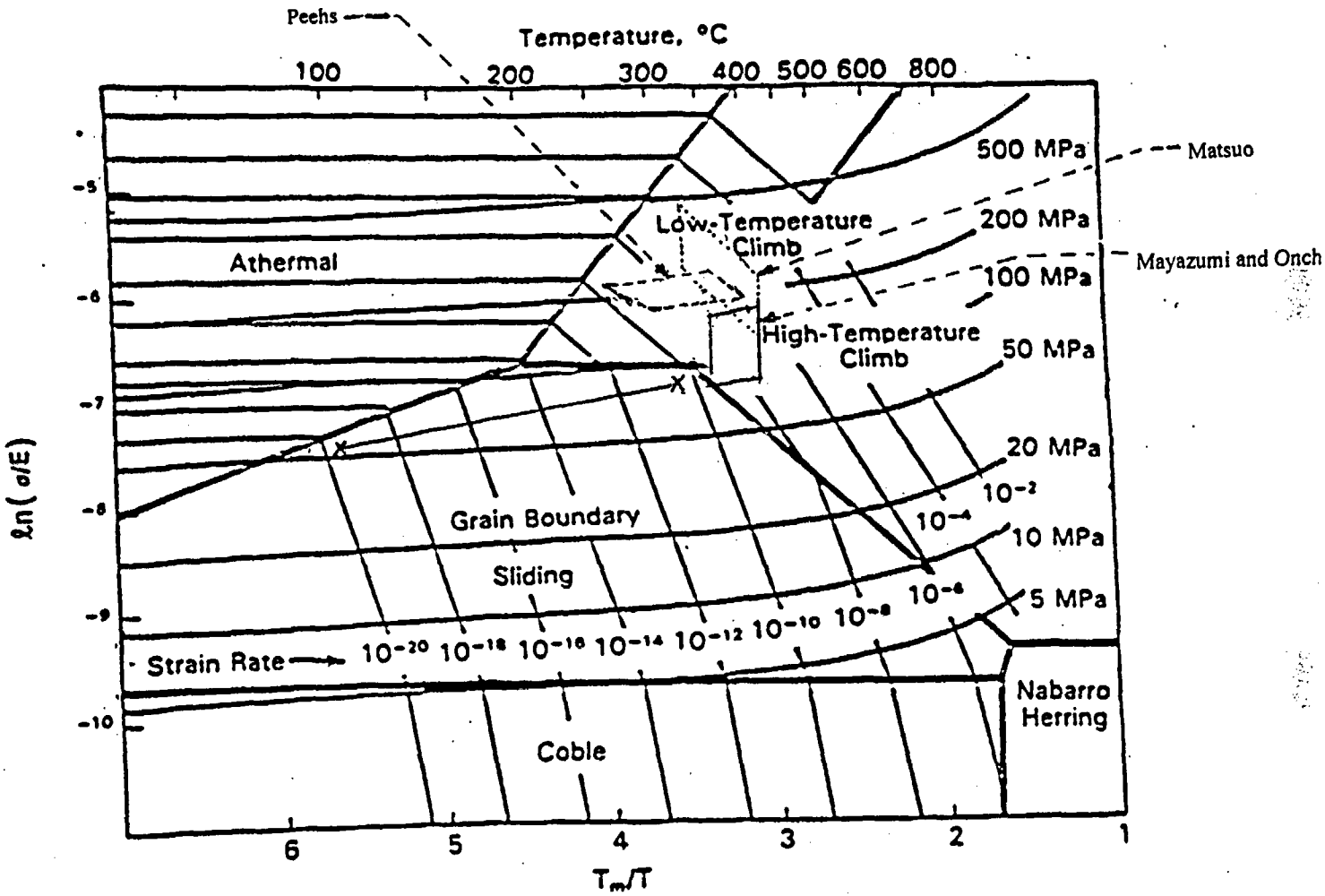


Figure D-1. Zircaloy Deformation Map Showing Range of Expected Yucca Mountain Disposal Conditions and Ranges of Experimental Creep Studies.

is rate limiting (i.e., produces the higher creep rate). Comparative total creep strains at 10,000 y[21], both experimentally determined and calculated using Chin's equation for grain boundary sliding with grain boundary diffusion, namely:

$$\dot{\epsilon}_{gbs} = A_{gbs} D_{0gb} \exp(-\frac{Q_{gb}}{RT})(\frac{Eb}{kT})(\frac{b}{d})^3(\frac{\sigma}{E})^2 \qquad \text{(D-1)}$$

are shown in Figure D-2. (Parameters used in equation D-1 were defined in Table 3.3b.) From this figure it can be seen that, at temperatures above about 470 K (197°C), the Chin grain boundary sliding model gives the most conservative results with the total creep strain being about twice as high at 550 K (277°C) as that based on Mayazumi and Onchi's experimental work. Below about 500 K (227°C), a 1% strain limit is not exceeded with any of the models when conservatively assuming isothermal conditions.

It should be noted that the parameter d in equation D-1 is the grain size of the material for which Chin assigns a value of 5 x $10^{-6}$ m. Since the strain rate is proportional to $1/d^3$, increasing the grain size to 10 x $10^{-6}$ m will decrease the calculated creep strain by a factor of 8.

In other work on deformation maps, Luthy *et al.*, 1979 describe a general equation for grain boundary sliding in materials where grain boundary diffusion is the rate controlling process as:

$$\dot{\epsilon} \approx 10^8 \frac{D_{gb}}{d^3} b (\frac{\sigma}{E})^2 \qquad \text{(D-2)}$$

[21] The total creep strains for Peehs, Matsuo, and Mayazumi and Onchi include primary creep strain but the total strains calculated from the Chin model include only steady-state creep effects.

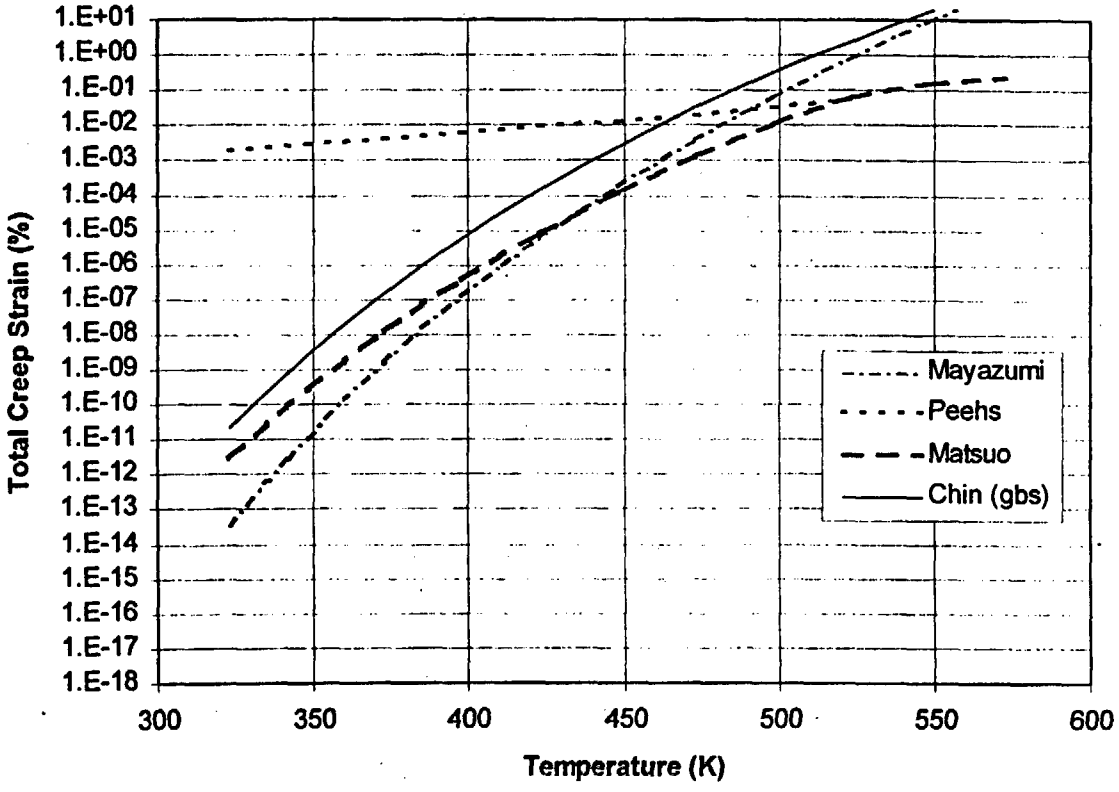


Figure D-2. Cumulative Creep Strains at 10,000 Y Based on Mechanistic and Empirical Creep Models.

This equation and a companion equation where lattice diffusion is rate controlling were shown to predict the creep rates from 56 separate investigations within an order of magnitude. Equation D-2 was converted to be comparable to constitutive equations equations used by Ashby and Frost, 1975 as follows:

$$\dot{\epsilon}_{gbs} \approx 6x10^{5} D_{gb} \frac{Gb}{kT} \left(\frac{b}{d}\right)^{3} \left(\frac{\tau}{G}\right)^{2} \qquad \text{(D-3)}$$

Assuming that $\tau = \sigma/2$, $E = 2(1+\mu)G$, and $\mu = 0.3$, this equation becomes:

$$\dot{\epsilon}_{gbs} \approx 4x10^{5} D_{gb} \frac{Eb}{kT} \left(\frac{b}{d}\right)^{3} \left(\frac{\sigma}{E}\right)^{2} \qquad \text{(D-4)}$$

Comparing equations D-1 and D-4 shows that the numerical constant, $A_{gbs,}$ is more than an order of magnitude lower based on the the approach of Luthy *et al.*, 1979 as compared to Chin and Gilbert. Additionally, Luthy, et al. 1979 note that grain boundary sliding is impossible below a normalized stress ($\sigma$/E) of 9.6 x 10-6 or $\ln(\sigma/E) = -11.6$. This is somewhat lower than the boundary of -9.8 proposed by Chin in Figure D-1.

More recently, Langdon 1994 has used equations of the same general form as those of Chin and Gilbert and Luthy, *et al.* and attempted to develop a consistent rationale to describe the role of grain boundary sliding in both creep and superplasticity. Based on experimental data for aluminum, Langdon derived the following equations for creep and superplasticity, respectively:

$$\dot{\epsilon}_{gbs} = \frac{A_{gbs} D_{l} Gb}{kT} \left(\frac{b}{d}\right) \left(\frac{\sigma}{G}\right)^{3} \qquad \text{(D-5)}$$

$$\dot{\epsilon}_{sp} = \frac{A_{sp} D_{gb} Gb}{kT} \left(\frac{b}{d}\right)^{2} \left(\frac{\sigma}{G}\right)^{2} \qquad \text{(D-6)}$$

In equation D-5, the grain size (d) is presumed to range from 10 to 1000 $\mu$m, while in equation D-6, the grain size range is 0.01 to 10 $\mu$m. Using d=10 $\mu$m in equation D-5 and d=5 $\mu$m in equation D-6 assuming that $Q_l$ is 250 kJ/mole and $Q_{gb}$ is 175 kJ/mole, strain rates were calculated using Langdon's equations. These and other calculated strain rates based on grain boundary sliding are summarized in Table D-1.

Table D-1. Calculated Strain Rates for Grain Boundary Sliding (per second)

| Temperature (K) | Mayazumi & Onchi[a] | Chin & Gilbert | Luthy, *et. al.* | Langdon (creep) | Langdon (superplas.) |
|---|---|---|---|---|---|
| 423 | 1.9E-19 | 4.5E-18 | 2.0E-19 | 7.3E-24 | 2.0E-19 |
| 523 | 2.7E-14 | 7.8E-14 | 3.4E-15 | 1.0E-17 | 3.7E-15 |

a - Experimental data obtained outside grain boundary sliding range.

From this table it can be noted that the Langdon formulations for both creep and superplasticity result in lower strains than predicted by either the results of Mayazumi and Onchi or of Chin and Gilbert. No doubt fortuitously, the strain rates proposed by Langdon for superplasticity are essentially the same as those proposed by Luthy, *et al.* for creep. There is reasonable agreement between the predictions of Mayazumi and Onchi and Luthy *et al.*

Several investigators, including Matsuo, Mayazumi and Onchi, and Murty have measured the activation energy for creep. As can be seen from Figure D-1, the experimental data were obtained under conditions where this activation energy should be the activation energy for lattice diffusion, $Q_l$. These data are summarized in Table D-2 along with estimates of the activation enery for grain boundary diffusion, $Q_{gb}$, assuming that $Q_{gb}/Q_l = 0.6$ (i.e, the minimum of the expected range).

Table D-2. Activation Energies for Lattice Diffusion and Grain Boundary Diffusion

| Source | $Q_l$ (kJ/mole) | $Q_{gb}$ (kJ/mole) | $Q_{gb}=0.6Q_l$ |
|---|---|---|---|
| Matsuo | -272 | | -163 |
| Mayazumi & Onchi | -215 | | -129 |
| Murty | -249 | | -149 |
| Chin et al. | -250 | -175 | -150 |

As noted earlier, the strain rate is proportional to $1/d^3$ where d is the grain size. In the ASTM Specification B 811-90 for Zircaloy tubing for nuclear fuel, the grain size for recrystallization annealed material is ASTM micrograin Size No. 7 or finer[22]. This is equivalent to an average grain diameter of 31.8 $\mu$m per ASTM Specification E 112 - 96. In practice, the grain size for BWR cladding runs about ASTM 12 (5.7 $\mu$m) (Marlowe 1998).

For stress-relief annealed tubes, ASTM specifies that the grain size must meet requirements agreed upon between the manufacturer and the purchaser. In the early 1960's, Bettis Atomic Power Laboratory obtained a variety of samples of Zircaloy-4 tubing from commercial suppliers for evaluation (WAPD 1966). Many of the samples were cold worked various amounts and stress-relief annealed. ASTM grain sizes ranged from 6 to 12.5 (45 to 4.7 $\mu$m). The mean grain size for 14 lots of cold-worked and stress relieved tubing was 9.7 (12 $\mu$m). The value of 12 $\mu$m was confirmed as representative of current practice for PWR fuel rods (Bale 1998). This information suggests that the grain size used by Chin, et al. is smaller than expected in commercial practice for PWR fuel rods and thus over-predicts creep strain.

References:

Ashby, M.F. and H.J. Frost, 1975. In *Constitutive Equations in Plasticity*, A.S. Argon (ed.) MIT Press, Cambridge, MA, p. 117.

[22] BWR cladding is generally in the recrystallized condition while PWR cladding is cold-worked and stress relief annealed.

Bale 1998. Private communication with Mike Bale, Framatome Technologies, (804) 832-2488, July 6, 1998.

Chin, B.A. and E.R. Gilbert, 1989. "Prediction of Maximum Allowable Temperature for Dry Stroage of Zircaloy-Clad Spent Fuel in Inert Atmosphere," *Nucl. Technol.*, vol. 85, pp. 57-65, April 1989.

Langdon, T.G., 1994. "Grain Boundary Sliding as a Deformation Process in Creep and Superplasticity," *International Conference on Superplasticity in Advanced Materials, Materials Science Forum Vols. 170-172*, pp. 53-58.

Langdon, T.G. and R.B. Vastava, 1982. "An Evaluation of Deformation Models for Grain Boundary Sliding," in *ASTM Conference on Mechanical Testing for Deformation Model Development*, Bal Harbour, FL November 12-13 1980, pp. 435-451, pub. 1982.

Luthy, H., R.A. White and O.D. Sherby 1979. "Grain Boundary Sliding and Deformation Mechanism Maps," *Mater. Sci. Eng.* 39 (2), pp. 211-216, August 1979.

Marlowe, M. 1998. Private communication with Mick Marlowe, GE Nuclear Energy, (910) 675-5418, July 6, 1998.

Matsuo, Y., 1987 "Thermal Creep of Zircaloy-4 Cladding under Internal Pressure," *J. Nucl. Sci. and Technol.*, 24[2], pp. 111-119.

Mayazumi, M. and T. Onchi, 1990, "Creep Deformation of Unirradiated Zircaloy Nuclear Fuel Cladding Tube Under Dry Storage Conditions," *J. Nuc. Mat.*, 171:383-388.

Murty, K.L., G.S. Clevinger, and T.P. Papazoglou 1977. "Thermal Creep of Zircaloy-4 Cladding." in *Transactions of the 4th International Conference on Structural Mechanics*, San Francisco CA, August 15-19, 1977.

Peehs, M., G. Kaspar, and E. Steinberg, 1986, "Experimentally Based Spent Fuel Dry Storage Performance Criteria," *Proc. 3rd International Spent Fuel Storage Technology Symposium/Workshop*, vol. 1, pp. S-316-S-331, USDOE-CONF-86041/UC-85.

WAPD 1966. "Properties of Zircaloy-4 Tubing," WAPD-TM-585, C.R. Woods (ed.), Bettis Atomic Power Laboratory, December 1966.